VOLUME 38 SEPTEMBER 1960 NUMBER 9

Canadian Journal of Physics

Editor: H. E. DUCKWORTH

Associate Editors:

L. G. ELLIOTT, *Atomic Energy of Canada, Ltd., Chalk River*
J. S. FOSTER, *McGill University*
G. HERZBERG, *National Research Council of Canada*
L. LEPRINCE-RINGUET, *Ecole Polytechnique, Paris*
B. W. SARGENT, *Queen's University*
G. M. VOLKOFF, *University of British Columbia*
W. H. WATSON, *University of Toronto*
G. A. WOONTON, *McGill University*

Published by THE NATIONAL RESEARCH COUNCIL

OTTAWA CANADA

CANADIAN JOURNAL OF PHYSICS

Under the authority of the Chairman of the Committee of the Privy Council on Scientific and Industrial Research, the National Research Council issues THE CANADIAN JOURNAL OF PHYSICS and five other journals devoted to the publication, in English or French, of the results of original scientific research. Matters of general policy concerning these journals are the responsibility of a joint Editorial Board consisting of: members representing the National Research Council of Canada; the Editors of the Journals; and members representing the Royal Society of Canada and four other scientific societies.

EDITORIAL BOARD

Representatives of the National Research Council

I. McT. Cowan (Chairman), *University of British Columbia*
L. Marion, *National Research Council*
H. G. Thode, *McMaster University*
D. L. Thomson, *McGill University*

Editors of the Journals

D. L. Bailey, *University of Toronto*
T. W. M. Cameron, *Macdonald College*
H. E. Duckworth, *McMaster University*
Léo Marion, *National Research Council*
J. F. Morgan, *Department of National Health and Welfare, Ottawa*
F. E. Chase, *Ontario Agricultural College*
J. A. F. Stevenson, *University of Western Ontario*

Representatives of Societies

D. L. Bailey, *University of Toronto*
Royal Society of Canada
T. W. M. Cameron, *Macdonald College*
Royal Society of Canada
H. E. Duckworth, *McMaster University*
Royal Society of Canada
Canadian Association of Physicists
P. R. Gendron, *University of Ottawa*
Chemical Institute of Canada
D. J. Le Roy, *University of Toronto*
Royal Society of Canada
J. F. Morgan, *Department of National Health and Welfare, Ottawa*
Canadian Biochemical Society
R. G. E. Murray, *University of Western Ontario*
Canadian Society of Microbiologists
J. A. F. Stevenson, *University of Western Ontario*
Canadian Physiological Society

Ex officio

Léo Marion (Editor-in-Chief), *National Research Council*
J. B. Marshall (Administration and Awards), *National Research Council*

Manuscripts for publication should be submitted to Dr. H. E. Duckworth, Editor, Canadian Journal of Physics, Hamilton College, McMaster University, Hamilton, Ontario.
For instructions on preparation of copy, see **NOTES TO CONTRIBUTORS** (back cover).

Proof, correspondence concerning proof, and orders for reprints should be sent to the Manager, Editorial Office (Research Journals), Division of Administration and Awards, National Research Council, Ottawa 2, Canada.

Subscriptions, renewals, requests for single or back numbers, and all remittances should be sent to Division of Administration and Awards, National Research Council, Ottawa 2, Canada. Remittances should be made payable to the Receiver General of Canada, credit National Research Council.

The journals published, frequency of publication, and subscription prices are:

Canadian Journal of Biochemistry and Physiology	Monthly	$9.00 a year
Canadian Journal of Botany	Bimonthly	$6.00 a year
Canadian Journal of Chemistry	Monthly	$12.00 a year
Canadian Journal of Microbiology	Bimonthly	$6.00 a year
Canadian Journal of Physics	Monthly	$9.00 a year
Canadian Journal of Zoology	Bimonthly	$5.00 a year

The price of regular single numbers of all journals is $2.00.

ERRATUM

Two errors in the Appendix have been pointed out to the author of the paper "Scattering of radio waves by an ionized gas in thermal equilibrium" (Can. J. Phys. **38**, 1114, 1960). These errors do not occur in the corresponding analysis of Pines and Bohm, which is correct within its range of validity.

The first error consists in the omission of the second order term in the expansion of the logarithm leading to equation (58). The second occurs in the final integration leading to equation (73), where the lack of independence of Fourier components with wave number vectors of equal magnitude and opposite direction was not taken into account.

The corrected forms of equations (6), (7), (73), and (76) are obtained by replacing T in the original equations by $T/2$. The corrected form of equation (8) is obtained by replacing λ^2 in the original equation by $2\lambda^2$. The results obtained for the frequency spectrum of scattered power are not affected.

Canadian Journal of Physics

Issued by THE NATIONAL RESEARCH COUNCIL OF CANADA

VOLUME 38 SEPTEMBER 1960 NUMBER 9

THE CRACKING ACTIVITY IN ICE DURING CREEP[1]

L. W. GOLD

ABSTRACT

Observations were made at one temperature on the cracks that form in ice during creep under constant compressive load. The ice had a hexagonal symmetry with respect to the grain boundaries. The load was applied perpendicular to the long axis of the grains. A piezoelectric crystal was used to detect the cracking activity in the ice.

Two stages of cracking were observed. The first occurred during the transient period of the creep, and the plane of these cracks tends to be parallel to the grain boundaries and to the direction of the stress. The rate at which these cracks formed decreased very markedly as the creep rate approached a constant value. Above a certain stress, the creep rate continuously increased with time. Under this condition the second stage of cracking was observed. These cracks tend to be more irregular in direction and to occur in planes that are at 45° to the applied stress.

INTRODUCTION

Observations on the elastic and creep behavior of ice under constant compressive stress have been carried out by Brown (1926). At lower stresses he observed a creep rate which, after the initial transient stage, tended to decrease with time to a constant value characteristic of the stress. At a critical stress range, between 190 and 200 p.s.i. for the temperature and load conditions of the experiment, the character of the creep–time curve changed radically from one for which the creep rate decreased with time to one for which it increased with time. The period of observation was never more than $3\frac{1}{2}$ hours.

Throughout his paper, Brown refers to internal cracking of the ice and associated audible "crackling" that occurred during a load test. Qualitatively, his comments indicate that the intensity of "crackling" depends on the temperature and on the magnitude of the applied stress.

The creep of ice and its general dependence on stress, temperature, and time is similar to that observed for many materials. Glen (1958), in his review of such investigations, found that the minimum observed strain rate is related to the applied stress according to the law:

$$\dot{e} = kc^n \tag{1}$$

[1]Manuscript received May 10, 1960.
Contribution from the Snow and Ice Section, Division of Building Research, National Research Council, Ottawa, Canada.
Issued as N.R.C. No. 5763.

where $\dot{e}$ is the strain rate, c is the applied stress, and k is a constant. The exponent n is observed to increase with c within the range $1.85 < n < 4.16$ for $1.0 < c < 15$ kg/cm^2. Glen (1955) observed that until accelerating creep occurs, ice obeys the Andrade law with the initial transient in the creep curve being proportional to the cube root of the time.

Cracking activity has been reported in other materials during compressive loading. Obert (1945) conducted investigations in the laboratory to see if the microseismic activity, which he observed in rock in the field, could also be detected with rock specimens subject to compressive loads in the laboratory. He observed a high "microseismic rate" when the load was between 1/8 to 1/2 the ultimate strength of the rock. This rate had decreased to a minimum when the load reached 1/2 to 3/4 the ultimate strength. As the load was increased, he observed that the rocks that tended to shatter showed a marked increase in "microseismic" activity at about 8/10 of the crushing strength, whereas the rocks that tended to crush showed comparatively little increase in activity. He was able to show that the first maximum in his observed "microseismic" activity was due to the geometry of loading. If he held the load constant at stresses up to 9/10 the ultimate load, the activity rate in the sample decreased with time to a constant value which depended on the magnitude of the load.

Bridgman (1949) attributed anomalies in the volume change during loading for loads approaching the ultimate strength of the material to the forming of internal cracks or interstices at grain boundaries, mechanical impurities, or around dislocations in the lattice.

Jones (1952) observed that the velocity of an ultrasonic pulse transmitted through a concrete specimen in a direction perpendicular to the applied compressive load began to decrease when the load was about 25 to 30% of the ultimate strength. He attributes this decrease to the formation of internal cracks. Because the velocity of a pulse propagated in the direction of the stress did not change, he concluded that the plane of the cracks must be parallel to the direction of the stress.

Rüsch (1959) using a crystal pickup, recorded the internal cracking in concrete subject to compressive loads. For loads within 85% of the 1-minute ultimate strength, he observed a high rate of cracking when the load was first applied. This rate dropped off but increased again rapidly just before failure occurred.

The purpose of the observations reported in this paper was to investigate at one temperature and under constant compressive load, the cracking activity that occurs in ice during creep. In particular, it was desired to investigate the sudden transition that Brown reported in the character of the creep–time curve and to see if this transition was in some way related to the internal cracking.

EXPERIMENTAL PROCEDURE

The observations were carried out on rectangular ice specimens 5×10 cm and 20 cm long prepared at $-10°$ C with a standard metal cutting lathe and a wood planer. A small, manually driven testing machine (Hounsfield

PLATE I

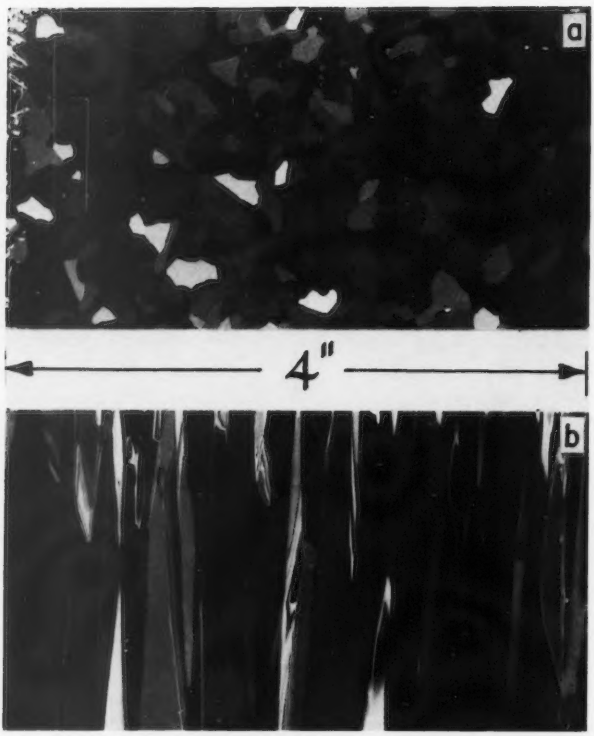

FIG. 2. Thin sections of test specimen viewed with polarized light: (*a*) section perpendicular to direction of growth, (*b*) section parallel to direction of growth.

tensometer) with a capacity of 2000 kg was used for applying the load. The test pieces were mounted between special loading heads one of which is shown in Fig. 1. The silicone grease, separated from the ice by the silicone rubber

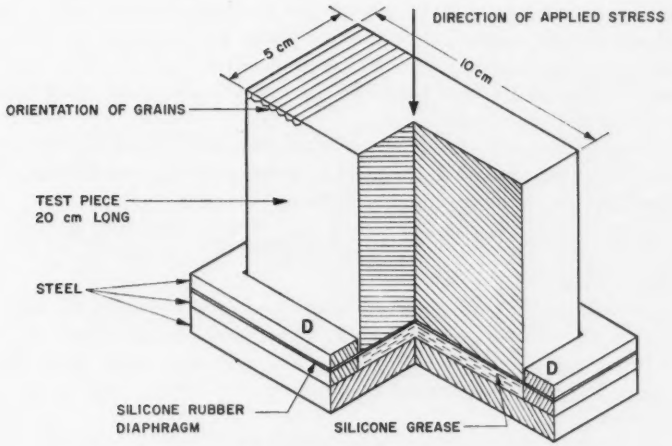

FIG. 1. Sketch of loading head construction.

diaphragm, ensured that the applied compressive stress was uniform over the test piece.

To keep the silicone rubber from shearing during an experiment, water was frozen in the small space between the test piece and D of the loading heads. The frozen bond between the ice and D failed as soon as a load was applied but the ice was constrained from deforming laterally. This constraint influenced the distribution of cracks in the vicinity of the loading head as will be shown later.

An extensometer with a 2-in. gauge length and a strain magnification of 3300 was used for measuring the creep. The gauge had to be remounted periodically because of its limited range. The creep was recorded on a Baldwin X-Y recorder, model MD-2. The pen of the recorder automatically and continuously traversed the chart paper at a constant rate of $2\frac{1}{4}$ inches per minute. The creep–time curve was constructed by aligning the measured sections on the known time base.

The ice used in the observations was prepared from ordinary tap water in a cylindrical container about 1 meter in diameter. The direction of freezing was perpendicular to the water surface. When the water surface cooled to 0° C, ice grains were sprinkled on the surface to act as centers of nucleation. The resulting grain structure as seen with polarized light is shown in Fig. 2. Figure 2*a* is a thin section cut parallel to the ice surface and Fig. 2*b* is a section cut perpendicular to the surface. The columnar structure is typical for multigrained ice often encountered under natural conditions.

The test specimens were cut so that the long axis of each grain was perpendicular to the 10×20 cm face and therefore perpendicular to the applied compressive stress as shown in Fig. 1. The stress applied to the test specimen was kept constant to ±1% of the applied load during the test.

To measure the cracking activity in the ice during creep, a piezoelectric crystal was frozen to one face of the test piece. The output from the crystal was fed into a high-gain amplifier and then recorded. Each time a disturbance occurred within the ice that would set up a shock wave, the event caused a deflection of the recorder pen.

The observations were carried out in a cold room maintained at $-10\pm0.5°$ C. The test pieces were stored in the room in kerosene for at least 24 hours before they were loaded in the testing machine.

OBSERVATIONS

Cracking Activity

Figure 3 shows that the observed creep–time curves for all tests exhibit an initial increase in creep rate with time. Those subjected to a stress less than about 16 kg/cm² had a decreasing creep rate with time after about the first half hour. Two of these showed a tendency to a later period of increasing creep rate with time.

Figure 4 shows the observed dependence of the total cracking activity on time for three test pieces subject to the applied stress given in the figure. Also shown are the associated creep–time curves. At a stress of 10 kg/cm², very little internal cracking occurred; at a stress of 15.2 kg/cm² the cracking activity was appreciable. Most of the activity occurred in the first hour during the transient portion of the creep–time curve. After 1½ hours, practically no further cracking occurred. When the stress was greater than about 16 kg/cm², and the creep rate showed no tendency to decrease with time, the cracking activity greatly increased.

Some of the details in the cracking–time curves are shown in Fig. 5 where the number of disturbances that occurred in a 5-minute interval are plotted against time. The resulting curve is an approximation to the rate of cracking activity. One further set of observations made at a stress of 15.4 kg/cm² is shown to illustrate the oscillatory character of the rate of cracking activity after the first maximum. The cracks seem to occur in bursts as though a critical situation developed within the test piece, which then was relieved by the formation of cracks. Figure 5 shows also that even when the applied stress was great enough that no decrease was observed in the rate of creep, a decrease was observed in the cracking rate but then the rate increased beyond the original maximum.

In Fig. 6, the logarithm of the total cracking activity that occurred during the first hour, which amounted to at least 60% of the total cracking activity observed, is plotted against the applied stress. The line drawn is the least squares fit to all the observations made. This figure shows the marked dependence that the cracking activity has on the applied stress.

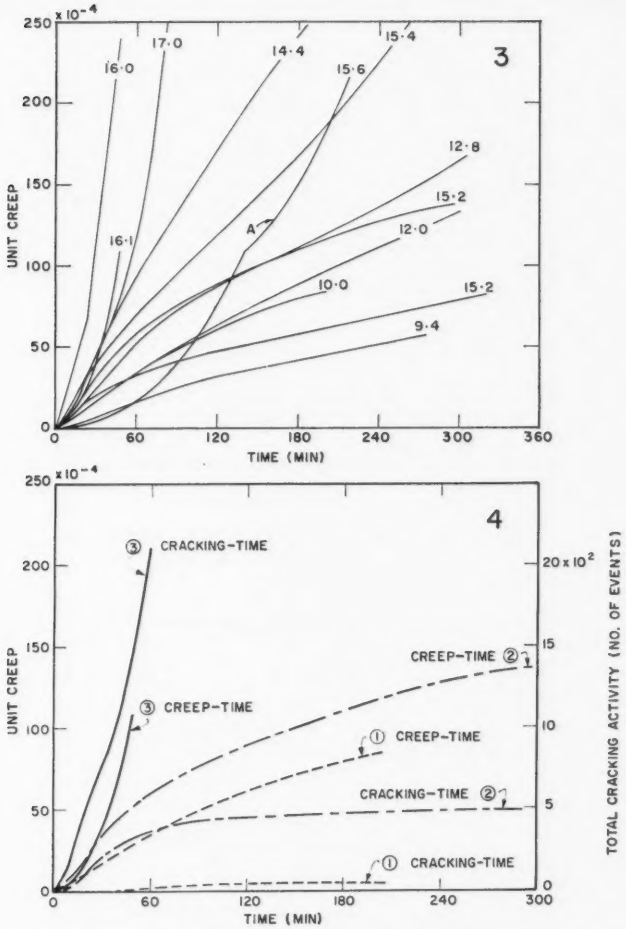

FIG. 3. Creep–time curves. The stress in kg/cm² is given for each curve.
FIG. 4. Three typical examples of the dependence of the total cracking activity and the creep on time at the applied stress given. (1) – – – stress = 10 kg/cm²; (2) — — — stress = 15.2 kg/cm²; (3) ——— stress = 16.1 kg/cm².

Crack Formation

The cracks were observed to propagate parallel to the long direction of the grain boundaries and perpendicular to the applied stress. This is shown in Fig. 7*b* where each light mark is a crack. The edge view shows that in some cases the cracks will propagate from face to face. For stresses below about 15 kg/cm², the crack distribution, which resulted during the period of loading,

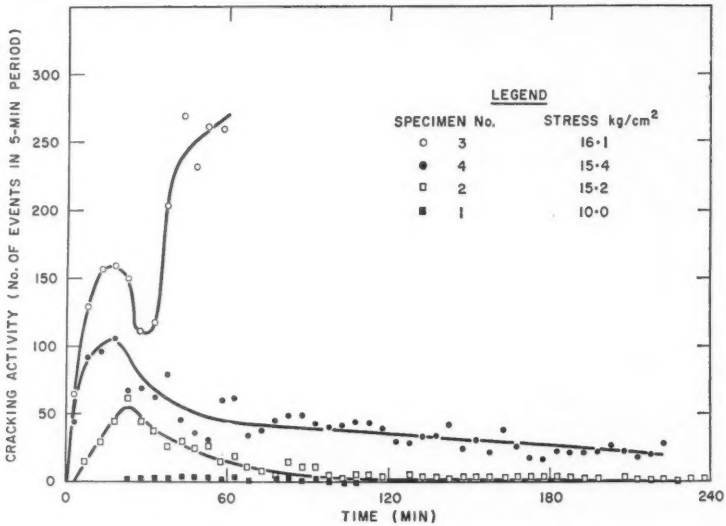

FIG. 5. Time dependence of the rate of cracking activity.

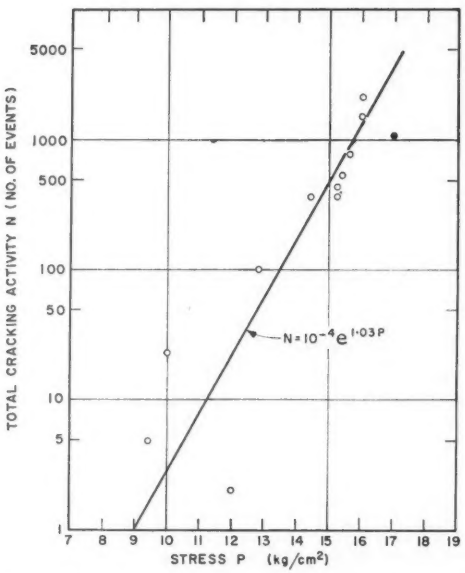

FIG. 6. Stress dependence of total cracking activity which occurred during the first 60 minutes.

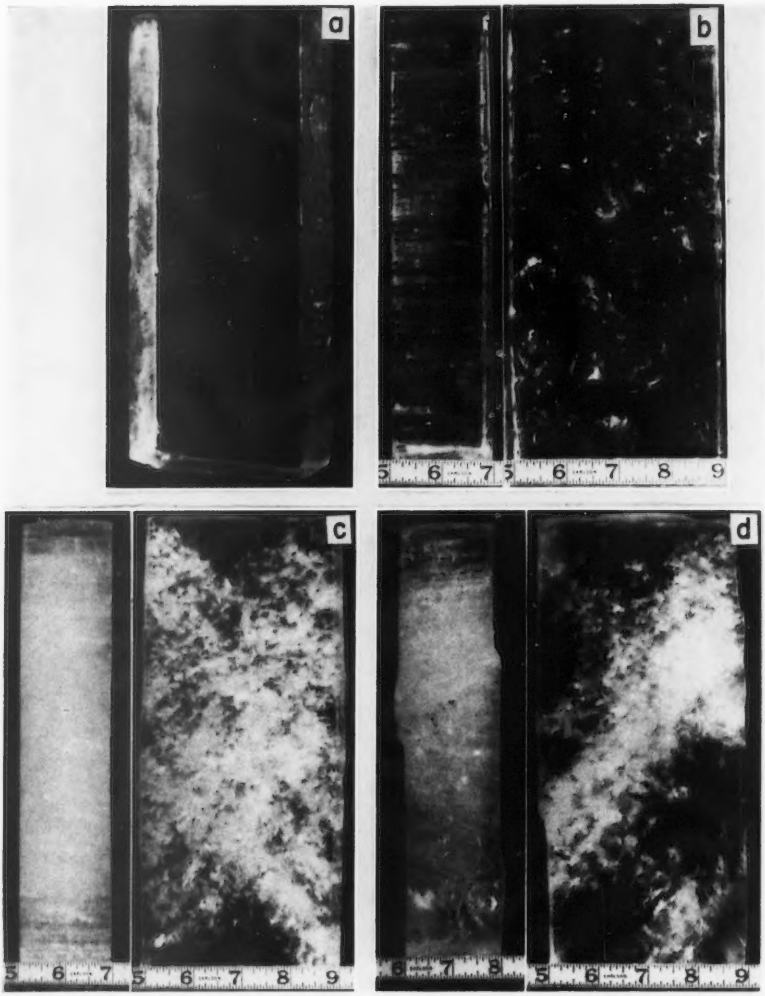

FIG. 7. Examples of crack development in ice during creep (scale in inches): (*a*) stress, 10 kg/cm²; duration of load, 180 minutes; (*b*) stress, 15.2 kg/cm²; duration of load, 300 minutes; (*c*) stress, 16 kg/cm²; duration of load, 50 minutes; (*d*) stress, 15.6 kg/cm²; duration of load, 225 minutes.

was fairly uniform as shown in Figs. 7*a* and 7*b*. For stresses greater than about 15.5 kg/cm², a marked change occurred in the character of the cracking and this change was associated with the increase in the cracking rate shown in Fig. 5 for specimen 3. In these cases, after an initial cracking period of 15 to 30 minutes, during which the cracks formed uniformly throughout the test piece, the cracks tended to form in planes that were about 45° to the applied stress and parallel to the grain boundaries as shown in Fig. 7*c*. In only one case out of the five in which these cracking planes developed was the plane not parallel to the grain boundaries. This is shown in Fig. 7*d*; its creep–time curve is designated by A in Fig. 3.

Most of the test pieces were quite free of cracks in a triangular zone adjacent to the loading heads as shown in Fig. 7*c*. This is thought to be due to the confining influence of the loading heads.

Two test pieces were subjected to stresses of the order of 14 kg/cm² and allowed to deform until a number of cracks had developed. The angle between the plane of each crack and the direction of the stress was measured. The resulting distribution diagram for 56 cracks observed, which is shown in Fig. 8, shows that there is a definite preference for a crack to form with its

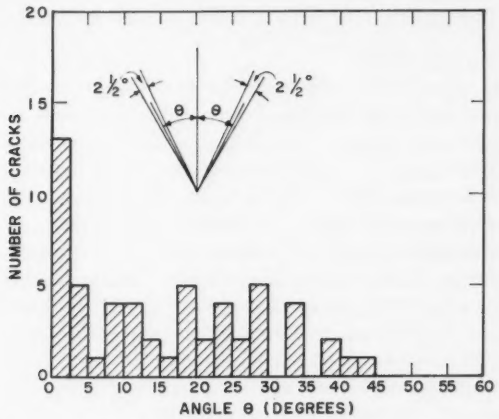

FIG. 8. Number of cracks in 2½-degree interval with plane of crack at angle θ to stress.

plane parallel to the direction of the applied stress. No cracks were observed with their plane at an angle greater than 45° to the stress. As already mentioned, the long direction of the cracks is parallel to the grain boundaries.

Out of 74 cracks studied, 22 occurred at grain boundaries. An additional eight occurred at grain boundaries but were also partly transcrystalline. The remainder were completely transcrystalline.

The water molecules in ice are loose-packed and the single crystal has an hexagonal symmetry. An attempt was made to see if there was any correlation between the direction of the axis of hexagonal symmetry and the direction of

the plane of those cracks that were transcrystalline. An etching technique described by Higuchi (1958) was used to determine the crystallographic orientation. No positive correlation was found because it proved to be almost impossible to form an etch pit in grains containing a crack using Higuchi's technique.

It was realized during the etch-pit observations and later confirmed by observations using polarized light that there was a bias in the crystallographic orientation of the grains. It had been hoped that seeding with snow would result in a random orientation. Hillig (1958) has shown that ice crystals grow more quickly perpendicular to the axis of the hexagonal symmetry than parallel to it. As a result, crystals with their symmetry axis perpendicular to the direction of growth tend to squeeze out those that are parallel. In the present experiments, no crystals were observed that had their axis of hexagonal symmetry within 45° of the direction of growth. Thus, the easy slip plane of the grains tended to be parallel to the grain boundaries. Because the symmetry axis tended to be normal to the grain boundaries and therefore parallel to the ice surface, it was impossible with the apparatus available to determine its direction accurately with polarized light. It was observed that at least 12 of the 44 transcrystalline cracks were either parallel or perpendicular to the symmetry axis and therefore parallel or perpendicular to the easy slip plane.

Deformation of the Test Pieces

Measurements were made on one specimen that had been subject to a stress of 17 kg/cm^2 to determine the change of volume that occurred over the section where the creep was measured. An increase in volume of approximately 3% was observed. This increase is probably due to the formation of the cracks. When the sample was immersed in kerosene for storage after the observations, air bubbles were observed to issue from some of the cracks.

All of the lateral deformation of the specimen was observed to be normal to the grain boundaries. No significant creep in the direction parallel to the long axis of the grains was observed in any of the tests. The ice deformed in a way similar to a pile of logs subject to a load perpendicular to the long dimension of the logs. At the completion of a test, the edges of most of the test pieces were very irregular and it was possible to recognize individual grains because of their displacement relative to their neighbors.

DISCUSSION

In an earlier paper, Gold (1958) presented evidence which indicated that when ice, at a temperature between 0° C and −40° C, is subject to a uniaxial compression normal to the grain boundaries, there is a relaxation of the shear stress at the grain boundaries. Consider the array of hexagonal grains shown in Fig. 9. If the shear stress relaxes at the grain boundaries, a tensile stress will be developed across the planes nearly parallel to the applied stress, such as A–A, whose average value is given approximately by

$$p = c(1 - a\cos^2 b) \tag{2}$$

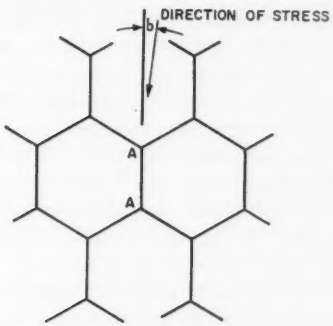

FIG. 9. Array of hexagonal grains.

where p is the average tensile stress,

c is the compressive stress,

$0 < a < 1$ is the proportion of shear stress still effective at the grain boundary,

b is the angle between the applied stress and the plane under consideration. For $b = 0°$,

$$p = c(1-a).$$

This demonstrates that under conditions of uniaxial compression, if the shear stress can relax at the grain boundaries, each grain will be subject to both compressive and tensile stresses. The magnitude of these stresses at each point will depend on the value of the applied stress, the local geometry of the grain boundaries, and their orientation with respect to the applied stress. In the present case, the stress field is biaxial because of the columnar nature of the grains. Under these conditions, one would expect cracks to form parallel to the grain boundaries with their plane tending to be parallel to the direction of the applied stress, that is, to form in planes across which tensile stresses can develop. Furthermore, it would be expected that the number of such sites available for crack formation would be limited and would depend on the magnitude of the stress as was observed (Fig. 4).

Figures 4 and 5 show that the initiation and extension of a crack in ice is time dependent. If one considers the conditions necessary for the development of a crack according to the theory put forward by Griffith (1924), this would imply that (*a*) the stress across the rupture plane increases with time, (*b*) imperfections in the single crystal or at the grain boundaries coalesce until in time a nucleus of the right size has formed from which a crack can develop (Cottrell 1959), or (*c*) both processes occur together.

Cottrell states that for holes at incoherent grain boundaries to grow, the following relation must be satisfied:

$$p = 2d/r, \tag{3}$$

where p is the tensile stress normal to the boundary,
d is the surface energy of ice per unit area,
r is the radius of the hole.

Figure 7 shows that for the duration of load associated with the observations, the compressive stress has to be greater than about 9 kg/cm² for a crack to develop. Assuming that the shear stress has completely relaxed at the grain boundary, this would give for p a value of about 9 kg/cm². The value of 120 ergs/cm² for d (Skapski *et al.* 1957) gives, for the critical radius, $r = 2.7 \times 10^{-5}$ cm. This value for r is a little smaller than that used by Cottrell in calculations of the critical tension p for metals.

Figure 4 shows that the transient portion of the creep–time curve occurs during the period when the cracking is maximum. Glen (1955) has attributed this transient stage, and the condition of an increasing creep rate with time, to recrystallization. In the present experiments it is apparent that the formation of cracks and the resulting disruption of the lateral constraint on the grains must make a significant contribution to the observed creep rate. The increasing creep rate with time at the start of the test would support the thesis that the tensile stress concentration across planes, such as A–A in Fig. 9, tends to increase with time. The formation of a crack would relieve the tensile stresses locally and thus change the stress distribution. This change in stress distribution would tend to decrease the creep rate of the grains involved. It would appear that under the conditions of the present experiments, during the first few minutes at least, Andrade's law for creep is not obeyed.

Steinemann (1954) gives evidence of the recrystallization of ice during the creep process. The ice used in his experiments had a granular rather than a columnar structure. It is possible that for compressive stresses less than about 9 kg/cm² at a temperature of $-10°$ C, creep and recrystallization of the grains ensures that concentrations of stress and imperfections will not develop to the magnitude necessary for the initiation of a crack.

Although the evidence indicates that it is the grain boundaries that control the formation of the cracks and the direction of the creep of multigrained ice, the possible influence of the easy slip direction, which tends to be parallel to the direction of the grain boundaries because of the bias in the crystallographic orientation, cannot be ruled out. This bias may certainly have been a contributing factor to the lack of creep in the direction of the long axis of the grains. It would also contribute to the ability of each grain to deform under the constraints imposed by its neighbors.

Each time a crack forms, the internal structure of the ice is altered. In the present situation it would appear that when enough cracks form, the ability of the ice to withstand shear stresses is lowered to the extent that large movements accompanied by extensive crack formation occur along preferred planes in which the shear stress is a maximum. When this condition is reached the ice can be considered to have failed. The cracking associated with the planes of shear failure is responsible for the high cracking rate observed after the first ½ hour for those test pieces that showed a continually

increasing creep rate with time. It is probable that, if the tests at lower stress had been continued long enough, failure along the planes of maximum shear would have developed in these cases also, resulting in a sudden increase in the cracking rate and a corresponding increase in the creep rate similar to that observed in concrete by Rüsch (1959).

Because of the movement that occurs at the planes of cracking in Fig. 7*c* and 7*d*, the creep measured by an extensometer similar to that used would depend on the location at which it is mounted. An obvious example of this is curve A in Fig. 3. It was also observed that if the cracking tended to occur on one side of the test piece, the creep would be greater on that side, that is, the test piece would develop a bow. These factors are responsible in part for the irregular dependence of the creep on the applied stress as seen in Fig. 3. Even so, the observed dependence of the creep rate on the stress does agree well with the dependence found by Steinemann (1954) for granular ice.

CONCLUSIONS

The purpose of these observations was to investigate, at one temperature and under constant compressive load, the cracking that occurs in ice during creep. In particular, it was desired to investigate the sudden transition in the creep–time curve that had been reported earlier and to see if this transition was in some way related to the internal cracking. From the present observations the following conclusions are drawn:

(1) During creep under uniaxial compressive stress greater than about 9 kg/cm² applied perpendicular to the grain boundaries of ice at −10° C, internal cracks form in the ice. The rate of formation of these cracks depends on the time and on the magnitude of the stress. For stresses below about 16 kg/cm², this rate goes through a maximum within the first hour after the application of the load and then decreases. The cracks tend to be long and narrow with their plane parallel to the direction of the grain boundaries and to the applied stress.

(2) The formation of these cracks is due to a tensile stress which is developed perpendicular to the applied stress because of the relaxation of shear stresses at the grain boundaries.

(3) The transient portion of the creep–time curve is due, in part, to the formation of internal cracks.

(4) The formation of internal cracks weakens the structure until a condition is attained where the specimen will fail along the planes of maximum shear.

(5) Because of the logarithmic dependence of the rate of cracking on the stress, this condition is attained very rapidly at stresses of about 16 kg/cm² and is responsible for the sudden change in the character of the creep–time curve that is observed in this stress range.

(6) Once failure begins along the planes of maximum shear the cracking activity greatly increases, the cracks forming primarily in the failure plane.

ACKNOWLEDGMENTS

The author acknowledges with gratitude the assistance of R. Wallace in obtaining the observations that form the basis of this paper. This paper is a contribution from the National Research Council of Canada, Division of Building Research, and is published with the approval of the Director.

REFERENCES

BRIDGMAN, P. W. 1949. J. Appl. Phys. **20**, 1241.
BROWN, E. 1926. Experiments on strength of ice, St. Lawrence Waterway Project, Report of Joint Board of Engineers, Appendix F, 423–453.
COTTRELL, A. H. 1959. Theoretical aspects of fracture. *In* Fracture (The Technology Press of Massachusetts Institute of Technology and John Wiley & Sons, Inc., New York).
GLEN, J. W. 1955. Proc. Roy. Soc. A, **228**, 519.
——— 1958. Phil. Mag. Suppl. **7**, 254.
GOLD, L. W. 1958. Can. J. Phys. **36**, 1265.
GRIFFITH, A. A. 1924. Proc. Intern. Congr. Appl. Mech., 1st Congr., 55–63. Delft, 1924.
HIGUCHI, K. 1958. Acta Met. **6**, 636.
HILLIG, W. B. 1958. The kinetics of freezing of ice in the direction perpendicular to the basal plane. *In* Growth and perfection of crystals (John Wiley & Sons, Inc., New York).
JONES, R. 1952. Brit. J. Appl. Phys. **3**, 229.
OBERT, L. and DUVALL, W. 1945. Microseismic method of predicting rock failure in underground mining. Part I. General method (U.S. Department of Interior, Bureau of Mines, RI 3797).
RÜSCH, H. VON. 1959. Zement-Kalk-Gips, **12**, 1.
SKAPSKI, A., BILLUPS, R., and ROONEY, A. 1957. J. Chem. Phys. **26**, 1350.
STEINEMANN, S. 1954. Flow and recrystallization of ice. *In* International Union of Geodesy and Geophysics. International Association of Scientific Hydrology, Rome general assembly, Tome IV, pp. 449–462.

TABLES OF ROTATIONAL ENERGY LEVELS OF DEFORMED EVEN–EVEN NUCLEI[1]

R. B. Moore and W. White

ABSTRACT

A digital computer has been used to extend calculations of rotational energy levels of deformed even–even nuclei treated in the manner of Davydov and Filippov. Tables are presented which may be useful for comparison with experimental energy levels of high spin such as are realized in Coulomb excitations by heavy ions.

Energy levels of axially asymmetric nuclei, given by the rotational Hamiltonian

$$\mathbf{H} = \frac{\hbar^2}{4B\beta^2} \sum_{i=1}^{3} \frac{\mathbf{I}_i^2}{2 \sin^2\{\gamma - (2\pi/3)i\}}$$

proposed by Bohr (1952), have been examined by Davydov and Filippov (1958), and Davydov and Rostovsky (1959). Here B is the mass transport parameter, β and γ are shape parameters corresponding to a deformation of order 2, and the $\mathbf{I}_i$ are operators of the projections of the total angular momentum along the body-fixed axes of the nucleus. Certain energy levels are excluded by symmetry conditions.

In a previous paper, DeMille *et al.* (1959) calculated the energy levels for the then experimentally known excited states. An important recent development in Coulomb excitation techniques (Stephens, Diamond, and Perlman 1959) has extended the observations and encouraged the present authors to calculate the energy levels for states of higher spin. The results of such calculations are presented in Tables I and II. These tables give the energy ratios $E(n+)/E(2+)$ and also the energy $E(2+)$ of the first excited state (in units of $\hbar^2/4B\beta^2$) so that the ratios may be converted to energies if desired. Figure 1 shows the ratios as a function of γ for the "ground state band" and the $2'+$ level.

The calculations were performed with the aid of an IBM 650 digital computer. Calculated final results for the energy levels have an accuracy of at least 0.02%. Spot checks were made for the levels of higher spin using the tables of King, Hainer, and Cross (1943), and the asymptotic method of Golden (1948).

Stephens, Diamond, and Perlman (1959), using multiple Coulomb excitation realized by bombarding with A^{40} ions, have succeeded in establishing experimentally the "ground state bands" of Th^{232} and U^{238} with spins up to 10 and 12 respectively. Assuming these nuclei to be axially symmetric, they show that the "ground state" level schemes may be given by

$$E = AI(I+1) - BI^2(I+1)^2 + CI^3(I+1)^3 \qquad I = 0, 2, 4, 6, \ldots$$

[1]Manuscript received May 16, 1960.
Contribution from the Radiation Laboratory, McGill University, Montreal, Que.

TABLE I

Energy ratios E(n+)/E(2+) and the energy E(2+) of the "ground state rotational band" of axially asymmetric even-even nuclei. γ is given in degrees and E(2+) in units of $\hbar^2/4B\beta^2$

γ	E(2+)	E(4+)/E(2+)	E(6+)/E(2+)	E(8+)/E(2+)	E(10+)/E(2+)	E(12+)/E(2+)
0	4.0000	3.3333	7.0000	12.000	18.333	26.000
3	4.0220	3.3333	7.0000	12.000	18.333	26.000
4	4.0392	3.3331	6.9987	11.996	18.323	25.979
5	4.0613	3.3327	6.9964	11.989	18.306	25.944
6	4.0887	3.3320	6.9929	11.978	18.280	25.891
7	4.1212	3.3309	6.9869	11.959	18.235	25.799
8	4.1590	3.3291	6.9774	11.929	18.163	25.654
9	4.2022	3.3265	6.9633	11.885	18.059	25.446
10	4.2510	3.3227	6.9430	11.822	17.912	25.158
11	4.3055	3.3175	6.9152	11.737	17.717	24.790
12	4.3658	3.3104	6.8776	11.624	17.467	24.338
13	4.4322	3.3010	6.8284	11.481	17.164	23.818
14	4.5048	3.2887	6.7656	11.306	16.813	23.246
15	4.5836	3.2729	6.6875	11.099	16.424	22.645
16	4.6688	3.2529	6.5930	10.866	16.010	22.028
17	4.7603	3.2280	6.4819	10.610	15.581	21.409
18	4.8582	3.1975	6.3557	10.341	15.148	20.796
19	4.9622	3.1608	6.2169	10.064	14.718	20.196
20	5.0718	3.1177	6.0690	9.7869	14.296	19.613
21	5.1864	3.0684	5.9164	9.5139	13.888	19.050
22	5.3047	3.0137	5.7632	9.2499	13.498	18.513
23	5.4251	2.9552	5.6138	8.9989	13.128	18.005
24	5.5451	2.8950	5.4721	8.7650	12.785	17.535
25	5.6613	2.8361	5.3420	8.5526	12.474	17.108
26	5.7691	2.7814	5.2273	8.3666	12.202	16.735
27	5.8629	2.7342	5.1320	8.2127	11.977	16.426
28	5.9365	2.6977	5.0601	8.0968	11.808	16.194
29	5.9837	2.6746	5.0153	8.0246	11.703	16.049
30	6.0000	2.6667	5.0000	8.0000	11.667	16.000

γ	E(14+)/E(2+)	E(16+)/E(2+)	E(18+)/E(2+)	E(20+)/E(2+)	E(22+)/E(2+)	E(24+)/E(2+)
0	35.000	45.333	57.000	70.000	84.333	100.000
3	35.000	45.333	57.000	70.000	84.333	100.000
4	34.962	45.270	56.899	69.847	84.111	99.687
5	34.897	45.160	56.725	69.584	83.730	99.153
6	34.800	44.996	56.467	69.198	83.175	98.382
7	34.633	44.718	56.032	68.554	82,264	97.142
8	34.373	44.290	55.376	67.605	80.958	95.420
9	34.005	43.701	54.500	66.384	79.340	93.362
10	33.513	42.940	53.415	64.928	77.481	91.075
11	32.907	42.043	52.188	63.345	75.518	88.715
12	32.200	41.042	50.868	61.686	73.502	86.322
13	31.424	39.985	49.512	60.011	71.490	83.952
14	30.606	38.903	48.147	58.344	69.499	81.612
15	29.772	37.820	46.795	56.701	67.541	79.316
16	28.937	36.747	45.463	55.087	65.620	77.063
17	28.110	35.691	44.156	53.504	63.737	74.855
18	27.299	34.659	42.880	51.960	61.900	72.701
19	26.508	33.655	41.637	50.457	60.112	70.604
20	25.740	32.681	40.434	49.000	58.380	68.572
21	25.002	31.743	39.276	47.598	56.712	66.616
22	24.296	30.849	38.170	46.260	55.119	64.747
23	23.631	30.004	37.126	44.997	53.616	62.983
24	23.013	29.221	36.158	43.824	52.220	61.344
25	22.453	28.511	35.280	42.761	50.954	59.859
26	21.964	27.890	34.512	41.831	49.847	58.560
27	21.559	27.376	33.877	41.062	48.932	57.485
28	21.254	26.990	33.399	40.484	48.243	56.676
29	21.065	26.749	33.101	40.123	47.813	56.172
30	21.000	26.667	33.000	40.000	47.667	56.000

TABLE II

Energy ratios E(n+)/E(2+) of the " γ - band " of axially asymmetric even-even nuclei. γ is given in degrees

γ	E(2'+)/E(2+)	E(3+)/E(2+)	E(4'+)/E(2+)	E(4"+)/E(2+)	E(5+)/E(2+)	E(5'+)/E(2+)	E(6'+)/E(2+)
0							
3	181.878	E(2'+)/E(2+) + 1	184.211	726.844	185.878	728.510	187.878
4	102.091		104.425	407.697	106.091	409.364	108.092
5	65.162		67.496	259.982	69.162	261.649	71.166
6	45.103		47.438	179.743	49.103	181.410	51.110
7	33.009		35.345	131.368	37.009	133.036	39.023
8	25.161		27.500	99.977	29.161	101.645	31.186
9	19.783		22.125	78.462	23.783	80.131	25.822
10	15.937		18.285	63.079	19.937	64.749	21.998
11	13.094		15.448	51.704	17.094	53.376	19.185
12	10.933		13.297	43.060	14.933	44.734	17.065
13	9.2543		11.631	36.340	13.254	38.017	15.438
14	7.9244		10.317	31.016	11.924	32.698	14.176
15	6.8541		9.2683	26.729	10.854	28.416	13.190
16	5.9811		8.4223	23.230	9.9811	24.924	12.420
17	5.2608		7.7358	20.340	9.2608	22.043	11.820
18	4.6608		7.1778	17.929	8.6608	19.643	11.359
19	4.1572		6.7253	15.900	8.1572	17.629	11.010
20	3.7320		6.3615	14.181	7.7320	15.928	10.751
21	3.3717		6.0735	12.717	7.3717	14.487	10.565
22	3.0659		5.8515	11.464	7.0659	13.263	10.437
23	2.8068		5.6879	10.391	6.8068	12.227	10.353
24	2.5888		5.5765	9.4725	6.5888	11.355	10.298
25	2.4078		5.5128	8.6899	6.4078	10.631	10.257
26	2.2610		5.4933	8.0305	6.2610	10.044	10.212
27	2.1472		5.5141	7.4874	6.1472	9.5886	10.151
28	2.0656		5.5677	7.0625	6.0656	9.2623	10.080
29	2.0164		5.6335	6.7741	6.0164	9.0657	10.022
30	2.0000		5.6667	6.6667	6.0000	9.0000	10.000

γ	E(6"+)/E(2+)	E(6'''+)/E(2+)	E(7+)/E(2+)	E(7'+)/E(2+)	E(8'+)/E(2+)	E(9+)/E(2+)	E(10'+)/E(2+)
0							
3	730.517	1634.898	190.211	732.844	192.878	195.878	199.211
4	411.364	916.819	110.424	413.697	113.095	116.090	119.433
5	263.649	584.459	73.495	265.983	76.173	79.160	82.521
6	183.411	403.922	53.435	185.745	56.124	59.099	62.485
7	135.037	295.078	41.341	137.372	44.049	47.002	50.433
8	103.648	224.449	33.492	105.983	36.230	39.150	42.652
9	82.134	176.039	28.111	84.472	30.894	33.764	37.370
10	66.753	141.426	24.263	69.094	27.110	29.908	33.659
11	55.383	115.832	21.416	57.726	24.349	27.050	30.995
12	46.744	96.382	19.251	49.092	22.298	24.870	29.061
13	40.032	81.261	17.566	42.386	20.758	23.164	27.655
14	34.719	69.281	16.227	37.080	19.597	21.800	26.635
15	30.445	59.635	15.146	32.816	18.724	20.685	25.899
16	26.963	51.760	14.259	29.347	18.073	19.756	25.366
17	24.095	45.254	13.521	26.494	17.593	18.966	24.974
18	21.711	39.826	12.898	24.131	17.240	18.280	24.667
19	19.718	35.257	12.367	22.162	16.980	17.671	24.398
20	18.045	31.383	11.908	20.517	16.784	17.122	24.120
21	16.642	28.081	11.507	19.144	16.623	16.618	23.794
22	15.469	25.253	11.152	18.005	16.469	16.151	23.398
23	14.502	22.827	10.836	17.069	16.295	15.717	22.942
24	13.729	20.744	10.555	16.313	16.084	15.315	22.458
25	13.150	18.960	10.306	15.723	15.838	14.951	21.982
26	12.771	17.444	10.090	15.281	15.582	14.632	21.549
27	12.605	16.172	9.9129	14.976	15.347	14.367	21.182
28	12.642	15.136	9.7790	14.788	15.160	14.167	20.902
29	12.837	14.355	9.6952	14.694	15.041	14.042	20.727
30	13.000	14.000	9.6667	14.667	15.000	14.000	20.667

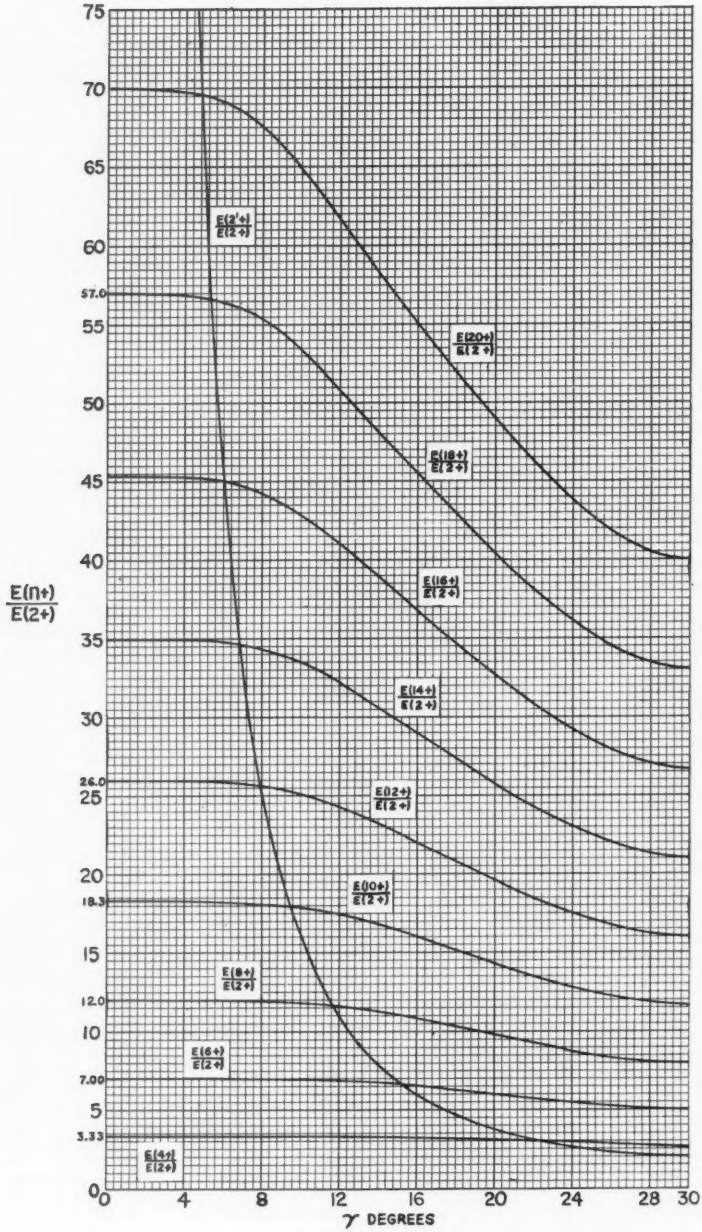

FIG. 1. Energy ratios.

and give appropriate values for the vibration–rotation constants B and C. The nucleus Th^{232} has a second known state of character $2+$ with energy $E(2'+) = 790$ kev (McGowan and Stelson 1957). The parameter γ may then be given as 10.0° by the usual Davydov–Filippov method of establishing γ by the ratio $E(2'+)/E(2+)$, and the observed levels matched within a few per cent. With this value of γ, corrections of the above type are still necessary for closer agreement with experiment, but the constants B and C are about one-half the values required by Stephens *et al.*

It may be significant that for Th^{232} and U^{238}, values of γ may be obtained from any two observed members of the "ground state band" such that the remaining levels of this band may be found within the experimental accuracy, without assuming any corrections. DeMille *et al.* (1959) have shown that this is true for many deformed nuclei. The values of γ so obtained are commonly a few degrees larger than those given by the ratio $E(2'+)/E(2+)$.

ACKNOWLEDGMENTS

The authors express their thanks to the National Research Council for scholarships held during the course of this work. Thanks are also extended to Mr. W. D. Thorpe, Technical Supervisor of the Computing Center, McGill University, for assistance with the computing program.

REFERENCES

BOHR, A. 1952. Kgl. Danske Videnskab. Selskab, Mat.-fys. Medd. **28**, No. 14.
DAVYDOV, A. S. and FILIPPOV, G. F. 1958. Nuclear Phys. **8**, 237.
DAVYDOV, A. S. and ROSTOVSKY, V. S. 1959. Nuclear Phys. **12**, 58.
DEMILLE, G. R., KAVANAGH, T. M., MOORE, R. B., WEAVER, R. S., and WHITE, W. 1959. Can. J. Phys. **37**, 1036.
GOLDEN, S. 1948. J. Chem. Phys. **16**, 78.
KING, G. W., HAINER, R. M., and CROSS, P. C. 1943. J. Chem. Phys. **11**, 27.
MCGOWAN, F. K. and STELSON, P. H. 1957. Bull. Am. Phys. Soc. **2**, 207.
STEPHENS, F. S., JR., DIAMOND, R. M., and PERLMAN, I. 1959. Phys. Rev. Letters, **3**, 435.

CENTRAL THREE-BODY FORCES IN HEAVY NUCLEI[1]

ROBERT C. SMITH[2] AND ROBERT T. SHARP

ABSTRACT

Three-nucleon potentials are calculated using the renormalized, static theory of Chew and Low. These potentials are used to evaluate the three-body contribution to the total energy per nucleon in nuclear matter as a function of nuclear density. It is found that while the three-body energy is greater than that predicted by unrenormalized theories by about one order of magnitude as a result of multiple-scattering effects, its dependence on the nuclear density in the region of the equilibrium density is very weak. Three-body forces are therefore not expected to change the saturation properties of nuclear matter as predicted by a hard core potential to any appreciable extent.

I. INTRODUCTION

Three-body forces have been of interest in nuclear physics for a considerable time (Janossy 1939; Primakoff and Holstein 1939; Drell and Huang 1953; Brueckner, Levinson, and Mahmoud 1954; Fujita and Miyazawa 1957). At first it was believed that many-body forces might be needed to account for the saturation of nuclear densities. More recently it has been shown, however, that the inclusion of a phenomenological infinite repulsive core in the two-body potential is sufficient to produce an equilibrium nuclear density which is in reasonable agreement with experiment (see, for example, Gomes, Walecka, and Weisskopf (1958)). However, it is still of interest to know if three-body forces are important, and if so, whether agreement with experiment is improved by taking them into account.

Two-body nuclear forces calculated with an unrenormalized, pseudoscalar meson theory and fixed, extended sources were studied extensively by Brueckner and Watson (1953). The three-body force obtained from this theory was calculated by Brueckner, Levinson, and Mahmoud (1954). In the non-relativistic approximation, where the effects of nucleon–antinucleon pair formation are small, the three-body forces are found to be negligible; in fact, using the approximation methods of Drell and Huang (1953) (which involve the neglect of Coulomb, nuclear surface, and core correlation effects) to evaluate the expectation value of the potential, they are found to produce only about 0.1 Mev of repulsion per particle.

That these estimates of the three-body energy are not reliable was pointed out by Chew (1954) and Klein (1957). The reason is that processes which involve the exchange of two or more pions are enhanced by multiple scattering; a resonance will occur when the energy of one of the virtual mesons present in the intermediate state is equal to the energy of the exchanged meson. This is the so-called (3,3) resonance—the resonance which occurs in the pion–nucleon "scattering" channel with total spin 3/2 and total isotopic spin 3/2. As Klein pointed out, the actual scattering in this channel is greater than the

[1]Manuscript received May 18, 1960.
Contribution from the Department of Mathematics, McGill University, Montreal, Que.
[2]Present address: Department of Physics, University of Ottawa, Ottawa, Ont.

Born approximation by a factor of 2 or more. It therefore seems likely that the three-body energy per nucleon in nuclear matter, with multiple scattering taken into account, will be appreciably greater than that predicted by an unrenormalized theory (i.e., when multiple scattering is neglected). Thus, a calculation of the three-body energy per nucleon using the renormalized, static theory of Chew (1954), and Chew and Low (1956), which takes these multiple-scattering effects into account, appears to be justified.

II. CALCULATION OF THE POTENTIAL

In order to calculate the three-body potential in lowest order (two pions exchanged), the following Chew–Low type Hamiltonian is chosen:

$$(1)\quad H = (H_M^1+\mathfrak{H}_1)+(H_M^2+\mathfrak{H}_2)+(H_M^3+\mathfrak{H}_3)+(\mathfrak{H}_2^1+\mathfrak{H}_3^2+\mathfrak{H}_1^3+\mathfrak{H}_3^1+\mathfrak{H}_1^2+\mathfrak{H}_2^3)$$
$$(2)\quad = H_0+\mathfrak{H}.$$

This is a natural extension of the Hamiltonian used by Sharp (1958) for the two-nucleon potential to the problem of three nucleons. The first six terms in (1), which are taken as the unperturbed Hamiltonian, comprise the Hamiltonians for three independent pion fields coupled to nucleons 1, 2, and 3, respectively; for example, H_M^1 is the energy of the pions associated with nucleon 1, and $\mathfrak{H}_1$ couples these pions to nucleon 1. The final six terms in (1) give the interactions between the three nucleons; that is, $\mathfrak{H}_2^1$ allows nucleon 2 to absorb a pion which has been emitted by nucleon 1, and so on. These terms are treated as a perturbation. By this means, the "renormalization effects" of the nucleons are treated exactly because they are contained in the unperturbed Hamiltonian, and only the interaction between nucleons is treated as a perturbation. The nucleon energies do not appear because, in the static approximation, the zero of energy can be chosen as the nucleon rest energy.

The interaction Hamiltonians are defined by the following expressions ($\hbar = c = 1$):

$$(3)\quad \mathfrak{H}_2^1 = f\sum_p V_p^2 a_p^1$$

$$(4)\quad V_p^2 = \frac{iN}{\mu} P_i \sqrt{\frac{2\pi}{\omega_p}}\, p\, v(p)(\sigma\tau)_{i\lambda}^2 e^{i\mathbf{p}\cdot\mathbf{r}_2}$$

where $\mathbf{p}$ is the momentum of the pion and λ is its charge state, N is a normalization factor, $P_i = p_i/p$ is a component of the unit vector in the direction of $\mathbf{p}$, $\omega_p = (p^2+\mu^2)^{\frac{1}{2}}$ is the energy of the pion, and $v(p)$ is the momentum cutoff factor which gives rise to extended nucleon sources for the pions. f is the unrenormalized coupling constant, and a_p is the annihilation operator for a pion of type p, λ. σ_i^2 and τ_λ^2 are the spin and isotopic spin operators respectively for nucleon 2.

The unperturbed, Hermitean part of the Hamiltonian gives a complete set of orthonormal eigenstates $|n_1, n_2, n_3\rangle$, where $|n_1\rangle$ is an eigenstate of $H_M^1+\mathfrak{H}_1$, and so on. The unperturbed ground state is $|\ ,\ ,\ \rangle$; this represents three "real" nucleons, and no free pions. (As used here, a "free" pion is one which is exchanged between nucleons.)

The potential due to the exchange of two mesons is now given directly by conventional second-order perturbation theory:

$$V = -\sum{}' \frac{\langle\, ,\, ,\, |\mathfrak{H}|n_1, n_2, n_3\rangle\langle n_1, n_2, n_3|\mathfrak{H}|\, ,\, ,\rangle}{E_{n_1}+E_{n_2}+E_{n_3}} \tag{5}$$

where $\mathfrak{H}$ is defined in (2). The exchange of one meson does not contribute to the three-body force, and processes involving the exchange of more than two mesons will be neglected in this calculation. The prime on the sum indicates that at least one of n_1, n_2, n_3 must be a state with one or more pions present; that is, the unperturbed state $|\, ,\, ,\rangle$ must not be included.

In order to simplify the calculations, we choose nucleon 1 as that with two vertices, and sum over all permutations of the three nucleons after the potential has been calculated.

We now invoke the one-meson approximation of Chew and Low (1956). Thus, we retain in our potential only those intermediate states $|n_1, n_2, n_3\rangle$ in which one of n_1, n_2, and n_3 is a one-meson state, and the others are real nucleon states. There are four essentially different Feynman diagrams which contribute to our potential, plus a number of others obtained by permuting the three nucleons; the basic diagrams are shown in Fig. 1. The term in the perturba-

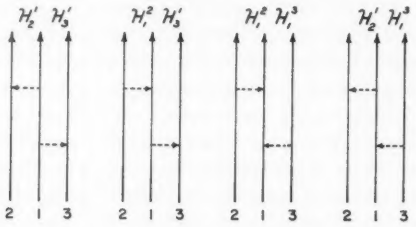

FIG. 1. Diagrams of the various processes contributing to the three-body potential. The terms in the Hamiltonian causing the absorption of the mesons are written above. All other diagrams obtained by permuting the three nucleons must also be included.

tion Hamiltonian which causes the absorption of the pion is written above the pertinent pion line (its emission is accomplished by the unperturbed Hamiltonian). The three-body potential can now be written down by inspection; it is

$$\begin{aligned} V = &-\sum_{pqs} \frac{\langle|a_q^1|s\rangle\langle s|a_p^1|\rangle\langle|fV_q^2|\rangle\langle|fV_p^3|\rangle}{\omega_s} \\ &-\sum_{pqs} \frac{\langle|fV_q^1|s\rangle\langle s|a_p^1|\rangle\langle|a_q^2|\rangle\langle|fV_p^3|\rangle}{\omega_s} \\ &-\sum_{pqs} \frac{\langle|fV_q^1|s\rangle\langle s|fV_p^1|\rangle\langle|a_q^2|\rangle\langle|a_p^3|\rangle}{\omega_s} \\ &-\sum_{pqs} \frac{\langle|a_q^1|s\rangle\langle s|fV_p^1|\rangle\langle|fV_q^2|\rangle\langle|a_p^3|\rangle}{\omega_s} \end{aligned} \tag{6}$$

plus all terms obtained by permuting the three nucleons. $|s\rangle$ is a one-meson state of nucleon 1 with momentum s, and the perturbation Hamiltonian has been written using equation (3).

In order to evaluate this expression for the potential, we use the following relationships for the matrix elements. They are rearrangements of equations (2.15), (5.32), (5.35), (5.37), (6.6), and (6.13), in the article by Wick (1955).

$$\langle |fV_p| \rangle = f_r V_p$$

$$\langle |a_p| \rangle = -f_r \frac{V_p^*}{\omega_p}$$

$$\langle s|a_p| \rangle = -\frac{\langle s|fV_p^*| \rangle}{\omega_p + \omega_s}$$

$$\langle |a_p|s \rangle = \delta_{ps} - \frac{\langle |fV_p^*|s \rangle}{\omega_p^* - \omega_s}$$

$$\langle q|fV_p| \rangle = \frac{6\pi N^2 pv(p)v(q)Q_j P_t}{q^2(\omega_p \omega_q)^{\frac{1}{2}}} g_u(\omega_q)(\Lambda_u)_{j\mu,\,t\lambda} e^{i(\mathbf{p}-\mathbf{q})\cdot\mathbf{r}}$$

where f_r is the renormalized coupling constant, $g_u(\omega)$ is the solution of the Low equation, and $(\Lambda_u)_{j\mu,\,t\lambda}$ is a charge–spin operator defined by Wick in his equation (6.12). Sums are understood over all repeated indices, and over all q. When the sums over momenta are replaced by integrals,

$$N^2 \sum_q \rightarrow \frac{1}{(2\pi)^3} \int_0^\infty q^2 dq \int d\Omega_q$$

the integrations over angles can be performed as follows:

$$\int d\Omega_s \langle |fV_q^*|s \rangle \langle s|fV_p| \rangle = \frac{48\pi^3 N^4 pv(p)qv(q)v^2(s)Q_j P_t |g_u(\omega_s)|^2}{s^4(\omega_p \omega_q)^{\frac{1}{2}}\omega_s} (\Lambda_{ju})_{\mu,\,t\lambda} e^{i(\mathbf{p}-\mathbf{q})\cdot\mathbf{r}}$$

$$\int d\Omega_p P_i P_j e^{i\mathbf{p}\cdot\mathbf{r}} = 4\pi\psi(pr)\delta_{ij} + 4\pi\phi(pr)R_i R_j$$

where

$$\psi(x) = \tfrac{1}{2}f(x) + \tfrac{1}{2}f''(x)$$

$$\phi(x) = -\tfrac{1}{2}f(x) - \tfrac{3}{2}f''(x)$$

and

$$f(x) = \frac{\sin x}{x}.$$

These results are applied to the potential of equation (6), resulting in the following expression:

$$\begin{aligned}
V(r_2, r_3) = & -\frac{3}{\pi^2}\left(\frac{f_r}{\mu}\right)^2 \int\int dpdq \frac{p^4 qv^2(p)v^2(q)}{\omega_p \omega_q^2(\omega_p + \omega_q)} g_u(\omega_q)\Psi^x(qr_3, pr_2)\xi_u^x \\
& -\frac{3}{\pi^2}\left(\frac{f_r}{\mu}\right)^2 \int\int dpdq \frac{p^4 qv^2(p)v^2(q)}{\omega_p^2 \omega_q^2} g_u(\omega_q)\Psi^x(qr_3, pr_2)\xi_u^x \\
& -\frac{3}{\pi^3}\left(\frac{f_r}{\mu}\right)^2 \int\int\int dpdqd\omega_s \frac{p^4 q^4 v^2(p)v^2(q)v^2(s)}{s^3\omega_s \omega_p \omega_q^2(\omega_p + \omega_s)} |g_u(\omega_s)|^2 \Psi^x(qr_3, pr_2)\xi_u^x \\
(7) \qquad & -\frac{3}{\pi^3}\left(\frac{f_r}{\mu}\right)^2 \int\int\int dpdqd\omega_s \frac{p^4 q^4 v^2(p)v^2(q)v^2(s)}{s^3\omega_s \omega_p^2 \omega_q^2} |g_u(\omega_s)|^2 \Psi^x(qr_3, pr_2)\xi_u^x \\
& -\frac{3}{\pi^3}\left(\frac{f_r}{\mu}\right)^2 \int\int\int dpdqd\omega_s \frac{p^4 q^4 v^2(p)v^2(q)v^2(s)}{s^3\omega_s \omega_p \omega_q(\omega_q^* - \omega_s)(\omega_p + \omega_s)} \\
& \qquad\qquad |g_u(\omega_s)|^2 \Psi^x(qr_3, pr_2)\xi_u^x \\
& -\frac{3}{\pi^3}\left(\frac{f_r}{\mu}\right)^2 \int\int\int dpdqd\omega_s \frac{p^4 q^4 v^2(p)v^2(q)v^2(s)}{s^3\omega_s \omega_p^2 \omega_q(\omega_q^* - \omega_s)} |g_u(\omega_s)|^2 \Psi^x(qr_3, pr_2)\xi_u^x
\end{aligned}$$

where

$$\Psi^1(x, y) = \psi(x)\,\psi(y)$$

$$\Psi^2(x, y) = \psi(x)\,\phi(y)$$

$$\Psi^3(x, y) = \phi(x)\,\psi(y)$$

$$\Psi^4(x, y) = \phi(x)\,\phi(y)$$

and

$$\xi_u^1 = (\Lambda_u^1)_{j\mu,\,i\lambda}(\sigma\tau)_{i\mu}^2(\sigma\tau)_{k\lambda}^3\delta_{jl}\delta_{ik}$$

$$\xi_u^2 = (\Lambda_u^1)_{j\mu,\,i\lambda}(\sigma\tau)_{i\mu}^2(\sigma\tau)_{k\lambda}^3\delta_{jl}R_i^2R_k^2$$

$$\xi_u^3 = (\Lambda_u^1)_{j\mu,\,i\lambda}(\sigma\tau)_{i\mu}^2(\sigma\tau)_{k\lambda}^3R_j^3R_l^3\delta_{ik}$$

$$\xi_u^4 = (\Lambda_u^1)_{j\mu,\,i\lambda}(\sigma\tau)_{i\mu}^2(\sigma\tau)_{k\lambda}^3R_j^3R_l^3R_i^2R_k^2.$$

In the factors in parentheses, the Latin indices refer to spin, the Greek to isotopic spin; as before, sums are understood over all repeated indices. The unit vectors **R** are now relative co-ordinates defined by

$$\mathbf{R}^2 = \mathbf{r}_1 - \mathbf{r}_3/|\mathbf{r}_1 - \mathbf{r}_3|\,.$$

We now make use of the effective range approximation of Chew, Goldberger, Low, and Nambu (1957). This amounts to the assumption that the (3,3) resonance dominates the scattering picture, so that in the sum over u in the above equations, only $u = 3$ contributes significantly. The potential can be simplified by the use of the integral equation of Low, which is, for $u = 3$

$$g_3(\omega_q) = \frac{4f_r^2q^3}{3\mu^2\omega_q} + \frac{q^3}{\pi}\int\frac{v^2(s)d\omega_s}{s^3}\left[\frac{|g_3(\omega_s)|^2}{\omega_s-\omega_q} + \frac{A_{3s}|g_s(\omega_s)|^2}{\omega_s+\omega_q}\right] \tag{8}$$

where A_{3s} is defined by Wick (1955). The second, or "crossing", term under the integral is small because $|g_1(\omega_s)|^2$ and $|g_2(\omega_s)|^2$ contain no resonances, and A_{33} is small; also, the energy denominator is large, so that this term can be neglected. In the limit of large q, the Low equation becomes

$$\frac{v^2(s)|g_3(\omega_s)|^2}{s^3} = \frac{4\pi f_r^2}{3\mu^2}\delta(\omega_s-\omega_r) \tag{8a}$$

where $\omega_r \simeq 2\mu$ is the resonance energy (see Chew, Goldberger, Low, and Nambu 1957).

In order to simplify the potential, the Low equation in the form of equation (8) (with the crossing term omitted) is substituted into the first two terms of equation (7). It is found that the resonant energy denominators in the fifth and sixth terms of (7) are just cancelled by similar parts of the first two terms. Upon application of (8*a*) to the resulting expressions, the potential is found to assume the form

$$V(r_2, r_3) = -\frac{8}{\pi^2}\left(\frac{f_r}{\mu}\right)^4\frac{1}{\omega_r}\int\int dpdqp^4v^2(p)q^4v^2(q)$$
$$\left[\frac{1}{\omega_p(\omega_p+\omega_r)\omega_q^2} + \frac{1}{\omega_p^2\omega_q^2}\right]\left[1+\frac{\omega_r}{2\omega_q}\right]\Psi^r(qr_3, pr_2)\xi_3^r$$

where ω_r has been neglected in comparison to $\omega_p+\omega_q$.

Tensor forces are not expected to produce any appreciable effect in heavy nuclei, because adjacent low-lying states which might have been admixed are already occupied. In fact, in the purely two-body problem which concerned them, Gomes, Walecka, and Weisskopf (1958) found that the neglect of tensor forces underestimates the binding energy by roughly 12 to 15% of the potential energy; for our purposes, this is quite negligible. We therefore average over the angular dependence of the potential, which is contained in the factors ξ_3^x, by replacing R_iR_j by $\frac{1}{3}\delta_{ij}$. Thus:

$$\xi_3^2 = \xi_3^3 = \tfrac{1}{3}\xi_3^1; \qquad \xi_3^4 = \tfrac{1}{9}\xi_3^1$$

$$\xi_3^1 = (\Lambda_3^1)_{j\mu,i\lambda}(\sigma\tau)_{j\mu}^2(\sigma\tau)_{i\lambda}^3 \tag{9}$$

$$= \tfrac{4}{9}(\mathfrak{d}^2\cdot\mathfrak{d}^3)(\tau^2\cdot\tau^3) - \tfrac{1}{9}(\mathfrak{d}^1\cdot\mathfrak{d}^2\times\mathfrak{d}^3)(\tau^1\cdot\tau^2\times\tau^3)$$

plus imaginary terms which are completely antisymmetric on exchange of particles 2 and 3, and so vanish when all possible nucleon permutations are taken into account.

The potential is therefore

$$V(r_2, r_3) = -0.3621\xi_3^1 \int\int dxdyx^4v^2(\mu x)y^4v^2(\mu y)$$

$$\left[\frac{1}{\sqrt{x^2+1}(\sqrt{x^2+1}+2)(y^2+1)} + \frac{1}{(x^2+1)(y^2+1)}\right]\left[1+\frac{1}{\sqrt{y^2+1}}\right] \tag{10}$$

$$\left[\psi(\mu r_3x)\psi(\mu r_2y) + \tfrac{1}{3}\psi(\mu r_3x)\phi(\mu r_2y) + \tfrac{1}{3}\phi(\mu r_3x)\psi(\mu r_2y) + \tfrac{1}{9}\phi(\mu r_3x)\phi(\mu r_2y)\right]$$

in Mev. A Gaussian form of cutoff was chosen, and these integrals were performed numerically.

III. THREE-NUCLEON CHARGE-SPIN STATES

There are various prescriptions for writing down states describing the 64 different ways in which the spins and isotopic spins of three interacting nucleons can combine (see, for example, Verde (1957) and Sachs (1953)). We propose a new representation, using spin states which are eigenfunctions of the total spin S, the Z component of spin S_Z, and the operator $\mathfrak{d}^1\cdot\mathfrak{d}^2\times\mathfrak{d}^3$, and isotopic spin states which are eigenfunctions of the analogous isotopic spin operators. This representation has the advantage of simplicity when used with the Hamiltonian of equation (1), as well as the fact that the states are eigenfunctions of the cyclic three-body exchange operator.

The spin states are

$$\chi^{0}_{\frac{3}{2},\frac{3}{2}} = \alpha^1\alpha^2\alpha^3$$

$$\chi^{0}_{\frac{3}{2},\frac{1}{2}} = \frac{1}{\sqrt{3}}(\alpha^1\alpha^2\beta^3+\alpha^1\beta^2\alpha^3+\beta^1\alpha^2\alpha^3)$$

$$\chi^{0}_{\frac{3}{2},-\frac{1}{2}} = \frac{1}{\sqrt{3}}(\beta^1\beta^2\alpha^3+\beta^1\alpha^2\beta^3+\alpha^1\beta^2\beta^3)$$

$$\chi^{0}_{\frac{3}{2},-\frac{3}{2}} = \beta^1\beta^2\beta^3$$

$$\chi^{+}_{\frac{1}{2},\frac{1}{2}} = \frac{1}{\sqrt{3}}(\alpha^1\alpha^2\beta^3+\omega^2\alpha^1\beta^2\alpha^3+\omega\beta^1\alpha^2\alpha^3)$$

$$\chi^{+}_{\frac{1}{2},-\frac{1}{2}} = \frac{1}{\sqrt{3}}(\beta^1\beta^2\alpha^3+\omega^2\beta^1\alpha^2\beta^3+\omega\alpha^1\beta^2\beta^3)$$

$$\chi^{-}_{\frac{1}{2},\frac{1}{2}} = \frac{1}{\sqrt{3}}(\alpha^1\alpha^2\beta^2+\omega\alpha^1\beta^2\alpha^3+\omega^2\beta^1\alpha^2\alpha^3)$$

$$\chi^{-}_{\frac{1}{2},-\frac{1}{2}} = \frac{1}{\sqrt{3}}(\beta^1\beta^2\alpha^3+\omega\beta^1\alpha^2\beta^3+\omega^2\alpha^1\beta^2\beta^3)$$

where ω and ω^2 are cube roots of unity. The subscripts are S and S_Z respectively; the superscript 0 indicates the fact that the eigenvalue of $\boldsymbol{\sigma}^1\cdot\boldsymbol{\sigma}^2\times\boldsymbol{\sigma}^3$ when operating on the $S = 3/2$ state vectors is zero, while $\pm$ indicates that its eigenvalues when operating on the $S = 1/2$ state vectors are $\pm 2\sqrt{3}$. The isotopic spin states, which are derived in an analogous manner, will be labelled similarly; we denote these states by ζ's. There is therefore a total of 64 charge–spin states, obtained by combining the charge states and spin states in all possible ways. We choose the following combinations:

(1) $$\frac{1}{\sqrt{2}}\left[\chi^{-}_{\frac{1}{2},S_z}\zeta^{+}_{\frac{1}{2},T_z}-\chi^{+}_{\frac{1}{2},S_z}\zeta^{-}_{\frac{1}{2},T_z}\right] \quad (4)$$

(2) $$\frac{1}{\sqrt{2}}\left[\chi^{-}_{\frac{1}{2},S_z}\zeta^{+}_{\frac{1}{2},T_z}+\chi^{+}_{\frac{1}{2},S_z}\zeta^{-}_{\frac{1}{2},T_z}\right] \quad (4)$$

(3) $$\chi^{0}_{\frac{3}{2},S_z}\zeta^{0}_{\frac{3}{2},T_z} \quad (16)$$

(4) $$\chi^{\pm}_{\frac{1}{2},S_z}\zeta^{0}_{\frac{3}{2},T_z}\ ; \qquad \chi^{0}_{\frac{3}{2},S_z}\zeta^{\pm}_{\frac{1}{2}} \quad (32)$$

(5) $$\chi^{\pm}_{\frac{1}{2},S_z}\zeta^{\pm}_{\frac{1}{2},T_z} \quad (8)$$

The states labelled (1) are completely antisymmetric upon interchange of any two particles, while those labelled (2) and (3) are completely symmetric. Those labelled (4) and (5) are states of mixed symmetry. The number of such states is shown in parentheses at the right; these numbers are measures of the statistical weights of the corresponding states.

The expectation value of the potential operator in these various states must now be evaluated. Since all of the spin – isotopic spin dependence of the potential is contained in the factor ξ_3^1 of equation (9), it will be sufficient simply to take matrix elements of this operator. These are shown in Table I.

TABLE I

Matrix elements of charge–spin operators

State	Symmetry	$(\sigma^2\cdot\sigma^3)(\tau^2\cdot\tau^3)$	$(\sigma^1\cdot\sigma^2\times\ ^3)(\tau^1\cdot\tau^2\times\tau^3)$	ξ_3^1
1	Antisymmetric	−3	−12	0
2	Symmetric	+5	−12	32/9
3	Symmetric	+1	0	4/9
4	Mixed	−1	0	−4/9
5	Mixed	+1	12	−8/9

The entry in the column labelled $(\sigma^2\cdot\sigma^3)(\tau^2\cdot\tau^3)$ is in reality

$$\tfrac{1}{3}[(\sigma^1\cdot\sigma^2)(\tau^1\cdot\tau^2)+(\sigma^2\cdot\sigma^3)(\tau^2\cdot\tau^3)+(\sigma^3\cdot\sigma^1)(\tau^3\cdot\tau^1)].$$

Thus, ξ_3^1 can be diagonalized simultaneously with the Hamiltonian.

The three-body force, because of its short range, should be strongest in symmetric spatial states, that is, in antisymmetric charge–spin states. But it is seen from Table I that the expectation value of ξ_3^1 in the antisymmetric charge–spin states vanishes, so that what might be expected to be the dominant three-body force is in fact zero. We must therefore consider contributions from charge–spin states which are not completely antisymmetric upon exchange of any two nucleons.

IV. THE SPATIAL WAVE FUNCTION

Besides the spatial states which are symmetric on interchange of any pair of nucleons, which have been found not to contribute to the three-body force due to the vanishing of the charge–spin matrix element associated with them, there exist spatial wave functions which are antisymmetric on interchange of any pair of particles, and wave functions of mixed symmetry. The antisymmetric spatial states will not contribute significantly to the three-body force because, roughly speaking, the antisymmetry of the wave function keeps the nucleons outside the range of the three-body force. This can be demonstrated by constructing a function which expresses the correlations imposed by the exclusion principle; the correlation function is derived in a manner which is analogous to that of Wigner and Seitz (1933) for two-body correlations due to the exclusion principle.

The spatial wave function is chosen to be

$$\psi = (1/\sqrt{6})\,\epsilon_{lmn}\,e^{i(\mathbf{k}_1\cdot\mathbf{r}_l+\mathbf{k}_2\cdot\mathbf{r}_m+\mathbf{k}_3\cdot\mathbf{r}_n)}$$

where ϵ_{lmn} is the Levi-Civita tensor density. The one-particle wave functions are chosen to be plane waves because no real scattering can take place in nuclear matter; all adjacent states are occupied. By averaging $|\psi|^2$ over all momenta from zero to the Fermi momentum k_F, one obtains the correlation function

$$P(r) = 1+2\prod_{i=1}^{3} f(r_i) - \sum_{i=1}^{3} f(r_i)$$

where

$$f(r_i) = \frac{3(\sin k_F r_i - k_F r_i \cos k_F r_i)}{(k_F r_i)^3}.$$

This function is shown graphically in Fig. 2 as a function of μr for various values of k_F, assuming two configurations: (i) the particles are equidistant

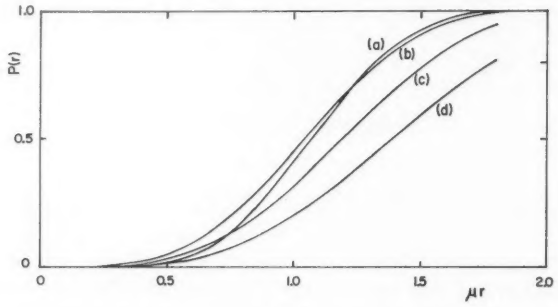

FIG. 2. The function which expresses correlations due to the exclusion principle in the antisymmetric spatial states plotted against μr. Curve (*a*): three colinear nucleons, $k_F = 1.69$ fermis^{-1}; curves (*b*), (*c*), and (*d*): three equidistant nucleons, $k_F = 1.69$, 1.48, and 1.27 fermis^{-1} respectively.

from each other ($r_1 = r_2 = r_3$), and (ii) the particles are colinear ($r_1 = 2r_2 = 2r_3$).

In the expression for the potential (equation (10)) it is found that the term with the longest range drops to half its maximum value at $r = 0.64\mu^{-1} = 0.9\times10^{-13}$ cm, at which point the correlation function $P(r)$ for $k_F = 1.69\times10^{13}$ cm^{-1} (the case when $P(r)$ is largest) is only 0.12, and rapidly becomes smaller at closer distances. There is therefore very little likelihood of the nucleons getting close enough together to be within the range of the three-body force. Thus, it is consistent with previous approximations to neglect the effect of antisymmetric spatial states.

It is seen therefore that the dominant three-body force arises in the spatial states of mixed symmetry. In order to calculate the binding energy due to this force, a function which takes into account the correlations induced in the wave function by the exclusion principle must again be calculated. Again using the methods of Wigner and Seitz (1933), the correlation function is found to be

$$P(r) = 1-\prod_{i=1}^{3} f(r_i)$$

where $f(r_i)$ has been defined previously. It is seen that this correlation function goes to zero only when all three of the r's vanish. Thus, the wave function vanishes only linearly at small distances instead of cubically, as was the case for a completely antisymmetric spatial wave function.

Account must also be taken of the correlation induced in the spatial wave function by the infinite repulsive core. High energy scattering data indicate the radius of this core to be $r_c = 0.4\times10^{-13}$ cm $= 0.283\mu^{-1}$. Since the potential is infinite inside the core, the wave function must vanish in this region. No real scattering is allowed in nuclear matter, however, due to the effect of the exclusion principle. Thus, there can be no permanent phase shift at large distances; the real wave function must approach the free-particle wave function asymptotically. The distance at which the difference between the real wave function and the free-particle wave function becomes small will be called the "healing distance" r_H, in accordance with the nomenclature of Gomes, Walecka, and Weisskopf (1958). This distance will be of order $\lambda_F = k_F^{-1}$.

In order to introduce this correlation, it will be sufficient for our purpose to multiply the previously calculated $|\psi|^2$ by a function which approaches unity asymptotically, but which is close to unity in a distance of order $r_H = k_F^{-1}$. We choose the function

$$K(r) = 0 \qquad r < r_c$$
$$= \left[1-\exp-\frac{r-r_c}{r_H-r_c}\right]^2 \qquad r > r_c$$

This function is plotted in Fig. 3 for various values of k_F.

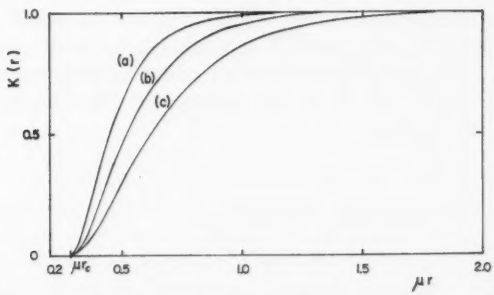

FIG. 3. The function which expresses correlations due to the infinite repulsive core plotted against μr. Curve (a): $k_F = 1.69$ fermis^{-1}; curve (b): $k_F = 1.48$ fermis^{-1}; curve (c): $k_F = 1.27$ fermis^{-1}.

The square of the spatial wave function is now

$$|\psi|^2 = [1-f(r_1)\,f(r_2)\,f(r_3)]\,K(r_1)\,K(r_2)\,K(r_3).$$

V. CALCULATION OF THE THREE-BODY BINDING ENERGY

In order to calculate the three-body contribution to the binding energy, the expectation value of the potential is evaluated in the previously specified three-body states of nuclear matter. Thus, the binding energy per particle is

$$\frac{E}{A} = \left(\frac{A}{\Omega}\right)^2 \int\int V(r_2, r_3)\,|\psi|^2 d\tau_2 d\tau_3 \quad . \tag{11}$$

The $V(r_2, r_3)$ which is used here is the potential energy before summing over all permutations of the three nucleons, as given in equation (10). The sum over all nucleon permutations is introduced by the factor $A(A-1)(A-2) \approx A^3$; one factor of A is then divided off to obtain the binding energy per particle. The factor of Ω^{-2}, where Ω is the nuclear volume, is used to normalize the one-particle wave functions to nuclear volume rather than to unit volume. Table II summarizes the results of this calculation.

TABLE II

Nuclear density relationships

k_F fermis^{-1}	ρ particles/fermi^3	r_0 fermis	E/A Mev per particle of repulsion
1.27	0.138	1.20	1.24
1.48	0.219	1.03	1.49
1.69	0.328	0.90	2.82

NOTE: $r_0 = RA^{-1/3}$, where R is the nuclear radius.

The binding energy is plotted as a function of k_F in Fig. 4, along with the total two-body energy per nucleon as calculated by Gomes, Walecka, and Weisskopf (1958) in the Born approximation to their "independent-pair model", and the sum of these two energies. Due to the weak dependence of the three-body energy on k_F in the region of the minimum in the two-body total energy curve, the equilibrium nuclear density is not changed to any appreciable extent. It can be concluded from this that the saturation of nuclear density is due principally to the hard core, since the three-body force (which is the strongest many-body force) has very little effect on the equilibrium density.

VI. CONCLUSIONS

The aim of the present work has been twofold: firstly, to construct a three-body potential using a Chew–Low coupling of static nucleons to the meson field; and secondly, using this potential, to calculate the effect of three-body forces on the saturation properties of nuclear matter, assuming a two-body potential with an infinite repulsive core. It has been found that the three-body force has a moderately short range, as would be expected from the fact that the process involves the exchange of two pions.

A new method of specifying the charge–spin states of three nucleons has been introduced. This representation has the advantage over previous schemes that the symmetry characteristics of the states are immediately apparent, as well as the fact that they are eigenstates of the Hamiltonian used in this calculation. Antisymmetric charge–spin states comprise 1/16th, symmetric states 5/16ths, and states of mixed symmetry the remaining 5/8ths of the total of 64 states.

It was shown that antisymmetric nuclear three-body spatial states could be neglected, because the antisymmetry of the spatial wave function keeps the nucleons outside the range of the three-body force. The contribution of

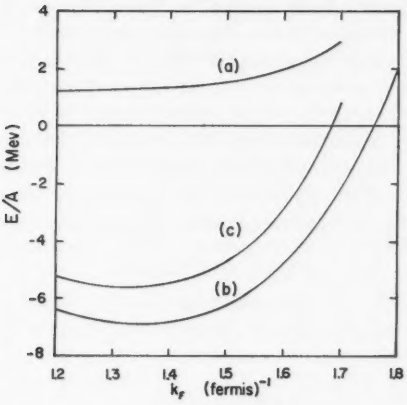

FIG. 4. The binding energy per nucleon as a function of the Fermi momentum k_F. Curve (a): three-body binding energy; curve (b): two-body binding energy calculated by Gomes, Walecka, and Weisskopf (1958); curve (c): the sum of these energies.

the symmetric spatial states, which might be expected to account for the dominant part of the binding, was found to be exactly zero, due to the fortuitous vanishing of the spin – isotopic spin matrix elements of the potential in these states. Thus, only the spatial states of mixed symmetry contribute significantly to the binding energy. In these states, the three-body force is repulsive, in agreement with unrenormalized calculations.

The belief that multiple-scattering effects, which give rise to the resonance in the (3,3) scattering channel, increase the magnitude of the three-body force is borne out by this calculation. The three-body repulsion obtained here is greater by about one order of magnitude than that obtained by Brueckner, Levinson, and Mahmoud (1954), who neglected all "renormalization effects" including multiple scattering.

Brueckner and Watson have suggested that iterated second-order terms, which appear implicitly in the potential obtained here, should not be included in the fourth order calculation. While agreement on this subject has not as yet been reached, it would be a simple matter to calculate the contributions of these processes to the potential by standard perturbation methods, and subtract them from the potential which has been calculated.

The three-body potential resulting from the exchange of three mesons cannot be calculated by present-day techniques. The difficulties arise in applying the one-meson approximation of Chew and Low to those terms whose diagrams have three vertices at one nucleon. One possible means of including these terms would be the use of experimental cross sections for multiple meson production in place of a more fundamental calculation of the nucleon – three-meson interaction.

While the neglect of angle-dependent forces seems reasonable, an investigation into their exact effect might prove fruitful, because the dependence of

these forces on the nuclear density may be quite different from that of the central forces. Since nuclear recoil has also been neglected, no velocity-dependent forces arise. It is by no means certain that these are not required; they may very well be important in both two- and three-body interactions.

It can be concluded that central three-body forces play a relatively small role in the saturation of nuclear densities, because the three-body binding energy per nucleon has little effect on the equilibrium nuclear density obtained from two-body forces. The repulsive core remains the dominant factor in explaining the saturation properties of nuclear binding energies.

ACKNOWLEDGMENTS

One of the authors (R. C. S.) is indebted to the National Research Council of Canada for the financial support given to this work in the form of three studentships.

REFERENCES

BRUECKNER, K. A., LEVINSON, C., and MAHMOUD, H. 1954. Phys. Rev. **95**, 217.
BRUECKNER, K. A. and WATSON, K. M. 1953. Phys. Rev. **90**, 699.
——— 1953. Phys. Rev. **92**, 1023.
CHEW, G. 1954. Phys. Rev. **94**, 1748, 1755.
——— 1954. Phys. Rev. **95**, 1669.
CHEW, G., GOLDBERGER, M., LOW, F., and NAMBU, Y. 1957. Phys. Rev. **106**, 1337.
CHEW, G. and LOW, F. 1956. Phys. Rev. **101**, 1570, 1579.
DRELL, S. D. and HUANG, K. 1953. Phys. Rev. **91**, 1527.
FUJITA, J. and MIYAZAWA, H. 1957. Progr. Theoret. Phys. **17**, 360.
GOMES, L. C., WALECKA, J. D., and WEISSKOPF, V. F. 1958. Ann. Phys. **3**, 241.
JANOSSY, L. 1939. Proc. Cambridge Phil. Soc. **35**, 616.
KLEIN, A. 1957. Proceedings of the Rochester High Energy Conference, IV, 41.
PRIMAKOFF, H. and HOLSTEIN, T. 1939. Phys. Rev. **55**, 1218.
SACHS, R. G. 1953. Nuclear theory (Addison-Wesley Publishing Co., Inc., Cambridge, Mass.).
SHARP, R. T. 1958. Nuovo Cimento, **9**, 23.
VERDE, M. 1957. Encyclopedia of Physics XXXIX, 144.
WICK, G. C. 1955. Revs. Modern Phys. **27**, 339.
WIGNER, E. P. and SEITZ, F. 1933. Phys. Rev. **43**, 804.

APPENDIX

The expression for the three-body binding energy (equation (11)) is an integral over the spaces of the vectors $\mathbf{r}_2$ and $\mathbf{r}_3$. It is complicated by the fact that in it appear correlation functions depending on the vector $\mathbf{r}_1$, which is related to $\mathbf{r}_2$ and $\mathbf{r}_3$ by

$$|\mathbf{r}_1| = (r_2^2+r_3^2-2r_2r_3\gamma)^{\frac{1}{2}} \tag{12}$$

where γ is the cosine of the angle between $\mathbf{r}_2$ and $\mathbf{r}_3$. The integrations over the two spaces are therefore not separable. It was accordingly decided to replace the r_2 and r_3 in equation (12) by effective values, in order to make the integrals separable. A different effective μr was calculated for each of the different products appearing in the expression for the binding energy, for each value of k_F, by calculating the expectation value of μr for the various terms in the potential.

When this is done, equation (11), which is of the form

$$E/A = \int\int F(r_1, r_2, r_3)\, d\tau_2\, d\tau_3$$

becomes

$$E/A = 8\pi^2 \int_{r_c}^{\infty} \int_{r_c}^{\infty} \int_{-1}^{1} G(r_2)G(r_3)Q(\gamma)r_2^2 dr_2 r_3^2 dr_3 d\gamma$$

where the functional dependence of $Q(\gamma)$ on r_2 and r_3 has been replaced by the effective values determined above, thereby making the integral separable.

The integrations over r_2 and r_3 extend from the core radius to infinity. However, the integration over γ from -1 to $+1$ does not prevent r_1 from becoming smaller than the core radius r_c. That this does not alter the value of the γ integration appreciably can be seen as follows. The core will make itself felt during a relatively small proportion of the time, because r_1 can become small only when r_2 and r_3 are approximately equal in magnitude. The worst case arises when both r_2 and r_3 are equal to the smallest effective distance calculated above; in this case, it is found that only 7.5% of the range of integration should be omitted if r_2 and r_3 are exactly equal in magnitude. This therefore represents an upper limit on the error.

The integrals themselves were performed on an I.B.M. 650 digital computer.

ON THE TEMPERATURE DEPENDENCE OF THE SHAPE OF PARAMAGNETIC RESONANCE LINES[1]

MALCOLM MCMILLAN[2] AND W. OPECHOWSKI

ABSTRACT

A theory of the temperature dependence of the shape of paramagnetic resonance lines is developed for temperatures sufficiently low to make the effects of the spin–lattice interaction and thermal expansion negligible. General expressions for the first and second moments of the line shape function as functions of the temperature are obtained, and the approximations used are discussed in detail. These expressions are applied to the case of effective spin $S = \frac{1}{2}$ and 1. As an illustration of the general theory numerical results are given for the paramagnetic resonance lines of nickel fluosilicate. In this case the moments become strongly temperature dependent below 10° K.

1. INTRODUCTION

At sufficiently low temperatures the effect of the variation of the temperature on the paramagnetic resonance absorption is mainly due to the temperature dependence of the average occupation numbers (as given by the Boltzmann factors) of the various energy levels of the absorbing system. The effects connected with lattice vibrations, the "spin–lattice relaxation" and thermal expansion, become small at these temperatures. In this paper we neglect them altogether and treat the lattice as perfectly rigid. In other words we regard the position and shape of a paramagnetic resonance line as determined solely by the nature of the paramagnetic unit systems ("spins") which constitute the paramagnetic crystal, and by the weak interactions of these unit systems ("spin–spin interactions"). On this assumption, we derive expressions which give the temperature dependence of the first and second moments of the absorption line for the case in which the "spin" is a paramagnetic ion subjected to an arbitrary crystalline electrostatic field, and to an external constant magnetic field.

The temperature dependence of the first two moments of a line has been considered by Pryce and Stevens (1950), and by Kambe and Usui (1952). Pryce and Stevens have derived some general approximate expressions containing Boltzmann factors but when specializing these expressions they have considered the temperature to be infinite. Kambe and Usui have set up quite general exact expressions for the moments, which we shall briefly rederive in Section 2 and use as the starting point of our calculations. However, Kambe and Usui have applied their general formulae only to the case in which no crystalline electrostatic field is present. From their results it is, however, quite clear that the well-known Van Vleck (1948) temperature-independent formulae for the moments could no longer be used to interpret experimental data on paramagnetic resonance lines at temperatures of the order of 10° K or lower, should such data of sufficient precision become available.

[1]Manuscript received May 17, 1960.
Contribution from the Department of Physics, University of British Columbia, Vancouver, B.C.

[2]Present address: Department of Mathematics, McGill University, Montreal, Que.

The results of the present paper can thus be regarded as a straightforward extension of the results of Pryce and Stevens, and Kambe and Usui. In fact, we use the methods of calculation developed by these authors, and we do not claim to have introduced any essentially new "tricks". However, we do discuss more explicitly than previous authors the meaning of various approximations, and especially of the temperature-independent approximation for the moments.

In the calculations which follow we assume that the amplitude of microwave radiation is very small. In other words, we assume the absence of saturation effects. This may seem incompatible with the assumption that the spin–lattice interaction is negligible which implies a long spin–lattice relaxation time and, consequently, an accumulation of energy in the spin system. However, the spin–lattice relaxation time may very well be short enough to prevent observable saturation effects to occur and still long enough not to contribute to the shape of the absorption line in an appreciable way.

The case of nickel fluosilicate treated in Sections 5 and 6 of this paper is intended mainly as an illustration of the application of the very complicated general formulae given in Section 4.

2. EXPRESSIONS FOR THE FIRST AND SECOND MOMENTS OF THE LINE SHAPE FUNCTION

As is implied by what we have said in the Introduction, we use in this paper the customary method of moments (Waller 1932; Broer 1943; Van Vleck 1948) in order to characterize the position and shape of a paramagnetic resonance line.

We shall define in this section a "line shape function" $f(\nu)$ such that $f(\nu)$is proportional to the imaginary part $\chi''(\nu)$ of the high frequency susceptibility and such that $\int_0^\infty f(\nu)d\nu = 1$. By the "moments" of a line we shall mean in this paper expressions of the type

$$\langle \nu^l \rangle = \int_0^\infty \nu^l f(\nu)d\nu \qquad (l = 1, 2, \ldots). \tag{2.1}$$

In order to be able to define the line shape function we must first describe more explicitly the "spin system" for which our formulae will be valid. The "spin system" is supposed to consist of N identical "spins" forming a rigid lattice, each spin being defined by a "spin-Hamiltonian" $\mathfrak{H}_i^{(0)}$, or some equivalent expression. The spin-Hamiltonian incorporates, as usual, the effect of the external constant magnetic field and of the crystalline electrostatic field.

The Hamiltonian of the spin system is then given by

$$\mathfrak{H} = \mathfrak{H}^{(0)} + \mathfrak{H}^{(1)} + \mathfrak{H}^{(2)}$$

where

$$\mathfrak{H}^{(0)} = \sum_{i=1}^{N} \mathfrak{H}_i^{(0)}$$

and $\mathfrak{H}^{(1)}$ describes the spin–spin interactions (which include magnetic dipole

and exchange interactions), and $\mathfrak{H}^{(2)}$ describes the effect of the high frequency oscillating magnetic field on the spins. We shall assume that the interactions are weak, i.e.,

$$\mathfrak{H}^{(0)} \gg \mathfrak{H}^{(1)}$$

and also

$$\mathfrak{H}^{(1)} \gg \mathfrak{H}^{(2)}$$

so that the Hamiltonian of the spin system can be written approximately as

$$\mathfrak{H} = \mathfrak{H}^{(0)} + \mathfrak{H}^{(1)}.$$

We shall consider $\mathfrak{H}^{(0)}$ to be the unperturbed energy and $\mathfrak{H}^{(1)}$ the perturbation energy. We shall treat $\mathfrak{H}^{(2)}$ as causing transitions between energy levels of $\mathfrak{H}^{(0)}+\mathfrak{H}^{(1)}$, with two qualifications however. Firstly, according to the well-known argument of Van Vleck (1948), which we will not repeat here, the term $\mathfrak{H}^{(1)}$ in the Hamiltonian must be "truncated" appropriately before we can use it for calculating the moments of the line shape function $f(\nu)$. The truncation of $\mathfrak{H}^{(1)}$ is necessary in order to eliminate the weak "secondary" lines from $f(\nu)$, and consists in discarding that part of $\mathfrak{H}^{(1)}$ which does not commute with $\mathfrak{H}^{(0)}$. We shall write $\overline{\mathfrak{H}}^{(1)}$ for the truncated $\mathfrak{H}^{(1)}$. Secondly, a further truncation is necessary, as pointed out by Kambe and Usui (1952), when a crystalline field is present, namely a truncation of $\mathfrak{H}^{(2)}$. This truncation has to do with the fact that when a crystalline field is present the energy levels of an unperturbed spin are, in general, not equidistant, and, hence, several absorption lines of comparable intensity, that is, several "primary" lines, will be observed. In order to calculate the characteristics of $f(\nu)$ for only one of these lines, one has then to modify $\mathfrak{H}^{(2)}$ in such a way as to make it cause transitions between only two levels of a spin. This kind of truncation will be denoted by a circumflex over $\mathfrak{H}^{(2)}$ (or over the operators which enter the expression for $\mathfrak{H}^{(2)}$), i.e., we shall write $\hat{\mathfrak{H}}^{(2)}$. We shall define $\hat{\mathfrak{H}}^{(2)}$ more explicitly later on, in terms of its matrix elements.

Before proceeding, we must say a few words about the notation to be used for the Boltzmann factors. Since over 100 Boltzmann factors occur in the equations of the present paper, we will consistently use the abbreviations

$$b = e^{-1/kT} \qquad \text{and} \qquad b^x = e^{-x/kT}$$

where x may be a number or an operator. Occasionally, when x is a complicated expression, it may be convenient to use the notation "bol x" for b^x, in analogy with the "exp" notation for the exponential function, i.e. to define a function bol x as follows:

$$\text{bol } x = \exp(-x/kT).$$

We shall label the eigenvalues of the Hamiltonian of the spin system $\overline{\mathfrak{H}} = \mathfrak{H}^{(0)}+\overline{\mathfrak{H}^{(1)}}$ by E_n and the corresponding eigenstates by $|n)$, and we shall assume $\mathfrak{H}^{(2)}$ to be of the form

$$\mathfrak{H}^{(2)} = 2H_1 \cos 2\pi\nu t \cdot M$$

where $2H_1$ is the amplitude of the oscillating magnetic field and M is the component of the magnetic moment of the spin system in the direction of the oscillating field. Then, in thermal equilibrium, the power $P(\nu)d\nu$ absorbed by the spin system from the oscillating field will be proportional to

$$h\nu \sum_{nn'}^{\Delta} (b^{E_n} - b^{E_{n'}}) |(n|\hat{M}|n')|^2$$

where $\sum_{nn'}^{\Delta}$ means summation over all states $|n)$ and $|n')$ such that

$$h\nu \leqslant E_{n'} - E_n \leqslant h\,(\nu + d\nu).$$

On the other hand, we have the well-known relation between $P(\nu)$ and the imaginary part $\chi''(\nu)$ of the high frequency susceptibility:

$$P(\nu) = 4\pi\nu H_1^2 \chi''(\nu).$$

If we now define the line shape function $f(\nu)$ as $\chi''(\nu)$ times a normalization constant,

$$f(\nu) = \frac{\chi''(\nu)}{\int_0^\infty \chi''(\nu)d\nu}, \qquad \int_0^\infty f(\nu)d\nu = 1,$$

then this equation combined with the two immediately preceding equations gives

$$f(\nu)d\nu = \frac{\sum_n \sum_{n'}^{\Delta} (b^{E_n} - b^{E_{n'}}) |(n|\hat{M}|n')|^2}{\sum_n \sum_{n'}^{+} (b^{E_n} - b^{E_{n'}}) |(n|\hat{M}|n')|^2},$$

where $\sum_{n'}^{+}$ means summation over all states $|n')$ such that $E_{n'} \geqslant E_n$.

Hence, using definition (2.1), we can write the expressions for the first two moments as follows:

$$h\langle\nu\rangle = \frac{\sum_n \sum_{n'}^{+} (E_{n'} - E_n)(b^{E_n} - b^{E_{n'}}) |(n|\hat{M}|n')|^2}{\sum_n \sum_{n'}^{+} (b^{E_n} - b^{E_{n'}}) |(n|\hat{M}|n')|^2}, \tag{2.2}$$

$$h^2\langle\nu^2\rangle = \frac{\sum_n \sum_{n'}^{+} (E_{n'} - E_n)^2 (b^{E_n} - b^{E_{n'}}) |(n|\hat{M}|n')|^2}{\sum_n \sum_{n'}^{+} (b^{E_n} - b^{E_{n'}}) |(n|\hat{M}|n')|^2}. \tag{2.3}$$

We shall calculate these two moments. As is usual in this kind of calculation, we shall first rewrite (2.2) and (2.3) in an invariant form, involving traces of operators. Following Kambe and Usui (1952), we get rid of the rather awkward summation Σ^+ by introducing the operators $\hat{M}_+$ and $\hat{M}_-$, which are defined as

$$(n|\hat{M}_+|n') = \begin{cases} (n|\hat{M}|n') & \text{if } E_n > E_{n'} \\ 0 & \text{otherwise,} \end{cases}$$

$$(n|\hat{M}_-|n') = \begin{cases} (n|\hat{M}|n') & \text{if } E_{n'} > E_n \\ 0 & \text{otherwise.} \end{cases}$$

Thus $(n|\hat{M}|n') = (n|\hat{M}_+|n') + (n|\hat{M}_-|n')$ for $n \neq n'$.

Equations (2.2) and (2.3) can then be rewritten, as has been shown by Kambe and Usui, in the following invariant form:

$$h\langle\nu\rangle = \frac{1}{2}\frac{\text{trace } (b^{\bar{\mathfrak{H}}}[\hat{M}, [\bar{\mathfrak{H}}, \hat{M}]])}{\text{trace } (b^{\bar{\mathfrak{H}}}[\hat{M}_-, \hat{M}_+])}, \tag{2.4}$$

$$h^2\langle\nu^2\rangle = \frac{\text{trace } (b^{\bar{\mathfrak{H}}}[[\hat{M}_-, \bar{\mathfrak{H}}], [\bar{\mathfrak{H}}, \hat{M}_+]])}{\text{trace } (b^{\bar{\mathfrak{H}}}[\hat{M}_-, \hat{M}_+])}. \tag{2.5}$$

Equation (2.4) can also be written as

$$h\langle\nu\rangle = \frac{\text{trace } (b^{\bar{\mathfrak{H}}}\hat{M}[\bar{\mathfrak{H}}, \hat{M}])}{\text{trace } (b^{\bar{\mathfrak{H}}}[\hat{M}_-, \hat{M}_+])}.$$

It should be noted that equations (2.4) and (2.5) have been derived without resorting to any assumptions as to the temperature T. These equations are quite general and are valid at all temperatures. Furthermore, they could be applied not only to the case of electron paramagnetic resonance but also to the case of nuclear magnetic resonance. However, in the latter case the region of temperatures for which the usual temperature-independent formulae of Van Vleck cease to be valid is far below 1° K and hence probably of no immediate experimental interest.

We shall now rewrite equations (2.4) and (2.5) in terms of $\mathfrak{H}$ and M rather than $\bar{\mathfrak{H}}$, $\hat{M}$, $\hat{M}_+$, and $\hat{M}_-$. To this end we shall introduce certain projection operators in the way Pryce and Stevens (1950) have done before.

We define a projection operator, P_λ, such that

$$P_\lambda|\mu, k) = \delta_{\lambda\mu}|\lambda, k) \tag{2.6}$$

where $|\mu,k)$ satisfies the eigenvalue equation

$$\mathfrak{H}^{(0)}|\mu,k) = E_\mu|\mu,k) \qquad (k = 1, 2, \ldots, g_\mu, \text{ the degeneracy of } E_\mu).$$

As a consequence of (2.6) we have that

$$P_\lambda P_{\lambda'} = P_\lambda \delta_{\lambda\lambda'}. \tag{2.7}$$

Now it is clear that any operator G can be written as

$$G = \sum_{\mu=1}^{\Omega}\sum_{\eta=1}^{\Omega} P_\mu G P_\eta$$

where Ω is the number of different eigenvalues of $\mathfrak{H}^{(0)}$. Using this and the fact that $[\bar{\mathfrak{H}}, \mathfrak{H}^{(0)}] = 0$ we can write

$$\bar{\bar{\mathfrak{H}}} = \sum_{\mu} P_{\mu}\mathfrak{H}P_{\mu}. \tag{2.8}$$

Let us now consider $\hat{M}$. We shall suppose that equations (2.4) and (2.5) give the first and second moments of the primary line at the frequency ν^*, say. That is, we consider $h\nu^*$ to be the energy difference of the two levels of the unperturbed spin between which $\hat{M}$ induces transitions. The circumflex has been introduced over M in order to eliminate from the expressions for the moments any of the primary lines in which we are not interested. Thus we have

$$(\alpha, i|\hat{M}|\beta, k) = \begin{cases} (\alpha, i|M|\beta, k) & \text{if } |E_\alpha - E_\beta| = h\nu^* \\ 0 & \text{otherwise.} \end{cases}$$

Then we can write

$$\hat{M} = \sum_{\alpha,\beta} (P_\alpha M P_\beta + P_\beta M P_\alpha) \tag{2.9}$$

where $\sum_{\alpha,\beta}$ means summation over all values of α and β wherein $E_\beta - E_\alpha = h\nu^*$.

Let us now suppose that $|\mu,k)$ also satisfies the equation

$$\bar{\mathfrak{H}}|\mu,k) = E_{\mu,k}|\mu,k).$$

(This is possible since $[\bar{\mathfrak{H}}, \mathfrak{H}^{(0)}] = 0$.) Then, if $\overline{\mathfrak{H}^{(1)}}$ is not too large, we have that $E_\alpha < E_\beta$ implies that $E_{\alpha,i} < E_{\beta,k}$ except for a negligible number of pairs of states $|\alpha,i)$, $|\beta,k)$. If this is the case then we can write

$$\hat{M}_+ = \sum_{\alpha,\beta} P_\beta M P_\alpha, \tag{2.10}$$

$$\hat{M}_- = \sum_{\alpha,\beta} P_\alpha M P_\beta. \tag{2.11}$$

Using equations (2.7) to (2.11), equations (2.4) and (2.5) can be rewritten, after some straightforward rearrangements, as follows

$$h\langle\nu\rangle = C/B, \tag{2.12}$$

$$h^2\langle\nu^2\rangle = D/B, \tag{2.13}$$

where

$$B = \sum_{\alpha,\beta} \text{trace}\{[\text{bol}(P_\alpha\mathfrak{H}P_\alpha)]P_\alpha M P_\beta M - [\text{bol}(P_\beta\mathfrak{H}P_\beta)]P_\beta M P_\alpha M\},$$

$$C = \sum_{\alpha,\beta} \text{trace}\{[\text{bol}(P_\alpha\mathfrak{H}P_\alpha)](P_\alpha M P_\beta\mathfrak{H}P_\beta M - P_\alpha\mathfrak{H}P_\alpha M P_\beta M) - [\text{bol}(P_\beta\mathfrak{H}P_\beta)](P_\beta\mathfrak{H}P_\beta M P_\alpha M - P_\beta M P_\alpha\mathfrak{H}P_\alpha M)\},$$

$$D = \sum_{\alpha,\beta} \text{trace}\{[\text{bol}(P_\alpha\mathfrak{H}P_\alpha)](P_\alpha M P_\beta\mathfrak{H}P_\beta\mathfrak{H}P_\beta M - 2P_\alpha\mathfrak{H}P_\alpha M P_\beta\mathfrak{H}P_\beta M + P_\alpha\mathfrak{H}P_\alpha\mathfrak{H}P_\alpha M P_\beta M) - [\text{bol}(P_\beta\mathfrak{H}P_\beta)](P_\beta\mathfrak{H}P_\beta\mathfrak{H}P_\beta M P_\alpha M - 2P_\beta\mathfrak{H}P_\beta M P_\alpha\mathfrak{H}P_\alpha M + P_\beta M P_\alpha\mathfrak{H}P_\alpha\mathfrak{H}P_\alpha M)\}.$$

We now define

$$\langle \Delta\nu^l \rangle = \langle (\nu - \nu^*)^l \rangle \qquad (l = 1, 2, 3 \ldots). \tag{2.14}$$

That is, $\langle \Delta\nu^l \rangle$ denotes the lth moment of $f(\nu)$ about the frequency ν^*. It should be noticed that $\langle \Delta\nu^l \rangle$ is not in general equal to the lth central moment of $f(\nu)$ this being defined as $\langle (\nu - \langle \nu \rangle)^l \rangle$.

Using equation (2.14) and the fact that

$$P_\alpha \mathfrak{H} P_\alpha = P_\alpha (\mathfrak{H}^{(0)} + \mathfrak{H}^{(1)}) P_\alpha = E_\alpha P_\alpha + P_\alpha \mathfrak{H}^{(1)} P_\alpha \tag{2.15}$$

equations (2.12) and (2.13) give

$$h \langle \Delta\nu \rangle = C^{(1)}/B \tag{2.16}$$

$$h^2 \langle \Delta\nu^2 \rangle = D^{(1)}/B \tag{2.17}$$

where the expressions for $C^{(1)}$ and $D^{(1)}$ differ from those for C and D only in the replacement of $\mathfrak{H}$ by $\mathfrak{H}^{(1)}$ everywhere except in the exponentials.

3. DISCUSSION OF VARIOUS APPROXIMATIONS INVOLVING THE TEMPERATURE

The expressions for the moments discussed in the previous section do not involve any assumption about the magnitude of the temperature.

As is well known, in most physical situations of experimental interest the temperature in such expressions can be regarded as infinite. In order to obtain the limiting values of these expressions for $T \to \infty$ it is not sufficient to replace the exponentials by unity, because this would lead only to indeterminate expressions of the form $0/0$ (a glance at equations (2.4) and (2.5) shows that this is so, since the trace of a commutator of two finite matrices always vanishes). However, by expanding the exponentials into powers of $1/kT$, one easily finds that the correct limiting values arise from terms linear in $1/kT$, and are given by

$$\lim_{T\to\infty} \langle \Delta\nu \rangle = \frac{\nu^* \langle \Delta\nu \rangle_V + \langle \Delta\nu^2 \rangle_V}{\nu^* + \langle \Delta\nu \rangle_V}, \tag{3.1}$$

$$\lim_{T\to\infty} \langle \Delta\nu^2 \rangle = \frac{\nu^* \langle \Delta\nu^2 \rangle_V + \langle \Delta\nu^3 \rangle_V}{\nu^* + \langle \Delta\nu \rangle_V} \tag{3.2}$$

where

$$\langle \Delta\nu \rangle_V = Q^{-1} \sum_{\alpha,\beta} \text{trace}(P_\beta \mathfrak{H}^{(1)} P_\beta M P_\alpha M - P_\alpha \mathfrak{H}^{(1)} P_\alpha M P_\beta M), \tag{3.3}$$

$$\langle \Delta\nu^2 \rangle_V = Q^{-1} \sum_{\alpha,\beta} \text{trace}(P_\beta \mathfrak{H}^{(1)} P_\beta \mathfrak{H}^{(1)} P_\beta M P_\alpha M - 2 P_\alpha \mathfrak{H}^{(1)} P_\alpha M P_\beta \mathfrak{H}^{(1)} P_\beta M + P_\alpha \mathfrak{H}^{(1)} P_\alpha \mathfrak{H}^{(1)} P_\alpha M P_\beta M), \tag{3.4}$$

$$\langle \Delta\nu^3 \rangle_V = Q^{-1} \sum_{\alpha,\beta} \text{trace}(P_\beta \mathfrak{H}^{(1)} P_\beta \mathfrak{H}^{(1)} P_\beta \mathfrak{H}^{(1)} P_\beta M P_\alpha M - 3 P_\beta \mathfrak{H}^{(1)} P_\beta \mathfrak{H}^{(1)} P_\beta M P_\alpha \mathfrak{H}^{(1)} P_\alpha M + 3 P_\beta \mathfrak{H}^{(1)} P_\beta M P_\alpha \mathfrak{H}^{(1)} P_\alpha \mathfrak{H}^{(1)} P_\alpha M - P_\alpha \mathfrak{H}^{(1)} P_\alpha \mathfrak{H}^{(1)} P_\alpha \mathfrak{H}^{(1)} P_\alpha M P_\beta M), \tag{3.5}$$

and

$$Q = \sum_{\alpha,\beta} \text{trace}\, P_\alpha M P_\beta M.$$

It is not difficult to show that these last three equations can be obtained from

$$h^l \langle \nu^l \rangle_V = \frac{\sum_n \sum_{n'}^{+} (E_{n'} - E_n)^l |(n|\hat{M}|n')|^2}{\sum_n \sum_{n'}^{+} |(n|\hat{M}|n')|^2} \qquad (l = 1, 2, \ldots) \tag{3.6}$$

by rewriting equation (3.6) for $l = 1, 2$, and 3 in terms of traces of operators then using equations (2.7) to (2.11) and equation (2.14). In the Appendix we show how we can arrive at equation (3.6) from equation (2.1).

Equation (3.6) is an obvious generalization of Van Vleck's (1948) equation (3) and for this reason we call $\langle \nu^l \rangle_V$ the "Van Vleck" approximation for the lth moment.

If $\langle \Delta\nu^l \rangle_V = 0$ for l odd, as is often the case (see Van Vleck (1948)), then, equations (3.1) and (3.2) can be written

$$\lim_{T\to\infty} \langle \Delta\nu \rangle = \langle \Delta\nu^2 \rangle_V / \nu^*,$$

$$\lim_{T\to\infty} \langle \Delta\nu^2 \rangle = \langle \Delta\nu^2 \rangle_V.$$

The exact limiting value of $\langle \Delta\nu \rangle$ is not zero as predicted by the Van Vleck approximation. However, if $\nu^{*2} \gg \langle \Delta\nu^2 \rangle_V$ it is a good approximation to take

$$\lim_{T\to\infty} \langle \nu \rangle = \nu^*, \qquad \lim_{T\to\infty} \langle (\nu - \langle \nu \rangle)^2 \rangle = \langle \Delta\nu^2 \rangle_V,$$

as is usually done.

The approximation consisting in treating the temperature as infinite can be expected to be reasonably good for most paramagnetic salts down to a temperature of a few degrees Kelvin. It breaks down as soon as $h\nu^*/kT$ becomes comparable with unity. (A few additional remarks about this point will be made at the end of Section 4.) Hence, a much better approximation will consist in making use of the fact that the interactions are weak, i.e., $\mathfrak{H}^{(1)} \ll \mathfrak{H}^{(0)}$ and expanding the exponentials in equations (2.16) and (2.17) as follows:

$$\text{bol}(P_\alpha \mathfrak{H} P_\alpha) = [\text{bol}(E_\alpha P_\alpha)]\left[1 - \frac{P_\alpha \mathfrak{H}^{(1)} P_\alpha}{kT} + \ldots\right]. \tag{3.7}$$

In obtaining (3.7) use has been made of equation (2.15). We shall call the approximation consisting in keeping only the first term in the square bracket "the first approximation", and the approximation consisting in keeping only the first and the second terms in the bracket "the second approximation". A straightforward calculation shows that the exact equations (2.16) and (2.17) reduce, in the first approximation, to

$$h\langle \Delta\nu \rangle_1 = B_1^{-1} \sum_{\alpha,\beta} b^{E\alpha}\, \text{trace}(P_\beta \mathfrak{H}^{(1)} P_\beta M P_\alpha M - P_\alpha \mathfrak{H}^{(1)} P_\alpha M P_\beta M), \tag{3.8}$$

$$(3.9)\quad h^2\langle\Delta\nu^2\rangle_1 = B_1^{-1}\sum_{\alpha,\beta} b^{E\alpha}\,\mathrm{trace}(P_\beta\mathfrak{H}^{(1)}P_\beta\mathfrak{H}^{(1)}P_\beta MP_\alpha M - 2P_\alpha\mathfrak{H}^{(1)}P_\alpha MP_\beta\mathfrak{H}^{(1)}P_\beta M + P_\alpha\mathfrak{H}^{(1)}P_\alpha\mathfrak{H}^{(1)}P_\alpha MP_\beta M),$$

where

$$B_1 = \sum_{\alpha,\beta} b^{E\alpha}\,\mathrm{trace}\,P_\alpha MP_\beta M.$$

Equations (3.8) and (3.9) are exactly equivalent to equations (1), (2), and (3) in Pryce and Stevens' paper (1950).

It may be pointed out that by letting T tend to infinity in equations (3.8) and (3.9) one obtains the Van Vleck approximation for the moments, i.e., equations (3.3) and (3.4) rather than equations (3.1) and (3.2). The latter equations contain small additional terms arising from the here neglected second term in the bracket in equation (3.7).

4. EXPRESSIONS FOR THE MOMENTS IN THE FIRST APPROXIMATION FOR A SYSTEM OF IDENTICAL "SPINS"

We shall now apply equations (3.8) and (3.9) to the case when the unperturbed spin has R energy values $a_1, a_2, a_3, \ldots, a_R$ which are all non-degenerate. We shall suppose that Q pairs of these energy values have energy separation $h\nu^*$. Now, let us suppose the Q pairs of levels have energies $(a_{x'}, a_x)$, $(a_{y'}, a_y)$, $\ldots$, $(a_{z'}, a_z)$. That is, we have

$$a_{x'} - a_x = a_{y'} - a_y = \ldots = a_{z'} - a_z = h\nu^*.$$

We shall denote the set of Q positive integers $(x, y, \ldots, z)$ by G, and we have that, if r is in the set G, then there exists an integer r' such that $a_{r'} - a_r = h\nu^*$, but if r is not in the set G, then $a_\zeta - a_r \neq h\nu^*$ for $\zeta = 1, 2, \ldots, R$.

In order to evaluate the traces and perform the summations in equations (3.8) and (3.9) we use the same methods as used by Pryce and Stevens (1950) in Section 4 of their paper. That is, we take

$$\mathfrak{H}^{(1)} = \frac{1}{2}\sum_{ij}{}' \mathfrak{H}_{ij}^{(1)} \quad \text{and} \quad M = \sum_{i=1}^{N} m_i$$

then evaluate the traces with respect to the functions

$$|a)_1\,|b)_2 \ldots |c)_i \ldots |d)_N = |a, b \ldots c \ldots d)$$

where, for example, $|c)_i$ satisfies the eigenvalue equation

$$\mathfrak{H}_i^{(0)}|c)_i = a_c|c)_i\,.$$

Any eigenvalue E_μ of $\mathfrak{H}^{(0)}$ can be written

$$E_\mu = \sum_{r=1}^{R} n_r a_r$$

where

$$0 \leqslant n_r \leqslant N \quad \text{and} \quad \sum_{r=1}^{R} n_r = N\,,$$

so that the summations over the α's and β's can be replaced by summations over n's.

As the method is not new, and the calculations are rather lengthy and somewhat cumbersome, we give here only the results.*

We introduce the following notation:

$|e')$ denotes the single spin state having the energy $a_{e'} = a_e + h\nu^*$;

$(e|m|e')$ denotes the matrix element of the single spin operator m between the single spin states $|e)$ and $|e')$;

$(ef|\mathfrak{H}_{ij}^{(1)}|ab)$ denotes the matrix element of $\mathfrak{H}_{ij}^{(1)}$ between the state $|e)_i|f)_j$ of the spins i and j and the state $|a)_i|b)_j$ of the same pair of spins;

$\sum_e$ means summation over all R states $|e)$ of a single spin,

S_e means summation over all integers in the set G defined at the beginning of this section,

$\sum_{ab}$ means summation over all positive integers a and b such that $a_a + a_b = a_e + a_f$,

S_{ab} means summation over all positive integers a and b such that $a_a + a_b = a_e + a_f$, and a is in the set G,

$\sum_{ab}^*$ means summation over all positive integers a and b such that $a_a + a_b = a_{e'} + a_f = a_e + a_f + h\nu^*$,

$\sum_{ij}'$ means summation over all i and j independently, excluding those terms for which $i = j$,

$\sum_{ijk}'$ means summation over all i, j, and k independently, excluding those terms for which any two of the three summation indices are equal.

Further,

$$Z = \sum_e b^{a_e}$$

$$\Gamma = S_e b^{a_e} |(e|m|e')|^2.$$

With this notation the first two moments are:

$$(4.1)\quad h\langle \Delta\nu \rangle_1 = (NZ\Gamma)^{-1} \left\{ S_e S_f b^{a_f} (b^{a_e} - b^{a_{e'}}) \Lambda_{11}(ef) + S_e \sum_f b^{a_e + a_f} \Lambda_{12}(ef) \right\}$$

$$(4.2)\quad h^2\langle \Delta\nu^2 \rangle_1 = (NZ\Gamma)^{-1} \left\{ S_e S_f b^{a_f} (b^{a_e} + b^{a_{e'}}) \Lambda_{21}(ef) + S_e \sum_f b^{a_e + a_f} \Lambda_{22}(ef) \right\}$$

$$+ (N\Gamma)^{-1} Z^{-2} \left\{ S_e S_f S_g b^{a_f} (b^{a_e} - b^{a_{e'}}) (b^{a_g} - b^{a_{g'}}) \Lambda_{23}(efg) \right.$$

$$\left. + S_e S_f \sum_g b^{a_f + a_g} (b^{a_e} - b^{a_{e'}}) \Lambda_{24}(efg) + S_e \sum_f \sum_g b^{a_e + a_f + a_g} \Lambda_{25}(efg) \right\}$$

*For some details of the calculations one may consult McMillan (1959).

where

$$\Lambda_{11}(ef) = (e|m|e')(f'|m|f) \sum_{ij}{}' (e'f|\mathfrak{H}_{ij}^{(1)}|ef'),$$

$$\Lambda_{12}(ef) = |(e|m|e')|^2 \sum_{ij}{}' [(e'f|\mathfrak{H}_{ij}^{(1)}|e'f) - (ef|\mathfrak{H}_{ij}^{(1)}|ef)],$$

$$\Lambda_{21}(ef) = (e|m|e')(f'|m|f) \sum_{ij}{}' \sum_{ab}{}^{*} (e'f|\mathfrak{H}_{ij}^{(1)}|ab)(ab|\mathfrak{H}_{ij}^{(1)}|ef'),$$

$$\Lambda_{22}(ef) = |(e|m|e')|^2 \sum_{ij}{}' \left[\sum_{ab} |(ef|\mathfrak{H}_{ij}^{(1)}|ab)|^2 + \sum_{ab}{}^{*} |(e'f|\mathfrak{H}_{ij}^{(1)}|ab)|^2 \right]$$
$$-2 \sum_{ij}{}' S_{ab} [(a|m|a')(e'|m|e)(ef|\mathfrak{H}_{ij}^{(1)}|ab)(a'b|\mathfrak{H}_{ij}^{(1)}|e'f)$$
$$+ (a|m|a')(e'|m|e)(ef|\mathfrak{H}_{ij}^{(1)}|ba)(ba'|\mathfrak{H}_{ij}^{(1)}|e'f)],$$

$$\Lambda_{23}(efg) = (e|m|e')(f'|m|f) \sum_{ijk}{}' (e'g|\mathfrak{H}_{ij}^{(1)}|eg')(fg'|\mathfrak{H}_{jk}^{(1)}|f'g),$$

$$\Lambda_{24}(efg) = (e|m|e')(f'|m|f) \sum_{ijk}{}' (e'f|\mathfrak{H}_{ij}^{(1)}|ef')[(e'g|\mathfrak{H}_{jk}^{(1)}|e'g)$$
$$+ (f'g|\mathfrak{H}_{jk}^{(1)}|f'g) - (eg|\mathfrak{H}_{jk}^{(1)}|eg) - (fg|\mathfrak{H}_{jk}^{(1)}|fg)],$$

$$\Lambda_{25}(efg) = |(e|m|e')|^2 \sum_{ijk}{}' [(e'f|\mathfrak{H}_{ij}^{(1)}|e'f) - (ef|\mathfrak{H}_{ij}^{(1)}|ef)][(e'g|\mathfrak{H}_{jk}^{(1)}|e'g)$$
$$- (eg|\mathfrak{H}_{jk}|eg)].$$

We have verified that in the absence of crystalline field, i.e. the case in which each unperturbed spin has $2S+1$ equidistant energy levels, equations (4.1) and (4.2) become identical with the expressions given for this case by Kambe and Usui (1952).

As pointed out in Section 3, equations for $\langle \Delta\nu \rangle_1$ and $\langle \Delta\nu^2 \rangle_1$ reduce, for $T \to \infty$, to the formulae for the moments in the Van Vleck approximation (equations (3.3) and (3.4)). A glance at equations (4.1) and (4.2) makes it clear that T can be regarded as "infinite" as soon as the energy differences $a_e - a_f$ are negligible when compared to kT. A more careful analysis of the expression (4.2) shows that

$$\langle \Delta\nu^2 \rangle_1 \text{ bol } [4(a_R - a_1)] \leqq \langle \Delta\nu^2 \rangle_V \leqq \langle \Delta\nu^2 \rangle_1 \text{ bol } [4(a_1 - a_R)] \tag{4.3}$$

if a_1 is the smallest and a_R the largest single spin energy value.

5. APPLICATION OF THE FIRST APPROXIMATION FORMULAE FOR THE MOMENTS

General equations (4.1) and (4.2) for the first and second moments are complicated, and it is not easy to see from them at a glance what sort of temperature dependence of $\langle \Delta\nu \rangle_1$ and $\langle \Delta\nu^2 \rangle_1$ they imply.

We will specialize equations (4.1) and (4.2) to the case in which each unperturbed spin has R not equidistant energy levels, and the set G defined in Section 4 consists of one element. For convenience, we will label the R energy levels such that $a_1 < a_2 \ldots < a_R$.

Equation (4.1) gives then the following formula in the case of an absorption line from the ground state to the first excited state of the unperturbed spin:

$$h\langle\Delta\nu\rangle_1 = (NZ)^{-1}\Big\{(b^{a_1}-b^{a_2})\sum_{ij}{}'(21|\mathfrak{H}_{ij}^{(1)}|12) + \sum_{f=1}^{R} b^{af}\sum_{ij}{}'[(2f|\mathfrak{H}_{ij}^{(1)}|2f)-(1f|\mathfrak{H}_{ij}^{(1)}|1f)]\Big\}. \tag{5.1}$$

Similarly one obtains from equation (4.2) an expression for the second moment of the same line. We do not give this expression here because it is not much simpler than equation (4.2) itself. We write it later on for two special cases (see equations (5.9) and (5.10)).

We further specialize the problem by assuming that the spin-Hamiltonian of a single spin has an axial symmetry, that the constant magnetic field H is directed along the axis of symmetry which we choose to be the z-axis, and that the eigenstates of the spin-Hamiltonian are also eigenstates of the operator corresponding to the z-component of the spin. We assume that the spin–spin interaction is a sum of magnetic dipole interaction and isotropic exchange interaction. We can then write the "truncated" spin–spin interaction operator in its usual form:

$$\bar{\mathfrak{H}}^{(1)} = \frac{1}{2}\sum_{ij}{}'\bar{\mathfrak{H}}_{ij}^{(1)}, \tag{5.2}$$

$$\bar{\mathfrak{H}}_{ij}^{(1)} = A_{ij}\mathbf{S}_i\cdot\mathbf{S}_j + B_{ij}S_{zi}S_{zj}, \tag{5.3}$$

or

$$\bar{\mathfrak{H}}_{ij}^{(1)} = A_{ij}\tfrac{1}{2}(S_{-i}S_{+j}+S_{+i}S_{-j})+(A_{ij}+B_{ij})S_{zi}S_{zj}, \tag{5.4}$$

$$A_{ij} = \tilde{A}_{ij}+\tfrac{1}{2}g_\perp^2\beta^2 r_{ij}^{-3}(3\gamma_{ij}^2-1), \tag{5.5}$$

$$B_{ij} = -\tfrac{1}{2}(2g_\parallel^2+g_\perp^2)\beta^2 r_{ij}^{-3}(3\gamma_{ij}^2-1); \tag{5.6}$$

γ_{ij} is the direction cosine of the line of length r_{ij} joining spin i to spin j relative to the z-axis; $\tilde{A}_{ij}$ are the exchange interaction constants, which we shall assume to be all equal to $\tilde{A}$ if spins i and j are nearest neighbors, and zero otherwise; $g_\perp$ and $g_\parallel$ are the g-factors perpendicular and parallel to the symmetry axis; β is the Bohr magneton.

Substituting the appropriate matrix elements of (5.4) in equation (5.1) one obtains in the case of the effective spin $S = \frac{1}{2}$ $(R = 2)$

$$h\langle\Delta\nu\rangle_1 = \frac{1}{2N}\tanh\left(\frac{a_1-a_2}{2kT}\right)\sum_{ij}{}'B_{ij}, \tag{5.7}$$

(the terms involving A_{ij} cancel out), and in the case of the effective spin $S = 1$ $(R = 3)$

$$h\langle\Delta\nu\rangle_1 = -(NZ)^{-1}\Big\{(b^{a_2}-b^{a_3})\sum_{ij}{}'A_{ij}+(b^{a_1}-b^{a_3})\sum_{ij}{}'B_{ij}\Big\}. \tag{5.8}$$

For the second moment of the same line one obtains in the case of $S = \frac{1}{2}$

$$h^2\langle\Delta\nu^2\rangle_1 = \frac{1}{4N}\left\{\sum_{ij}{}'B_{ij}^2+\tanh^2\left(\frac{a_1-a_2}{2kT}\right)\sum_{ijk}{}'B_{ij}B_{jk}\right\}, \tag{5.9}$$

and in the case of $S = 1$

$$(5.10)\quad h^2\langle\Delta\nu^2\rangle_1 = (NZ)^{-1}\sum_{ij}{}'\,[(b^{a_2}+2b^{a_3})A_{ij}^2+(b^{a_1}+b^{a_3})B_{ij}^2+2b^{a_3}A_{ij}B_{ij}]$$
$$+N^{-1}Z^{-2}\sum_{ijk}{}'\,[(b^{a_2}-b^{a_3})^2A_{ij}A_{jk}+(b^{a_1}-b^{a_3})^2B_{ij}B_{jk}$$
$$+2(b^{a_2}-b^{a_3})(b^{a_1}-b^{a_3})A_{ij}B_{jk}].$$

If the shape of the sample is spherical, and the lattice of spins is cubic (each spin having z nearest neighbors) one has

$$(5.11)\qquad \sum_{ij}{}'B_{ij}=0, \qquad \sum_{ij}{}'A_{ij}=zN\tilde{A}.$$

Equations (5.7) and (5.8) become then

$$(5.12)\qquad h\langle\Delta\nu\rangle_1 = 0, \qquad (S=\tfrac{1}{2})$$

$$(5.13)\qquad h\langle\Delta\nu\rangle_1 = -z\tilde{A}Z^{-1}(b^{a_2}-b^{a_3}). \qquad (S=1)$$

To obtain some still more specific expressions for the moments we consider, as an example, the case of nickel fluosilicate. In this paramagnetic crystal there is only one Ni^{++} ion in the unit cell, which greatly simplifies the problem. The paramagnetic resonance absorption lines of nickel fluosilicate have been observed by Holden, Kittel, and Yager (1949), and by Penrose and Stevens (1950), and the theoretical expressions for the moments have been obtained by Ishiguro, Kambe, and Usui (1951), using the Van Vleck approximation.

While Ishiguro, Kambe, and Usui assumed exchange interaction in nickel fluosilicate to be isotropic, it would appear from Ollom and Van Vleck's (1951) theoretical analysis of experimental evidence that it is in fact strongly anisotropic. As some points of that analysis were rather uncertain, we have assumed for simplicity that exchange interaction is isotropic, and we have used equations (5.3) to (5.6) as they stand. However, after our calculations were essentially concluded a new experimental evidence in support of the anisotropy of exchange interaction in nickel fluosilicate was obtained by Walsh (1959). It seems thus that our quantitative predictions concerning nickel fluosilicate ought not to be taken too literally; but they should help in any case to clarify the situation on this point when relevant experimental data become available.

It has long been known (Becquerel and Opechowski 1939; Penrose and Stevens 1950) that each Ni^{++} ion in nickel fluosilicate has effective spin $S=1$, and that the spin-Hamiltonian of Ni^{++} ions can be written as

$$(5.14)\quad \mathfrak{H}^{(0)} = \sum_{i=1}^{N}\mathfrak{H}_i^{(0)} = \sum_i\{-\beta[g_\perp(S_{xi}H_x+S_{yi}H_y)+g_\parallel S_{zi}H_z]-\delta S_{zi}^2\}$$

where δ, $g_\parallel$, and $g_\perp$ are positive constants. We consider here only the case in which the constant magnetic field H is parallel to the symmetry axis of the crystal so that

$$(5.15)\qquad \mathfrak{H}_i^{(0)} = -\beta g_\parallel S_{zi}H-\delta S_{zi}^2,$$

and the three eigenvalues of $\mathfrak{H}_i^{(0)}$ are

$$(5.16)\qquad a_1=-g_\parallel\beta H-\delta, \qquad a_2=0, \qquad a_3=+g_\parallel\beta H-\delta,$$

where, since we have introduced the convention $a_1 < a_2 < a_3$, we assumed that H is large enough to make $g_\parallel \beta H > \delta$. There are only two absorption lines, corresponding to

$$h\nu^* = a_2 - a_1 = g_\parallel \beta H + \delta \tag{5.17}$$

and

$$h\nu^* = a_3 - a_2 = g_\parallel \beta H - \delta. \tag{5.18}$$

The line corresponding to $h\nu^* = a_3 - a_1$ is forbidden.

We shall assume, as has been done by Ishiguro, Kambe, and Usui (1951), that the lattice of the Ni^{++} ions can be approximated by a simple cubic lattice (lattice constant d), and we shall take for granted the following numerical result due to them:

$$\frac{1}{4} \sum_{ij}{}' r_{ij}^{-6} (3\gamma_{ij}^2 - 1)^2 = 0.626\, N d^{-6}.$$

We shall further assume that the crystal has the shape of a sphere so that equations (5.11) hold. From these equations one easily derives the following identities:

$$\sum_{ijk}{}' r_{ij}^{-3} r_{jk}^{-3} (3\gamma_{ij}^2 - 1)(3\gamma_{jk}^2 - 1) = -\sum_{ij}{}' r_{ij}^{-6} (3\gamma_{ij}^2 - 1)^2,$$

$$\sum_{ij}{}' \tilde{A}_{ij} r_{ij}^{-3} (3\gamma_{ij}^2 - 1) = \sum_{ijk}{}' \tilde{A}_{ij} r_{jk}^{-3} (3\gamma_{jk}^2 - 1) = 0.$$

On these assumptions the first two moments of the line corresponding to $h\nu^* = a_2 - a_1$, as obtained from equations (5.8) and (5.10), are

$$h\langle \Delta\nu \rangle_1 = -6\tilde{A} Z^{-1} (b^{a_2} - b^{a_3}) \tag{5.19}$$

$$\begin{aligned} h^2 \langle \Delta\nu^2 \rangle_1 = 6\tilde{A}^2 [&Z^{-1} (b^{a_2} + 2b^{a_3}) + 5Z^{-2} (b^{a_2} - b^{a_3})^2] \\ &+ 0.626 \beta^4 d^{-6} \{ g_\perp^4 [1 - Z^{-2} (b^{a_1} - b^{a_2})^2] \\ &+ 4 g_\parallel^4 [Z^{-1} (b^{a_1} + b^{a_2}) - Z^{-2} (b^{a_1} - b^{a_2})^2] \\ &+ 4 g_\parallel^2 g_\perp^2 [Z^{-1} b^{a_1} - Z^{-2} (b^{a_1} - b^{a_2})(b^{a_1} - b^{a_2})] \}. \end{aligned} \tag{5.20}$$

The first two moments of the line corresponding to $h\nu^* = a_3 - a_2$ can be found by appropriately relabelling the eigenstates in equation (5.1) and in the equation (not written here explicitly) for the second moment: one has to replace 1 by 2, and 2 by 3 in the matrix elements and Boltzmann factors. One then obtains using the same assumptions as before

$$h\langle \Delta\nu \rangle_1 = -6\tilde{A} Z^{-1} (b^{a_1} - b^{a_2}), \tag{5.21}$$

$$\begin{aligned} h^2 \langle \Delta\nu^2 \rangle_1 = 6\tilde{A}^2 [&Z^{-1} (b^{a_2} + 2b^{a_1}) + 5Z^{-2} (b^{a_1} - b^{a_2})^2] \\ &+ 0.626 \beta^4 d^{-6} \{ g_\perp^4 [1 - Z^{-2} (b^{a_2} - b^{a_3})^2] \\ &+ 4 g_\parallel^4 [Z^{-1} (b^{a_1} + b^{a_3}) - Z^{-2} (b^{a_1} - b^{a_3})^2] \\ &+ 4 g_\parallel^2 g_\perp^2 [Z^{-1} b^{a_3} - Z^{-2} (b^{a_1} - b^{a_3})(b^{a_2} - b^{a_3})] \}. \end{aligned} \tag{5.22}$$

The first and second moments for the two lines, as given by equations (5.19) to (5.22), are plotted as a function of the temperature on Figs. 1 to 4.

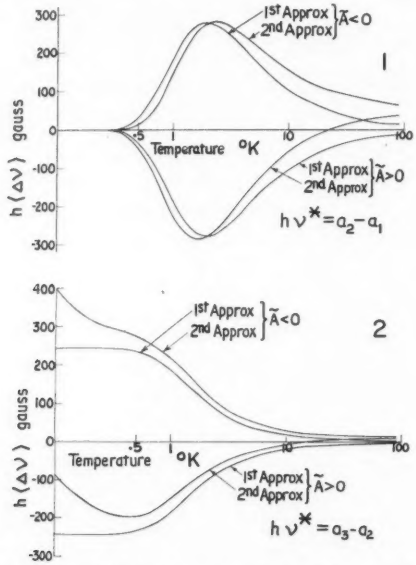

FIG. 1. The first moment of the line corresponding to $h\nu^* = a_2 - a_1 = g_\parallel \beta H + \delta$ as a function of the temperature in the first and second approximation for the positive and negative sign of the exchange interaction constant $\tilde{A}$. Conversion factor: 1 gauss corresponds to 2.19×10^{-20} erg.

FIG. 2. The first moment of the line corresponding to $h\nu^* = a_3 - a_2 = g_\parallel \beta H - \delta$ as a function of the temperature. For further explanations, see the caption of Fig. 1.

We have assumed $H = 12$ kilogauss, $g_\parallel = 2.36$, $g_\perp = 2.29$, $\delta = 0.12$ cm^{-1}. The numerical values of these constants are taken from Penrose and Stevens (1950). In fact δ is temperature dependent between room and liquid hydrogen temperatures, but below 20° K it seems to become constant, and it is this constant value that we have used. We regard d and $\tilde{A}$ as also temperature independent, which probably they really are at the very low temperatures we are interested in. Their numerical values are taken from Ishiguro, Kambe, and Usui (1951). They obtained two different values of $|\tilde{A}|$ for the two lines using the experimental data of Holden, Kittel, and Yager (1949): $|\tilde{A}| = 7.5 \times 10^{-18}$ erg for the line corresponding to $h\nu^* = a_2 - a_1$, and $|\tilde{A}| = 8.8 \times 10^{-18}$ erg for the line corresponding to $h\nu^* = a_3 - a_2$. We have used these values in our numerical calculations. From the point of view of our theory it would have been more logical of course to use the same value of $\tilde{A}$ for both lines.

On Figs. 3 and 4 we have also shown the second central moment $\langle \Delta\nu^2 \rangle_{c1} = \langle (\nu - \langle \nu \rangle)^2 \rangle_1$ as a function of the temperature.

The conversion factor from gauss to erg has been chosen equal to $g_\parallel \beta$, i.e. 1 gauss corresponds to 2.19×10^{-20} erg.

Some rather obvious comments on Figs. 1 to 4 are made in Section 6.

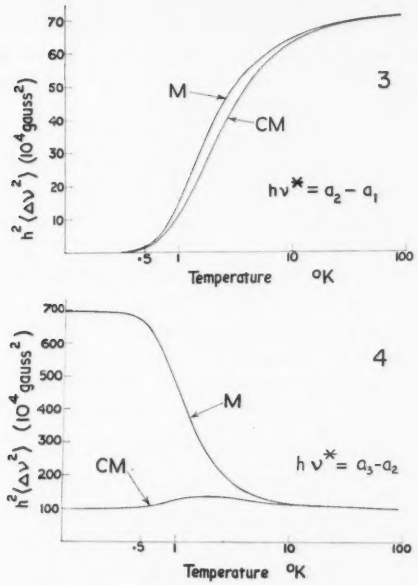

FIG. 3. The second moment (curve M) and the second central moment (curve CM) of the line corresponding to $h\nu^* = a_2 - a_1$ in the first approximation.

FIG. 4. The second moment (curve M) and the second central moment (curve CM) of the line corresponding to $h\nu^* = a_3 - a_2$ in the first approximation.

6. SECOND APPROXIMATION FORMULAE FOR THE FIRST MOMENT

The general expressions for the first and second moments in the second approximation are rather complicated. We have applied to special cases only the general expression for the first moment (the general expression for the second moment in the second approximation can be found in McMillan (1959)).

One obtains

$$h\langle\Delta\nu\rangle_2 = \frac{C_1+C_2/kT}{D_1+D_2/kT} \approx \frac{C_1}{D_1}+\frac{1}{kT}\left(\frac{C_2}{D_1}-\frac{C_1D_2}{D_1^2}\right), \tag{6.1}$$

$$C_1 = \sum_{\alpha,\beta} (b^{E_\alpha}-b^{E_\beta}) \text{ trace } (P_\beta \mathfrak{H}^{(1)} P_\beta M P_\alpha M - P_\alpha \mathfrak{H}^{(1)} P_\alpha M P_\beta M),$$

$$C_2 = \sum_{\alpha,\beta} [b^{E_\beta} \text{ trace } P_\beta \mathfrak{H}^{(1)} P_\beta \mathfrak{H}^{(1)} P_\beta M P_\alpha M$$

$$+ b^{E_\alpha} \text{ trace } P_\alpha \mathfrak{H}^{(1)} P_\alpha \mathfrak{H}^{(1)} P_\alpha M P_\beta M$$

$$- (b^{E_\alpha}+b^{E_\beta}) \text{ trace } P_\alpha \mathfrak{H}^{(1)} P_\alpha M P_\beta \mathfrak{H}^{(1)} P_\beta M],$$

$$D_1 = \sum_{\alpha,\beta} (b^{E_\alpha}-b^{E_\beta}) \text{ trace } P_\alpha M P_\beta M,$$

$$D_2 = \sum_{\alpha,\beta} (b^{E_\beta} \text{ trace } P_\beta \mathfrak{H}^{(1)} P_\beta M P_\alpha M - b^{E_\alpha} \text{ trace } P_\alpha \mathfrak{H}^{(1)} P_\alpha M P_\beta M).$$

Applying this expression to the case of the two absorption lines of nickel fluosilicate, and using the assumptions formulated in Section 5 one obtains expressions which, when evaluated numerically, give the second approximation curves on Figs. 1 and 2. We do not reproduce here these expressions, because they are very long. They are of the form

$$h\langle\Delta\nu\rangle_2 = h\langle\Delta\nu\rangle_1+\frac{1}{kT}\left[\tilde{A}^2G_1+0.626G_2\frac{\beta^4}{d^6}\right]$$

where G_1 depends on the Boltzmann factors only, and G_2 depends on the Boltzmann factors and the g-factors.

We should like to emphasize the following features of the curves given in Figs. 1 and 2:

The sign of $\langle\Delta\nu\rangle$, that is the sign of the shift of the mean frequency of the line relative to "unperturbed" frequency ν^*, is determined for both lines by the sign of the exchange interaction constant $\tilde{A}$. Apart from this the temperature dependence of the mean frequency shift is even qualitatively different for the two lines. This is due to the fact that the line corresponding to $h\nu^* = a_2-a_1$ originates in the ground state of a single ion while the other line corresponds to a transition between excited states. At very low temperatures it is the former line (transition from the ground state) which is of main interest. For this line the absolute value of the mean frequency shift goes through a maximum at about 2° K as the temperature decreases and becomes negligible below 0.4° K.

The second approximation curves differ very little from the first approximation curves. This means that one could obtain from the measured mean frequency shift a very good estimate of the exchange interaction constant $\tilde{A}$ since in the first approximation the shift is simply proportional to $\tilde{A}$.

One can prove quite generally that

$$\lim_{T\to 0}\langle\Delta\nu\rangle_1 = \lim_{T\to 0}\langle\Delta\nu\rangle_2$$

in the case of transitions from the ground state to any excited state for an arbitrary value of the effective spin S; no assumption about the structure of the crystal or its shape need be made nor is it necessary to assume that S_{zi} commutes with the spin-Hamiltonian.

The second central moment $\langle\Delta\nu^2\rangle_{c1}$ in the case of transitions from the ground state (as in Fig. 3) to the first excited state can be shown to vanish for $T = 0$ for arbitrary S and quite generally.

We should add that we have not seriously tried to investigate the question at what temperature the second approximation breaks down. Of course, it is possible that the qualitative features of the temperature dependence of the mean frequency shift remain unchanged in higher approximations.

ACKNOWLEDGMENTS

We are indebted to Dr. Myer Bloom for some conversations about the experimental aspects of the problem discussed in this paper.

A part of this work was carried out during the tenure of a grant-in-aid from the National Research Council of Canada. One of us (M. M.) would also like to acknowledge the financial help in the form of a N.R.C. scholarship.

REFERENCES

BECQUEREL, J. and OPECHOWSKI, W. 1939. Physica, **6**, 1039.
BROER, L. J. F. 1943. Physica, **10**, 801.
HOLDEN, A. N., KITTEL, C., and YAGER, W. A. 1949. Phys. Rev. **75**, 1443.
ISHIGURO, E., USUI, T., and KAMBE, K. 1951. Physica, **17**, 310.
KAMBE, K. and USUI, T. 1952. Progr. Theoret. Phys. **8**, 302.
McMILLAN, M. 1959. M. Sc. Thesis, University of British Columbia, Vancouver, B.C.
OLLOM, J. F. and VAN VLECK, J. H. 1951. Physica, **17**, 205.
PENROSE, R. P. and STEVENS, K. W. H. 1950. Proc. Phys. Soc. A, **63**, 29.
PRYCE, M. H. L. and STEVENS, K. W. H. 1950. Proc. Phys. Soc. A, **63**, 36.
VAN VLECK, J. H. 1948. Phys. Rev. **74**, 1168.
WALLER, I. 1932. Z. Physik, **79**, 380.
WALSH, W. M., JR. 1959. Phys. Rev. **114**, 1473.

APPENDIX

We can arrive at equation (3.6) in the following way.

Using definitions and notation explained in Section 2, one can easily see that the general expression for the lth moment of the line shape function $f(\nu)$ is

$$h^l\langle\nu^l\rangle = \frac{\sum_{\alpha=1}^{\Omega}\sum_{\beta}^{+}\sum_{i=1}^{g_\alpha}\sum_{j}^{+}(E_{\beta,j}-E_{\alpha,i})^l\,(b^{E_{\alpha,i}}-b^{E_{\beta,j}})\,|(\alpha,i|\hat{M}|\beta,j)|^2}{\sum_{\alpha=1}^{\Omega}\sum_{\beta}^{+}\sum_{i=1}^{g_\alpha}\sum_{j}^{+}(b^{E_{\alpha,i}}-b^{E_{\beta,j}})\,|(\alpha,i|\hat{M}|\beta,j)|^2}. \tag{A.1}$$

The summations over β and j are restricted to those values for which $E_{\beta,j} > E_{\alpha,i}$.

We now evaluate this expression in the "first approximation" as defined in Section 3. In others words, we replace the energy values $E_{\alpha,i}$ of the spin system in the Boltzmann factors by the energy values E_α in the absence of interactions:

$$h^l\langle\nu^l\rangle = \frac{\sum_{\alpha}\sum_{\beta}^{+}(b^{E_\alpha}-b^{E_\beta})\sum_{i}\sum_{j}^{+}(E_{\beta,i}-E_{\alpha,i})^l\,|(\alpha,i|\hat{M}|\beta,j)|^2}{\sum_{\alpha}\sum_{\beta}^{+}(b^{E_\alpha}-b^{E_\beta})\sum_{i}\sum_{j}^{+}|(\alpha,i|\hat{M}|\beta,j)|^2}. \tag{A.2}$$

According to the definitions given in Section 2, the matrix elements $(\alpha, i|\hat{M}|\beta, j)$ vanish unless $|E_\beta - E_\alpha| = h\nu^*$, and the summation has to be taken over only those values of α and β for which $|E_\alpha - E_\beta| = h\nu^*$. This means that the numerator as well as the denominator of equation (A.2) contains the factor $1-\text{bol}\,h\nu^*$. After removing this common factor, one obtains

$$h^l\langle\nu^l\rangle = \frac{\sum_{\alpha}\sum_{\beta}^{+}b^{E_\alpha}\sum_{i}\sum_{j}^{+}(E_{\beta,i}-E_{\alpha,i})^l\,|(\alpha,i|\hat{M}|\beta,j)|^2}{\sum_{\alpha}\sum_{\beta}^{+}b^{E_\alpha}\sum_{i}\sum_{j}^{+}|(\alpha,i|\hat{M}|\beta,j)|^2} \tag{A.3}$$

This expression becomes identical, except for the notation, with the right-hand side of equation (3.6) if all Boltzmann factors are replaced by unity. A sufficient condition for the validity of such a step is of course the validity of the inequality

$$\frac{|E_\alpha - E_{\alpha'}|}{kT} \ll 1, \qquad \text{(for all values of } \alpha \text{ and } \alpha'\text{)} \tag{A.4}$$

which would, however, imply very high temperatures indeed. The reason why the temperature-independent equation (3.6) can be used down to a temperature of the order of 10° K is of course due to the fact that condition (A.4) is sufficient without being necessary. It is rather obvious that it is sufficient for the temperature to be large compared with the differences between energy values of a single spin. A formal proof of this much weaker sufficient condition is given at the end of Section 4; see inequality (4.3).

DOMAIN STRUCTURE IN YTTRIUM IRON GARNET[1]

ARCHIBALD W. SMITH AND GERALD W. WILLIAMS

ABSTRACT

The magnetic domain structure in thin slices of yttrium iron garnet crystals has been studied by transmitted polarized light. The transmitted light exhibits Faraday rotation and magnetic birefringence, and both effects have been used to observe the domain structure. An example of structure in samples having a growth face on one side is presented for each of the (110) and (112) planes. The structure for the (110) face is similar to that for an ideal sample in this plane. The structure for the (112) face differs from an ideal sample due to a large strain anisotropy.

1. INTRODUCTION

It has recently been found that many ferromagnetic oxides become optically transparent when the thickness is reduced to a few thousandths of a centimeter. The transmitted light exhibits Faraday rotation and magnetic birefringence, and these effects have been used to observe the magnetic domain structure (Dillon 1958; Sherwood, Remeika, and Williams 1959). In contrast to transparent films of ferromagnetic metals, the oxide samples are sufficiently thick that the domain structure is still characteristic of the bulk material. In this paper, some observations on domain structure in single crystals of yttrium iron garnet are presented. These structures are analyzed briefly in terms of the appropriate magnetic theory.

Yttrium iron garnet (abbreviated YIG) has previously been studied by Dillon (1958). He found that with samples ground on both sides, the domain structure usually took the form of irregular strips, in which the magnetization was perpendicular to the plane of the sample, and antiparallel in adjacent domains. This was interpreted as being due to strain in the crystal caused by the grinding and polishing operations. The strain results in an approximately uniaxial anisotropy perpendicular to the surface which overrides the intrinsic cubic anisotropy. For convenience, this type of structure will be referred to as normal strain structure. Dillon's work also suggested that the strain might be less important if only one side of the sample were ground, the other being a growth face. A number of samples were prepared to investigate this point. Although some of these exhibited the normal strain structure, the majority showed different types of structure. Examples of the two most interesting, occurring in the (110) and (112) planes, are discussed below. The other structures observed were variations of these two.

2. EXPERIMENTAL

2.1 Sample Preparation

The crystals of yttrium iron garnet ($Y_3Fe_5O_{12}$) were grown by the method of Nielsen and Dearborn (1958). A melt of Y_2O_3, Fe_2O_3, and PbO in the mole

[1]Manuscript received March 25, 1960.
Contribution from the Electronics Laboratory of the Defence Research Telecommunications Establishment, Ottawa, Ontario. This work was carried out under Project No. D48-55-03-08.

ratio 0.525:0.440:0.035 was formed at 1350° C. The temperature was then lowered at 3° C/hr to about 950° C. Small crystals were obtained, usually not over 2 mm along any direction, showing both (110) and (112) growth faces. The method of grinding and polishing was similar to that described by Dillon and Earl (1959). The samples were mounted in an adjustable grinding jig, the piston of which was left unclamped. With this arrangement, the sample was free to ride over any slight irregularities in the grinding surface without damage. Grinding was done with 5 μ alumina on glass, polishing with 1 μ alumina on phenolic-impregnated linen. Only one side of the sample was ground, the other being a growth face. The crystallographic plane of the growth faces was determined by X-ray techniques.

2.2 Domain Observation

When light which is plane-polarized passes through a ferromagnetic crystal parallel to the magnetization, the plane of polarization is rotated. This is a type of Faraday effect which arises from the internal magnetic field of the crystal. In general, the specific rotation varies rapidly with wavelength, but falls between 10^3 and 4×10^3 degrees/cm for YIG (Dillon 1959). As an example of how the Faraday effect may be used to reveal domain structure, consider plane-polarized light passing through a sample which has the normal strain structure discussed in the Introduction. Because of the alternation in the direction of the magnetization, the rotation will be equal but opposite in the two sets of domains. If the sample is viewed through another polarizer at right angles to the first, the two sets of domains will have equal intensity. The domain walls will appear black, however, because much of their magnetization is perpendicular to the line of sight and hence does not cause any rotation. Contrast between the two sets of domains can be obtained by uncrossing the two polarizers slightly. YIG also exhibits magnetic circular dichroism (Dillon 1959): the absorption of right- and left-handed circularly polarized light is slightly different, and the sign of the difference depends on whether the light is travelling parallel, or antiparallel, to the direction of the magnetization. This effect can also be used to detect domain structure but does not give as good contrast as the first method.

When plane-polarized light passes through a magnetic crystal perpendicular to the magnetization, in general it emerges elliptically polarized due to the magnetic birefringence. The ellipticity varies from zero when the magnetization is either parallel or perpendicular to the plane of polarization, to a maximum when the magnetization is at 45° to the plane. The magnetic birefringence is very weak, giving retardations of only a few millimicrons for transparent samples. This effect provides a means of determining the direction of the magnetization in the plane perpendicular to the line of sight, with an ambiguity of 90°.

The apparatus for domain observation consisted of a standard polarizing microscope* with photographic attachment, and two small electromagnets which could be fixed to the rotating stage. One magnet gave a field perpendic-

*Model LI-2, Bausch and Lomb Optical Co., Rochester, N.Y.

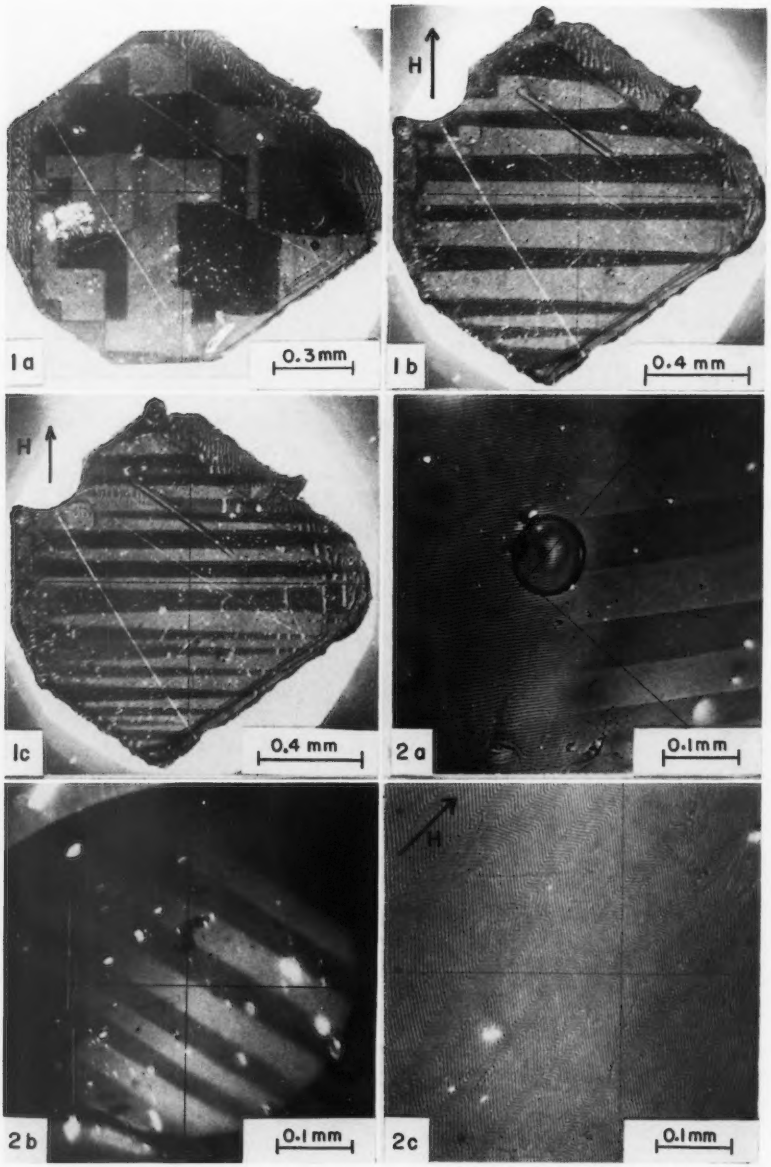

FIG. 1. Domain structure in the (110) plane: (*a*) zero field, (*b*) $H = 11$ oersteds (increasing field), and (*c*) $H = 21$ oersteds (decreasing field).

FIG. 2. Domain structure in the (112) plane: (*a*) narrow and broad strips, zero field, (*b*) sample tilted about axis perpendicular to strips, and (*c*) field perpendicular to narrow strips.

ular, the other parallel, to the line of sight. When using these magnets, the regular condensing lens was replaced by a suitable strain-free objective lens. Fields were measured with a Hall-effect gaussmeter. The retardation of elliptically polarized light was measured by the quarter-wave plate method (Goranson and Adams 1933). In order to carry this out, a quarter-wave plate was mounted below the stage in a specially-constructed holder, and the lower polarizer was provided with a finely-graduated angular scale. The latter was also used to measure the Faraday rotation.

3. RESULTS AND DISCUSSION

3.1 Domain Structure in the (110) Plane

The domain pattern in Fig. 1*a* was characteristic of strain-free samples cut from (110) growth faces. A less extensive example of this pattern was shown by Dillon (1958). The sample exhibited only magnetic birefringence and thus the magnetization lay in the plane of the sample. When the sample was viewed between crossed polarizers only, the contrast between the domains was very low. Therefore, in taking the photographs of this sample, the contrast was increased by using a quarter-wave plate. Normal strain structure occurred along two edges of the sample. The vertical and horizontal crosslines in Fig. 1 are parallel to the [001] and [$\bar{1}$10] directions, respectively, and at the same time indicate the position of the crossed polarizers. The crystallographic directions are explicitly marked in Fig. 3, which is an idealized drawing of Fig. 1*a*.

Two types of domain boundaries could be discerned in this sample. The first, which will be called type *A*, was clearly visible as the boundaries between the light and dark areas, and lay in the [001] and [$\bar{1}$10] directions. The second, type *B*, took the form of fine white or black lines cutting through either a light or a dark region, and ending at the right-angle junctions of type *A* boundaries. The acute angle between type *B* boundaries and the [001] direction was approximately 57°. In several cases, these boundaries were rather broad, and appeared to be inclusions of the normal strain structure. The type *B* boundaries were barely visible in the original photograph of Fig. 1*a*, and may be lost in reproduction. For clarity, the boundaries have been shown schematically in Fig. 3.

The change in intensity which occurs on crossing type *A* boundaries indicates that these are neither 90° nor 180° walls. Conversely, type *B* are either 90° or 180° walls. It is clear from Fig. 3 that the only consistent interpretation is to let type *A* be 114° and 66° walls in the [001] and [$\bar{1}$10] directions, respectively, and to let type *B* be 180° walls. In order to prevent the formation of poles within the sample, the 180° walls must terminate at junctions of 114° and 66° walls, i.e. at right-angle corners. It will be seen that the four orientations of the magnetization, and the 180° walls, are nearly parallel to the four ⟨111⟩ directions in the plane.

When a field was applied along one of the ⟨111⟩ directions in the plane, one set of domains, presumably that with the magnetization in the field direction, grew at the expense of the others. The type *A* boundaries moved at right

angles to their length, in such a way as to maintain 66°, 114°, and 180° walls until the domains were swept out. This occurred at a field of about 25 oersteds. However, a few hazy, wedge-shaped domains were left in the sample at this field, and about 40 oersteds was required to remove all traces of structure.

The behavior with the field in the [001] direction was more complex. Initially, two sets of domains, one light and one dark, began to increase in size, with the boundaries moving as before. These two sets formed strips across the sample perpendicular to the field, as shown in Fig. 1*b*, so that only 114° walls remained. As the field was further increased, the strips became narrower and their number increased. At the same time, another type of domain with intermediate intensity began to appear, again in the form of strips perpendicular to the field. These domains can be seen in Fig. 1*c*. At still higher fields, the contrast between the light and dark strips decreased, and finally they merged with the intermediate domains at a field of 100 oersteds. However, some traces of structure remained until a field of 140 oersteds was reached.

With the field in the [$\bar{1}$10] direction, the behavior was similar to the previous case. Strips again formed perpendicular to the field, but the intermediate domains entered much earlier in this case, and clear-cut strip pattern like that of Fig. 1*b* did not occur. A rather hazy pattern with wedges instead of strips was obtained, somewhat similar to Fig. 1*c*. The sample became nearly uniform in appearance at a field of 50 oersteds, although some traces of structure remained until the field reached 70 oersteds.

The behavior in the two latter cases may be understood by taking the magnetization in the light and dark strips to be along the two ⟨111⟩ directions which were closest to the field direction. In order to saturate the sample, the magnetization had to be rotated until it was parallel to the field. This was evidently occurring in two ways: by gradual rotation within the black and white strips, and by sudden rotation, leading to the formation of the intermediate strips.

The domain structure predicted for an ideal sample in the (110) plane will now be briefly described. For further details and references, the review article of Kittel and Galt (1956) may be consulted. YIG has a negative cubic anisotropy, and so the four ⟨111⟩ directions in the (110) plane are directions of easy magnetization. These are separated by angles of 70°32′ and 109°28′. The simplest domain structure is expected to occur when the sample is an equilateral parallelogram with the sides in the ⟨111⟩ directions. It consists of four quadrants, each with the magnetization in one of the easy directions, in such a way as to give flux closure within the sample. The boundaries are in the [001] and [$\bar{1}$10] directions, ending at opposite corners of the sample and crossing at right angles. When a field is applied along a ⟨111⟩ direction, the boundaries are expected to move perpendicularly to their length until the three unfavorable domains are eliminated. When a field is applied along either the [001] or [$\bar{1}$10] direction, the structure changes to a series of strips perpendicular to the field, with the magnetization alternating in the two favorable easy directions. The number of strips increases with increasing field, and the magnetization rotates towards the field. The fields required for saturation are approximately $4\pi Mn$,

$4\pi Mn-2K/M$, and $4\pi Mn-K/M$ in the [$\bar{1}$11], [001], and [$\bar{1}$10] directions, respectively, where M is the magnetization, K is the anisotropy constant, and n is the demagnetization factor in the plane of the sample.

The observed structure and its behavior under an applied field are consistent with these predictions. The differences can be readily understood on the basis of the irregularities in the crystal structure and shape of the sample. In addition, the occurrence of the intermediate domains when the field is in the [001] or [$\bar{1}$10] direction is probably connected with the low value of the demagnetization factor n. The value of n estimated from the dimensions of the sample is only 0.013. The predicted saturation fields are 22, 106, and 64 oersteds in the [$\bar{1}$11], [001], and [$\bar{1}$10] directions, respectively, with $4\pi M$ = 1750 g, $K/M = -42$ oersteds, and $n = 0.013$. These are in reasonable agreement with the experimental fields of 25, 100, and 50 oersteds required to remove the gross domain structure.

3.2 Domain Structure in the (112) Plane

The sample in Fig. 2*a* was cut from a (112) growth face. It displays two domain patterns: narrow and broad strips, both parallel to the [11$\bar{1}$] direction. (The circle near the center of this figure is a bubble in the mounting wax.) As before, the cross hairs indicate the position of the polarizers. With the polarizers exactly crossed, the contrast between the narrow strips was a maximum when they were oriented at 45° to the polarizers, and was practically zero when they were parallel to the polarizers. Under the same conditions, the contrast between the broad strips was very low, regardless of orientation. It was found that better contrast could be obtained by uncrossing the polarizers a few degrees, and this has been done in Fig. 2*a*. The region with the narrow strips exhibited a permanent birefringence, independent of the magnetization. The direction of vibration of the slow wave was parallel to the [11$\bar{1}$] direction. The retardation was 14 millimicrons, about five times the expected magnetic birefringence. The region with the broad strips exhibited a weaker permanent birefringence, being about the same as the magnetic birefringence. Closure domains could just be discerned in this region, near the edge of the sample. They took the form of spikes protruding into the strips. The thickness of the sample in this region was about half that in the region of the narrow strips.

The behavior of this sample with an external field applied was investigated for three orientations of the field. (1) Field in the plane, parallel to the strips. The domain walls moved perpendicularly to themselves, so that one set of strips in each region expanded, while the other shrank. The narrow strips merged at a field of 550 oersteds, the broad strips at 20 oersteds. (2) Field in the plane, perpendicular to the strips. Initially the region with the narrow strips brightened slightly, and then the narrow strips formed a zigzag pattern as shown in Fig. 2*c*. As the field was increased, the contrast between the strips decreased. At the same time the angle between the strips and the field direction decreased, and became almost zero when the pattern disappeared at 600 oersteds. The widths of the light and dark strips appeared to remain equal,

but decreased somewhat as the field increased. The broad strips were unstable with this field orientation, and again disappeared at a relatively low field. (3) Field perpendicular to the plane. Initially the domain walls moved as in case (1). At 600 oersteds the broad strips became unstable, and an irregular set of domains with the magnetization perpendicular to the plane began to appear. At higher fields, the broad strips were engulfed by these irregular domains, which grew until they merged together at 1750 oersteds. The narrow strips merged at 930 oersteds. As the field was further increased, the Faraday rotation in this region increased until it reached a maximum value at 2300 oersteds. This indicated that the magnetization was being rotated into a position perpendicular to the plane.

With negative cubic anisotropy, there is one easy direction in the (112) plane, namely $[11\bar{1}]$. Ideally the zero-field domain structure would be expected to consist of strips, with the magnetization in the plane of the sample and antiparallel in adjacent strips. The results for case (1) above are consistent with such a structure. However, neither the Faraday rotation nor the magnetic birefringence would provide any contrast between the domains. The existence of such contrast shows that the magnetization has a component $M_\perp$ perpendicular to the plane. This is consistent with the results for case (3), which also require a perpendicular component, antiparallel in adjacent domains. Thus the magnetization is inclined to the plane, and this, together with the existence of the permanent birefringence, requires that the crystal be strained, with the strain axis inclined to the plane. The strain must induce an approximately uniaxial anisotropy which overrides the cubic anisotropy in the region of the narrow strips, but is much weaker in the region of the broad strips. To explain the existence of strips in the $[11\bar{1}]$ direction, the projection of the strain axis on the plane must lie in this direction, which is consistent with the orientation of the optical axes.

The contrast between the narrow strips can be explained in terms of the circular dichroism which occurs in YIG. Consider first the case in which the strips are at 45° to the polarizers. When linearly polarized light passes through the sample, it emerges with a small circular component due to the weak birefringence. The linear component may be broken down into two equal circular components rotating in opposite directions. The small circular component can be added to one of these, giving two circular components with slightly different amplitudes. As the magnetization has a component $M_\perp$ parallel to the light path, one of the circular components will be absorbed more than the other, due to the circular dichroism. For one direction of $M_\perp$, the difference between the circular components will be reduced, and for the opposite direction, increased. The resulting difference in intensity for the two directions of $M_\perp$ is detected by the second polarizer. When the strips are parallel to the polarizers, the light emerges linearly polarized, and the absorption affects all domains equally. For the broad strips, the birefringence is apparently too weak to provide appreciable contrast by this mechanism. However, this can be overcome by making use of the Faraday rotation associated with $M_\perp$, i.e. by uncrossing the polarizers slightly, as in Fig. 2*a*.

The fact that the magnetization was inclined suggested that the sample be tilted under the microscope. An apparent depth measurement showed that the index of refraction of YIG was about 2.2. Therefore, in order to increase the internal ray angle, the sample was immersed in methylene iodide, which has an index of 1.75. The methylene iodide was placed in a small container with windows perpendicular to the line of sight. The experiment was carried out with the tilt axis perpendicular to the strips, which were at 45° to the polarizers. As was expected, the contrast between the strips varied with the angle of tilt. Positions of minimum contrast existed for both sets of domains. With the sample suitably tilted, another set of broad strips becomes visible, superimposed on the narrow strips. This is illustrated in Fig. 2*b*. By noting the optimum focussing positions, it was established that the two sets of strips existed in separate layers, with the narrow strips closer to the growth face. As can be seen in Fig. 2*b*, a smooth transition occurred between the two sets of broad strips.

The position of minimum contrast between the narrow strips occurred at a tilt of 20°. The contrast could be restored by uncrossing the polarizers slightly, indicating that the internal ray direction was parallel to the magnetization. For the first set of broad strips, this position occurred at 4°, but the contrast was not affected by uncrossing the polarizers. This indicated that the internal ray direction was perpendicular to the magnetization. For the second set of broad strips (under the narrow ones), the corresponding position occurred at 0°. The inclination of the magnetization to the plane was calculated to be 75°, 3°, and 0°, respectively, for the three cases.

It may be concluded that the highly strained material occurs as a layer on a base of unstrained material. The region without the narrow strips is essentially a continuation of the base layer, but a weak strain has been introduced.

The behavior with an applied field can be easily understood, at least qualita-

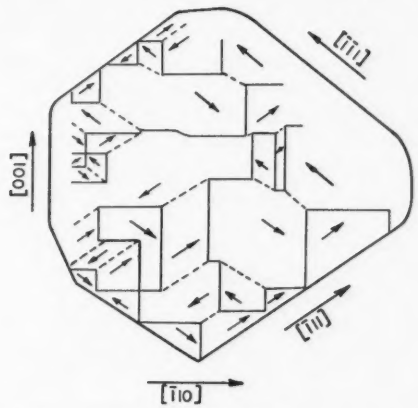

FIG. 3. A schematic representation of Fig. 1*a*. The solid and dotted lines represent type *A* and *B* boundaries, respectively, and the arrows indicate the direction of the magnetization.

tively, except when the field is perpendicular to the strips (case 2). The initial brightening of the sample can be attributed to the saturation of the unstrained base layer. The reduction in contrast between the narrow strips indicates that magnetization in the strained layer is rotating into the plane. It appears that the magnetization is remaining parallel to the domain walls. In order to get a net component of magnetization in the field direction with this arrangement, the component of magnetization in the plane must be in the same direction for all parallel strips. However, this can only be achieved if the magnetization in every second strip has flipped over to a position with the opposite tilt. The formation of the zigzag pattern permits the boundaries to remain a simple variant of the original 180° walls, instead of becoming more complex walls. Thus this analysis requires that the increase in anisotropy energy due to the flipping of the magnetization is more than offset by the avoidance of complex domain walls.

The permanent birefringence was found in all of the four samples which were cut from (112) growth faces. In addition to the present sample, one other was completely analyzed. There were no layers in this case, and the magnetization was inclined at an angle of 60° throughout the sample. The direction of vibration of the slow wave was again parallel to the $[11\bar{1}]$ direction. A permanent birefringence was also found in one sample cut from a (110) growth face. It is clear that the strain giving rise to the birefringence was introduced during the growth of the crystals. Although the present evidence is rather limited, it appears probable that all (112) growth faces are strained. This would be consistent with the observation of Nielsen and Dearborn (1958) that (112) faces predominate when the crystals are grown rapidly.

CONCLUSIONS

It has been found that samples having a growth face on one side are less likely to develop strain from the grinding and polishing operations. The domain structure in samples which are free from this type of strain depends on the particular crystallographic plane. Those cut from (110) faces have structure which is similar to that expected for an ideal sample in this plane. Those cut from (112) faces have unusual structure, due to a large strain anisotropy which is introduced during the growth of the crystals.

We wish to thank Mr. Peter Buratynski for grinding and polishing the samples, and Mr. Jack R. MacDonald for making some preliminary observations.

REFERENCES

DILLON, J. F. 1958. J. Appl. Phys. **29**, 1286.
——— 1959. J. phys. radium, **20**, 374.
DILLON, J. F. and EARL, H. E. 1959. Am. J. Phys. **27**, 201.
GORANSON, R. W. and ADAMS, L. H. 1933. J. Franklin Inst. **216**, 475.
KITTEL, C. and GALT, J. K. 1956. Ferromagnetic domain theory. *In* Solid state physics, Vol. 3 (Academic Press Inc., New York).
NIELSEN, J. W. and DEARBORN, E. F. 1958. J. Phys. Chem. Solids, **5**, 202.
SHERWOOD, R. C., REMEIKA, J. P., and WILLIAMS, H. J. 1959. J. Appl. Phys. **30**, 217.

THE POLAR RADIO BLACK-OUT OF THE IONOSPHERE OF 7 JULY, 1958[1]

JOHN H. CHAPMAN

ABSTRACT

Ionospheric sounding station data, particularly *f*-plots, were used to study the ionospheric storm of 7 July, 1958, which is shown to have consisted clearly of two stages. Polar cap absorption began shortly after an importance 3+ flare was observed at 0039 U.T., and a magnetic storm and auroral absorption event followed at 0749 U.T. on July 8.

The polar cap absorption spread towards the geomagnetic equator, but the use of higher than first order magnetic dipole terms was found necessary in order to arrange the data properly in latitude. The absorption began some hours earlier at northern stations than at most southern stations, the main cause of the differences in time of onset being thought to be due to the presence or absence of sunlight.

The inference is drawn that ionospheric absorption measured at about 3 Mc/s is caused by ionization at 50- to 80-km heights, in which case the data suggest that electrons first precipitated to the earth above 83° corrected geomagnetic latitude, and then protons and helium ions to lower latitudes. The cutoff latitude was 59°, corresponding to a particle magnetic rigidity of 9.6×10^8 ev/*c*. This storm was compared with the more severe event of 23 February, 1956, and showed to be of a similar nature.

INTRODUCTION

The phenomenon of prolonged periods of severe radio absorption in the polar regions has been known for some years (Obayashi 1959; Leinbach and Reid 1959; and Bailey 1959). Until the I.G.Y., however, there were insufficient data available for an adequate description. It is now clear that during a major ionosphere storm of this type, there is an absorbing blanket over the whole of the polar cap, which has led to the name "polar cap absorption" being applied. Such an event occurred during the period 7 July to 10 July, 1958, coinciding with a Special World Interval (July 8 to 9) (Harang and Troim 1959; Hultqvist, Aarons, and Ortner 1959; and Hultqvist 1959*a*).

The event is presumed to have begun shortly after midnight on 7 July, 1958, with an importance 3+ solar flare which was observed from 0039 to 0324 U.T. by the Tokyo Astronomical Observatory at Mitaka and from 0040 to 0214 U.T. at Honolulu, Hawaii, and which reached its maximum intensity at about 0103. The identification of the time of beginning of this storm is reasonably certain, the only possible confusion arising from an importance 2+ flare, observed at Mitaka from 0032 to 0117 U.T. on 7 July. Both of these flares were situated near the central median of the sun at about 25 degrees north latitude. There were no flares of importance greater than 1 observed during the previous day, which was an international magnetically quiet day for the month.

Major radio noise bursts were recorded as shown in the following table (CRPL F Series, and High Altitude Observatory, Boulder).

[1]Manuscript received June 1, 1960.
Contribution from the Defence Research Telecommunications Establishment, Ottawa, Canada.

TABLE I

Solar radio noise emission

Time duration (U.T.)	Frequency (Mc/s)	Location of observatory	Remarks
0027–0038	10,000	Ottawa, Canada	
0029–0058	458	Boulder, Colo.	
0029–0131	167	Boulder, Colo.	
0027–0028	100–580	Fort Davis, Texas	Type III fast drift burst
0028–0029	100–580	Fort Davis, Texas	Continuum, intensity 3
0052–0147	100–580	Fort Davis, Texas	Type IV, continuum, intensity 3
0055–0152	10,000	Ottawa, Canada	
0058–0207	458	Boulder, Colo.	
0131–0214	167	Boulder, Colo.	

These data appear to fall into two groups, one beginning at about 0027 U.T., and the second at 0052 U.T. The second group might be associated with the 3+ flare at 0039 U.T., and the first with the 2+ flare observed earlier. The maximum intensity of the noise bursts at 0104 coincided with the peak in solar flare activity of the later flare.

These flares and noise storms were also associated with short-wave fade-outs (SWF), in particular a widespread slow SWF of major importance from 0025 to 0230 hours U.T.

The first evidence of the onset of the storm was a gradual increase in ionospheric absorption observed at the ionospheric stations within the northern auroral zone, north of 65° geomagnetic latitude. By 0500 U.T., a severe black-out was in effect over the whole of the north polar cap, followed at 1100 U.T. by a similar event in the southern polar region. This black-out continued with no letup until the beginning of 10 July.

The polar cap black-out was accompanied by relatively minor magnetic activity. At 0749 U.T. on July 8, a severe world-wide geomagnetic storm began with a sudden commencement (SC) (Shapley 1959). Although the north polar regions are largely sunlit at this time of the year, the evidence suggests that a severe auroral storm followed.

Cosmic ray monitors in the northern hemisphere recorded a Forbush decrease, beginning between 0900 and 1000 U.T. on July 8, and continuing until July 12.

The purpose of this paper is to present the data of this particular polar radio black-out, and to describe some significant features, in the hope that similar features can be recognized in other storms of this type.

IONOSPHERIC SOUNDING DATA

The data used in this study were obtained by the ionospheric sounding network established during the I.G.Y., from the stations shown in Fig. 1 for the northern hemisphere, and in Fig. 2 for the southern hemisphere.

The principal data used in this study were *f*-plots, showing the frequencies reflected from the ionosphere as a function of time of day. The progress of the storm can be seen in Fig. 3, which shows the *f*-plots for six Canadian ionospheric

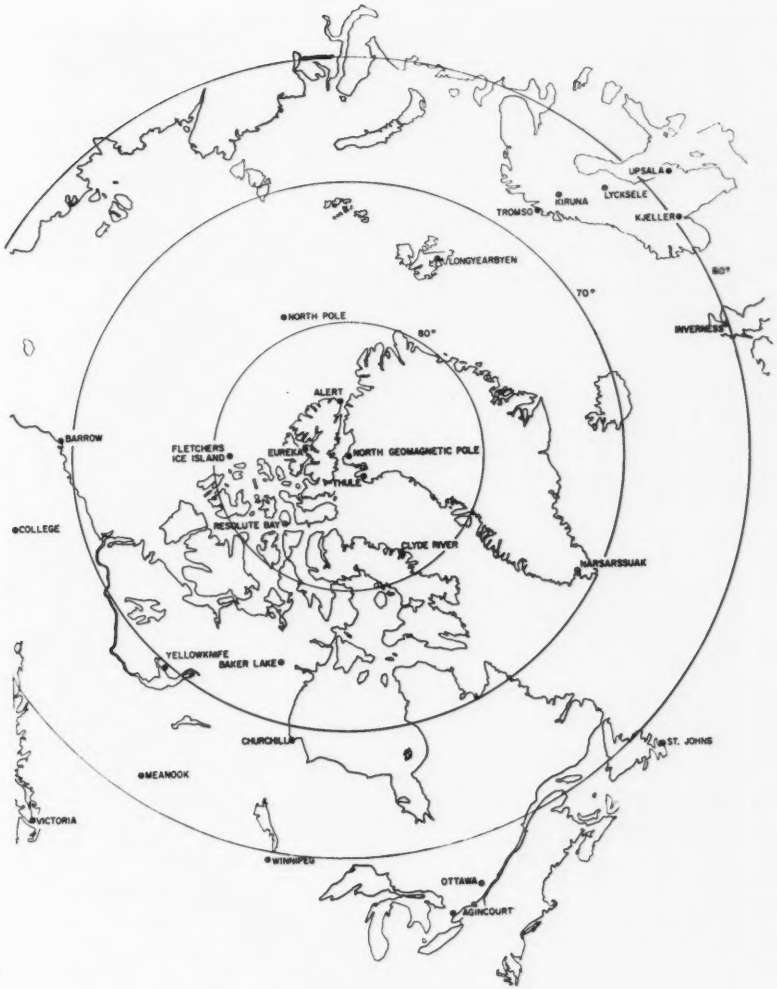

FIG. 1. Locations of stations in the northern hemisphere.

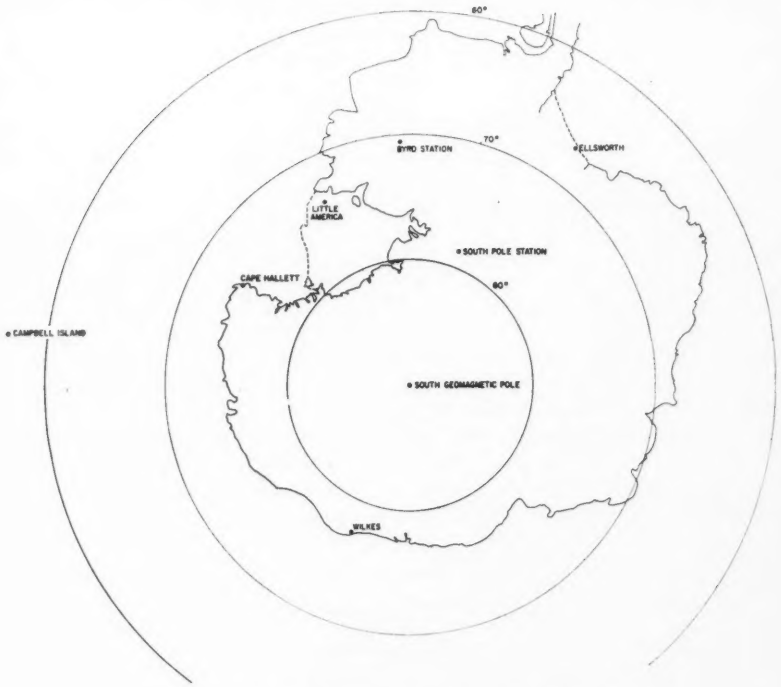

FIG. 2. Locations of stations in the southern hemisphere.

stations, for the period July 6 to July 12, arranged in order of geomagnetic latitude. The ordinate shows the critical reflection frequency in megacycles measured every 15 minutes, the abscissa the time of day.

The beginning of the storm can be seen at Resolute Bay, Baker Lake, Yellowknife, and Churchill by a gradual increase of the minimum frequency echo from the ionosphere ($f_{\min}$), denoted by a vertical line extending up from the base line and terminated by a dot. A solid vertical line extending to the top of the graph indicates a complete black-out, with no echoes being received from the ionosphere at any frequency. It should be noted particularly that the f-plot from Ottawa showed no unusual absorption following the time of the flare, until the sudden commencement 31 hours later.

The extent of the polar black-out can be seen in Figs. 4 and 5, showing the north and south polar regions respectively with data from the various stations arranged in order of geomagnetic latitude. It is apparent that the storm began later in the south than in the north, except for a short period of black-out at Wilkes Station at 0500 U.T. on July 7, which corresponds with the time of black-out at northern stations of comparable geomagnetic latitude.

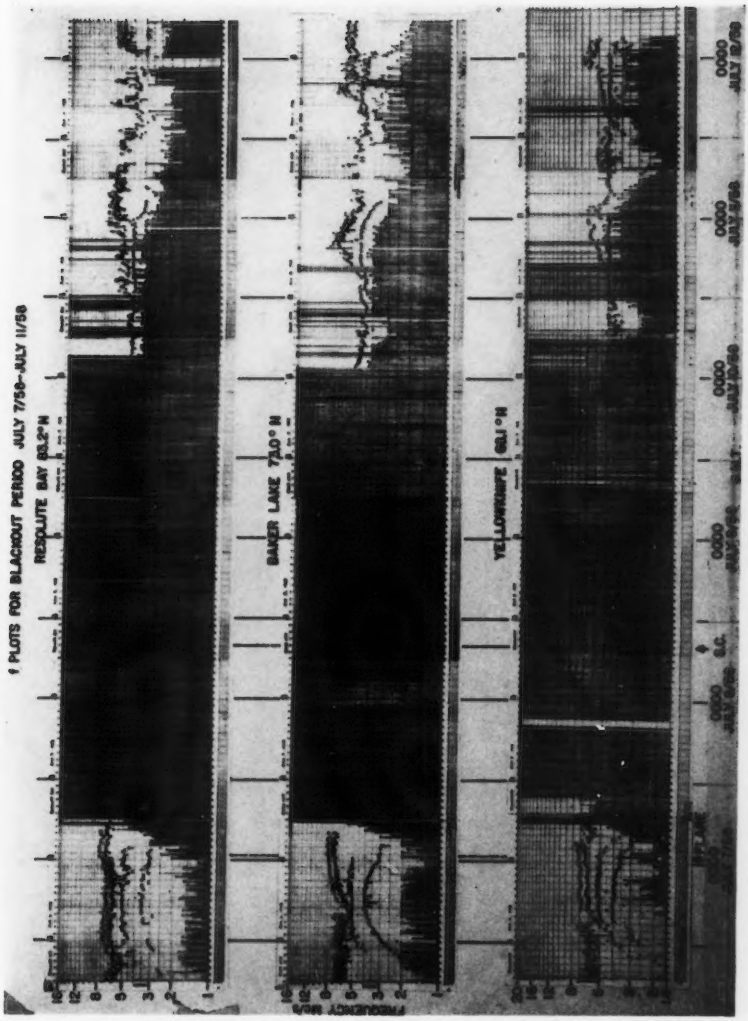

FIG. 3*a*. *f*-Plots from three Canadian stations, showing reflection frequencies and $f_{\min}$ measured every 15 minutes.

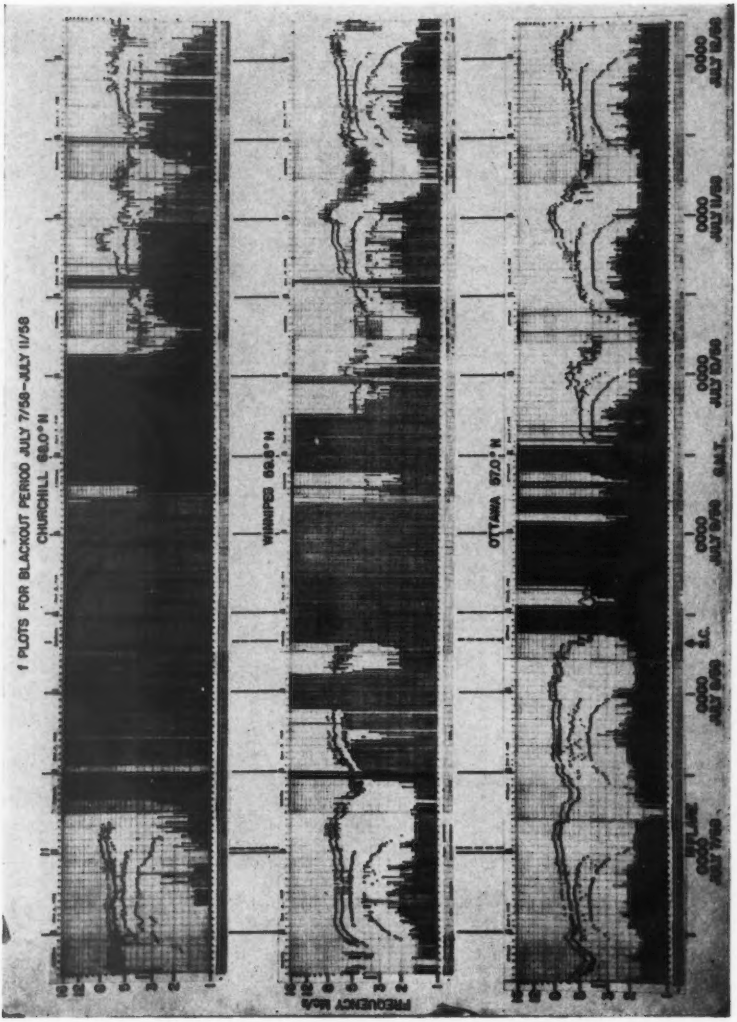

FIG. 3b. f-Plots from three Canadian stations, showing reflection frequencies and $f_{\min}$ measured every 15 minutes.

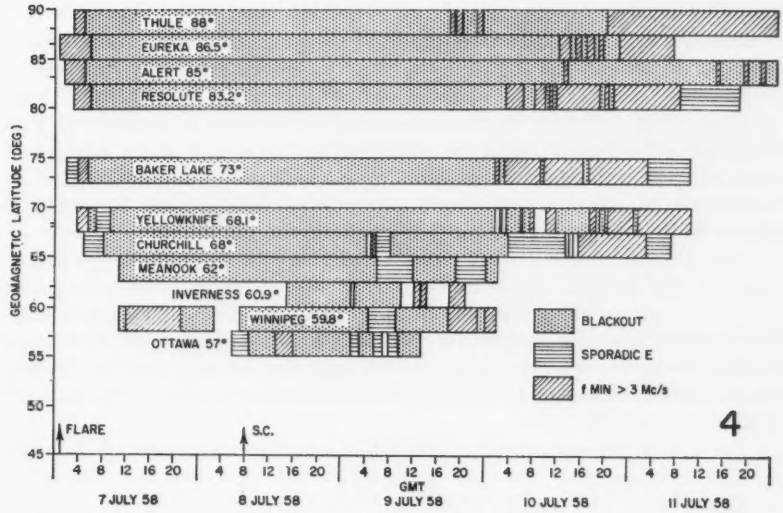

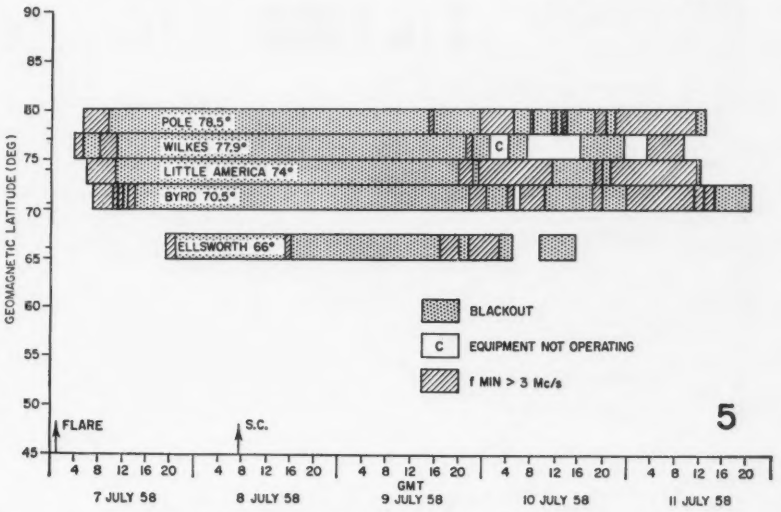

FIG. 4. Extent of black-out in northern hemisphere.
FIG. 5. Extent of black-out in southern hemisphere.

FIG. 36. J-Plots from three Canadian stations, showing reflection frequencies and f_{min} measured every 15 minutes.

MAGNETIC, AURORAL RADAR, AND COSMIC RAY DATA ON JULY 7

In order to show the two main phases of the storm, magnetic, auroral radar, and cosmic ray data are shown in Fig. 6 for the period from July 7 to July 10.

The main features of the variations of the horizontal component H of the magnetic field shown for Agincourt were similar at Baker Lake, Resolute Bay, and Alert. The fluctuations in the magnetic field prior to 0749 on July 8 were relatively minor. The severe magnetic storm which followed the sudden commencement caused large and rapid magnetic field fluctuations for about 12 hours, which were similar at the four magnetic observatories.

The v.h.f. auroral radars at Ottawa and Resolute Bay showed no returns prior to the sudden commencement. However, strong auroral echoes were observed north of the Ottawa station at the time of the sudden commencement and continued off and on until July 10. The geometry of reflection is such that these echoes come from the vicinity of the auroral zone maximum. At Resolute Bay, no radar aurora echoes were observed except for a weak echo present for $1\frac{1}{2}$ hours on July 9.

The cosmic ray data show a typical Forbush decrease beginning about the

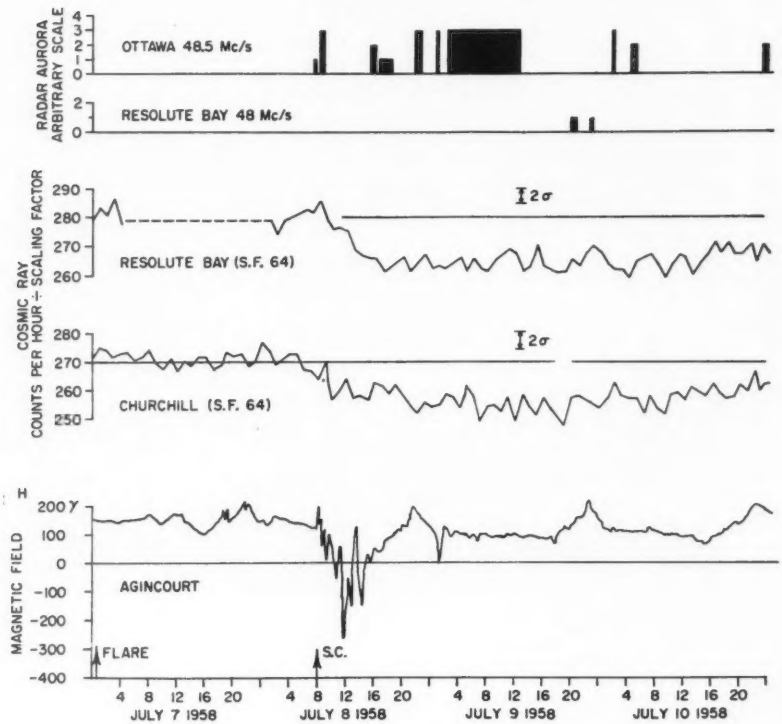

FIG. 6. Radar aurora, cosmic ray, and magnetic field data, 7 to 10 July, 1958.

same time as the sudden commencement. The cosmic ray count did not return to normal until about July 12. It should be noted that there was no noticeable increase of cosmic ray intensity before the Forbush decrease, as there was at the time of the February 23, 1956, event. The peak at 0800 at Resolute Bay is not considered significant in this regard.

The storm may therefore be divided into two distinct phases. The first began with the solar flare activity, the second with the sudden commencement of the geomagnetic storm. Because these two phases are separated by a period of 31 hours, it is possible to study each one separately. The intent of this paper is to examine in detail only the first phase.

TIME OF ONSET OF POLAR BLACK-OUT

The results of a detailed study of the time of onset of polar black-out are shown in Fig. 7, which gives the deviations of f_{min} from the monthly medians in a similar manner to that used by Shapley and Knecht (1958) for the

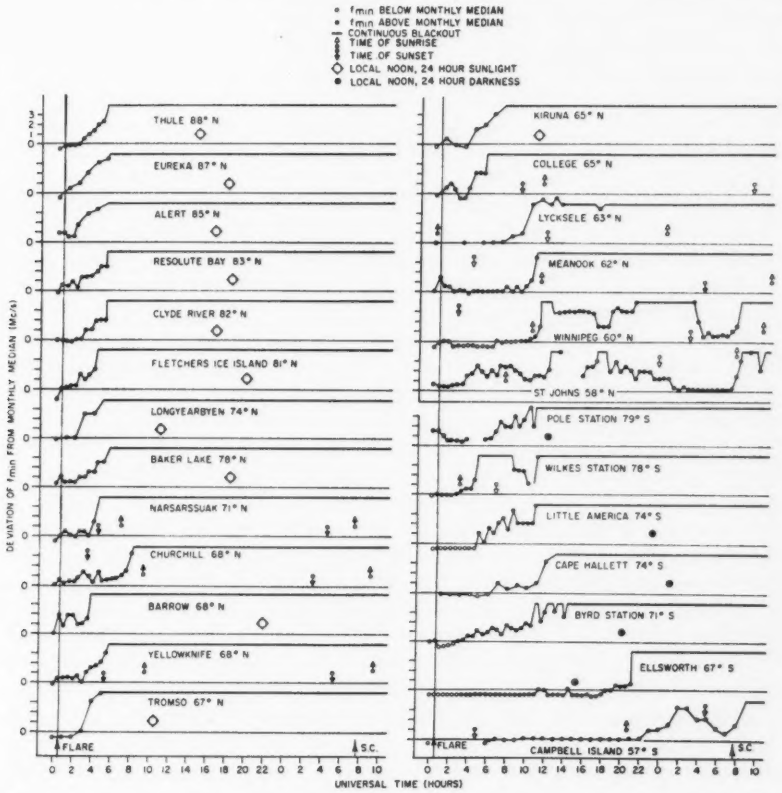

FIG. 7. Deviation of f_{min} from monthly median, for stations arranged in order of (dipole) geomagnetic latitude 7 July, 1958.

23 February, 1956, event. The times of last normal sounding, of first possible and first definite increase of f_{min}, and of the first black-out are shown in Table II for later analysis.

These data show the gradual increase of absorption from the time of the flare, until complete black-out at about 0500, at northern stations. Evidence of the short-wave fade-out (SWF) can be seen at some of the stations in sunlight by an increase of f_{min} immediately after the flare, before the polar cap absorption began. The initial black-out extended to St. John's, at 58° geomagnetic latitude. Three stations, however, in Table II, Inverness, Kjeller, and Upsala are clearly out of order, since black-out did not occur at these stations until after the sudden commencement on July 8.

In the south the black-out extended north to Ellsworth (67°), and there was evidence of increased absorption at Campbell Island (57°) during daylight hours. The late appearance of absorption at Ellsworth is, however, difficult to explain for a station at this high geomagnetic latitude.

The solution to these inconsistencies connected with the latitude of the stations is to be found in use of more precise values for the geomagnetic latitude. Studies have been made by Hultqvist (1958, 1959*b*) and Quenby and Webber (1959) using fifth and sixth order harmonics of the geomagnetic field in order to obtain a better representation of the effective magnetic latitude. These authors have shown that application of such corrections lead to a more accurate representation of auroral isochasms.

The calculations of Hultqvist (1958) have been used to compute a corrected geomagnetic latitude as tabulated in Table II.

The inconsistencies mentioned above disappear when the stations are considered in order of corrected geomagnetic latitude. Inverness, Kjeller, and Upsala are placed south of St. John's, which at 59° corrected latitude is at the southern limit of the polar black-out.

In the southern hemisphere, Ellsworth (62°) and Campbell Island (61°) compare well with Winnipeg (61°) and St. John's (59°) when times of black-out are compared, taking into account the amount of daylight at each station. The cutoff magnetic latitude for this storm, therefore, is about 59°.

It was shown by Reid and Collins (1959) that polar cap absorption is greater during daylight hours. It is presumed that sunlight causes the dissociation of negative ions, maintaining high electron densities in the lower ionosphere. This effect can be seen at Winnipeg, St. John's, Wilkes Station, and Campbell Island. The early onset of black-out at Wilkes Station presumably is partially due to the short period of daylight at that station, which, though high geomagnetically, is at 66.4° S. geographic latitude. The second onset of black-out at Wilkes at about 1100 hours roughly corresponds with the time of black-out at Pole Station, Little America, Cape Hallett, and Byrd Station in the south, and Lycksele, Meanook, Winnipeg, and St. John's in the north.

It is therefore suggested that the main reason for the late onset of polar cap absorption at southern stations is due to these stations being in darkness. The alternative explanation, that the inclination of the earth's magnetic field dipole axis away from the sun at this time of year reduced the incoming particle flux

seems less likely, since an attempt to correlate local time of particle precipitation with opening of the Störmer cone, using the graphs produced by Alpher (1950), was inconclusive.

The onset of black-out within an hour of the sudden commencement, at Winnipeg, St. John's, Ottawa, and Campbell Island presumably shows either the beginning of auroral absorption at stations outside the auroral zones, or the equatorial extension of polar cap absorption due to the distortion of the earth's magnetic field.

LATITUDE VARIATIONS OF TIME OF FIRST ABSORPTION

The times of first increase of absorption at the stations listed in Table II were rearranged according to corrected geomagnetic latitude, and plotted on Fig. 8. In principle, the time of first increase of $f_{\min}$ should be relatively more reliable than, for example, time of first black-out, since the latter is a function

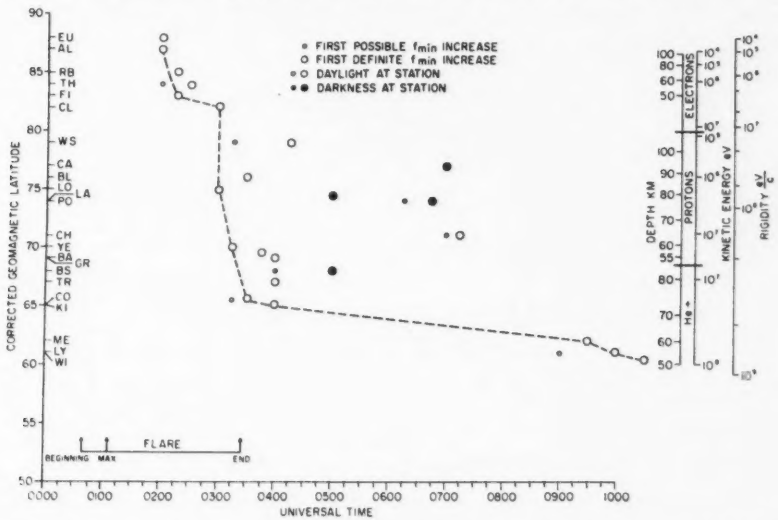

FIG. 8. Time of first increase of $f_{\min}$, arranged in order of corrected geomagnetic latitude, 7 July, 1958.

of equipment sensitivity, antenna pattern, ionospheric critical frequency, and so on. The increase $f_{\min}$ is a relative measurement based on average characteristics of the equipment and the ionosphere at each frequency.

The early beginning of absorption at highest latitude stations and the subsequent spread of absorption to lower latitudes are clearly evident. At the highest latitude stations, the measurement of the precise time of onset of absorption is made somewhat more difficult by the short-wave fade-out, which is evident at a number of the stations in sunlight. It should be noticed particularly that the first possible increase of absorption at Wilkes Station in Antarctica occurred at approximately the same time as the increase at northern

TABLE II

Station	Abbr.	Operated by:	Geo-magnetic dipole latitude	Corrected geo-magnetic latitude	Last normal f_{min}	First possible increase U.T.	First definite increase U.T.
Thule	TH	U.S. Signal Corps	88° N.	84° N.	0130	0200	0230
Eureka	EU	Canada D.R.B.	87° N.	88° N.	(0000)	(0100)	(0200)
Alert	AL	Canada D.R.B.	85° N.	87° N.	0145	0200	0200
Resolute Bay	RB	Canada D.O.T.	83° N.	85° N.	0100	0215	0215
Clyde River	CL	Canada D.R.B.	82° N.	82° N.	0245	0300	0300
Fletchers Ice Id.	FI	U.S. Signal Corps	81° N.	83° N.	0200	0215	0215
Longyear byen	LO	Norwegian Def. Research Est.	74° N.	75° N.	(0200)	(0300)	(0300)
Baker Lake	BL	Canada D.O.T.	73° N.	76° N.	0315	0330	0330
Narsarssuak	GR	CRPL	71° N.	69° N.	0330	0400	0400
Churchill	CH	Canada D.O.T.	68° N.	71° N.	0645	0700	0715
Barrow	BA	CRPL	68° N.	69° N.	0300	0345	0345
Yellowknife	YE	Canada D.R.B.	68° N.	70° N.	0300	0315	0315
Tromso	TR	Norwegian Def. Research Est.	67° N.	67° N.	(0300)	(0400)	(0400)
Kiruna	KI	Research Inst. Nat. Defence, Sweden	65° N.	65° N.	0300	0400	0400
College	CO	Union of Alaska	65° N.	65° N.	0300	0315	0330
Lycksele	LY	Research Inst. Nat. Defence, Sweden	63° N.	61° N.	(0900)	(1000)	(1000)
Meanook	ME	Canada D.R.B.	62° N.	62° N.	0915	0930	0930
Inverness	IN	DSIR, U.K.	61° N.	57° N.			
Kjeller	OS	Norwegian Def. Research Est.		60° N.	58° N.		
Winnipeg	WI	Canada D.O.T.	60° N.	61° N.	1000	1030	1030
Upsala	UP	Research Inst. Nat. Defence, Sweden	58° N.	57° N.			
St. John's	SJ	U.S. Signal Corps	58° N.	59° N.	1200	1215	1215
Ottawa	OT	Canada D.O.T.	57° N.	59° N.			
Victoria	VI	Canada D.R.B.	54° N.	53° N.			
Godley Head	GH	Christchurch Geophys. Obs.	48° S.	52° S.			
Campbell Id.	CI	Christchurch Geophys. Obs.	57° S.	61° S.			
Ellsworth	EL	CRPL	67° S.	62° S.	1800	1915	2100
Byrd Station	BS	CRPL	71° S.	68° S.	0300	0400	0500
Little America	LA	CRPL	74° S.	74° S.	0445	0500	0500
Cape Hallett	CA	Christchurch Geophys. Obs.	74° S.	77° S.	(0500)	(0700)	(0700)
Wilkes Station	WS	CRPL	78° S.	79° S.	0300	0315	0415
Pole Station	PO	CRPL	79° S.	74° S.	0530	0615	0645

stations of the same latitude. The delay in time of first absorption at dark stations was of the order of 3 hours except at Churchill which showed some absorption and then recovered, which made an assessment of the time of first increase very uncertain.

A striking observation on this graph is that one group of data appear to be clustered above 83° effective magnetic latitude, at about 0200 U.T. Absorption

LE II

First definite crease U.T.	Black-out begins U.T.	Duration of black-out, hr	6 July range of F_{max} Mc	Absorption during 7 July	Remarks
0230	0500	78	6.0–7.5	Black-out in progress	
0200)	0515	79	5.2–6.3	Black-out in progress	*f*-Plot, hourly values only
0200	0500	116	4.3–5.9	Black-out in progress	
0215	0515	79	5.0–6.8	Black-out in progress	
0300	0500	78	5.2–6.9	Black-out in progress	
0215	0415	97	5.1–6.7	Black-out in progress	
0300)	0500	85	4.6–7.0	Black-out in progress	No *f*-plot, hourly values only
0330	0545	67	5.0–7.3	Black-out in progress	
0400	0430	75	3.9–7.2	Black-out in progress	
0715	0815	67	5.4–7.0	Black-out in progress	
0345	0345	24	5.0–6.4	Black-out in progress	Equipment unserviceable 64 hr
0315	0545	66	5.0–6.5	Black-out in progress	
0400)	0500	76	5.4–7.5	Black-out in progress	No *f*-plot, hourly values only
0400	0700	39	4.5–7.3	Black-out in progress	Equipment unserviceable 35 hr
0330	0515	76	5.2–6.6	Black-out in progress	
(1000)	1400	50	4.5–7.7	Black-out in progress	No *f*-plot, hourly values only
0930	1030	51	4.5–6.7	Black-out in progress	
		19	5.2–8.6	Black-out began 1500 hr July 8	
		13	5.5–8.2	Black-out began 1500 hr July 8	11 hr "C" No *f*-plot, hourly values only
1030	1100	20	3.8–6.8	Absorption high, black-out intermittent	
		16	5.3–8.2	Black-out began 1500 hr July 8	No *f*-plot, hourly values only
1215	1215	19	4.6–7.6	Intermittent until black-out 0815 July 8	9 hr "C"
		22	3.8–7.3	Black-out began 0900 hr July 8	
		6	4.6–8.0	Intermittent black-out began 1415 hr July 8	
		0	3.1–13	Normal	No *f*-plot, hourly values only
		31	2.8–13	Black-out began 0900 hr July 8	No *f*-plot, hourly values only
2100	2100	43	1.9–5.2	Black-out in progress	
0500	1045	61	2.4–9.5	Black-out in progress	12 hr "C"
0500	1045	59	2.2–8.0	Black-out in progress	
(0700)	1300	39	2.9–8.4	Black-out in progress	No *f*-plot, hourly values only
0415	0445	62+	3.3–8.0	Intermittent black-out	
0645	1000	62+	3.6–8.2	Blackout in progress	

did not occur at any station at lower latitude before 0300 U.T. The lowest latitude at which absorption was evident before the sudden commencement was 59°, as has been pointed out previously.

For comparison Fig. 9 shows the time of onset of black-out. Again the stations in daylight blacked about 6 hours before stations in darkness, except for those stations below 62°.

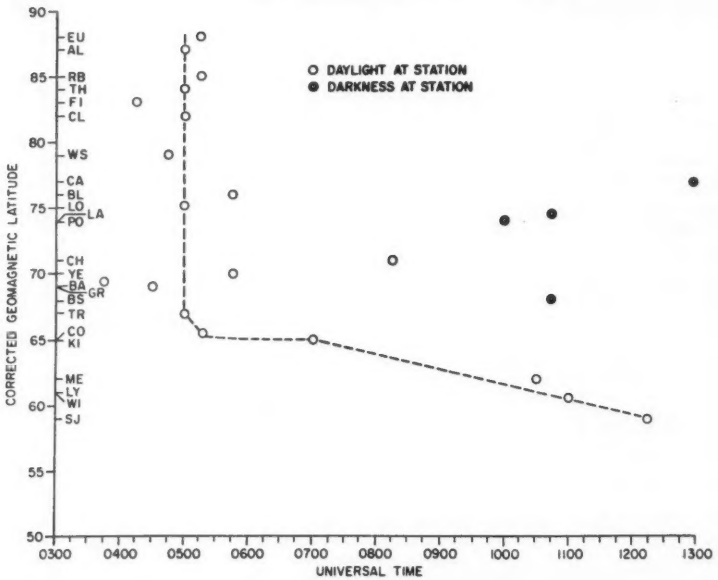

FIG. 9. Time of onset of black-out, arranged in order of corrected geomagnetic latitude, 7 July, 1958.

MECHANISM OF ABSORPTION

An increase of electron density in the lower ionosphere (50–80 km) is undoubtedly the cause of the increased absorption. The coefficient of absorption is given by the following equation:

$$k = \frac{2\pi e^2}{mc} \frac{N\nu}{\nu^2+\omega^2}$$

where e and m are the electronic charge, N the electron density, ν the collision frequency, and ω the radio wave angular frequency. The usual approximations have been made by neglecting the magnetic field and assuming that the index of refraction is not significantly different from unity.

When N is constant, the absorption coefficient reaches a maximum at the height at which $\nu = \omega$. At decreasing heights the collision frequency ν becomes much greater than ω, and $k \propto (N/\nu)$, so that absorption soon becomes unimportant. The variation of collision frequency with height was measured in a rocket from 60 to 80 km over Churchill during a polar black-out by Kane (1959). The measured values, extrapolated down to 45 km and up to 95 km are shown in Table III.

From this table it is evident that absorption at about 3 Mc/s ($\omega = 19\times10^6$) will be small below about 50 km ($\nu > 10\omega$) and will reach its maximum about 65 km ($\nu = \omega$). Measurements by Seddon and Jackson (Friedman 1959) on the same rocket flights above Churchill, when, however, the electron density

TABLE III

Collision frequencies

Height (km)	45	55	65	75	85	95
$\nu(\text{sec}^{-1}\times 10^{-6})$	400	90	20	4.3	.95	.21

was not constant, showed that absorption on 7.75 Mc/s began at about 55 km on the rocket's upward flight, reached its maximum at 65 km, and decreased rapidly above this height.

It can be inferred from this argument that ionospheric sounding method of observation of absorption is selective. The measurements reported in this paper emphasize the effects which produce ionization at heights from approximately 50 to 80 km.

SOLAR PARTICLE PRECIPITATION

The causative agent for the ionization at these heights in the ionosphere is believed to be the precipitation of charged particles from the sun produced by some mechanism, as yet unspecified, beginning with a flare of major importance (Leinbach and Reid 1959; Hultqvist 1959*a*; Reid and Collins 1959; and Obayashi 1959).

The particles lose their energy by collisions in the atmosphere. Each particle produces a very large number of ion pairs (3×10^5 ion pairs for a 10-Mev proton), the majority being produced in the last few kilometers of air where the solar particle is losing energy rapidly.

The particles are constrained to move in Störmer orbits by the earth's magnetic field since the particle flux is extremely low. The lack of reaction on the earth's magnetic field during the first hours of a polar cap absorption event confirms this low flux density. As a consequence it is reasonable to use the undisturbed magnetic field values to compute the magnetic cutoff rigidity R.

The magnetic cutoff rigidity, at a corresponding magnetic latitude given by Störmer (1955) is

$$R = (M/4r_e^2)\cos^4\lambda$$

where M is the magnetic dipole moment of the earth, and r_e the radius of the earth. The values of R for the appropriate latitude are plotted on the right-hand ordinate axes of Fig. 8. Also plotted are the kinetic energies and penetration depths in the atmosphere for particles of corresponding rigidity. Proton and helium ranges from the summary by Whaling (1958), electron ranges after Heitler (1954), and atmospheric parameters after Nicolet (1959) were used. Following Bailey (1959) it has been assumed that the helium ions are singly charged coming from the sun, but that they lose their second electron through collision on entering the atmosphere, and penetrate to depths appropriate for alpha-particles.

It is apparent that the 83° cutoff of Fig. 8 could be interpreted as due to electrons with energies of about 2 Mev, providing the earth's magnetic field

is essentially dipole in character at these latitudes. It is difficult to see how heavier particles could be responsible for this effect, since a proton or He+ ion flux which would penetrate 50 to 80 km into the atmosphere, would also be evident at much lower geomagnetic latitudes. The solar radio noise burst following the solar flare has been widely interpreted as due to radiation from energetic electrons, and so their precipitation into the earth's atmosphere is not entirely unexpected.

There is some indication in Fig. 8 of a break at 70°, which might be due to protons, while the low latitude cutoff of 59° suggests that He+ is present in the particle flux.

It is well known that protons are present during polar cap absorption events (Leinbach and Reid 1959). The presence of He has been discussed by Hultqvist (1958) and balloon observations of cosmic particles in July 12 have been interpreted as possible evidence of solar alpha-particle flux by Meyer (1959). It is, of course, well known that about 15% of the galactic cosmic ray flux is due to He ions.

COMPARISON WITH 23 FEBRUARY, 1956, EVENT

It is interesting to compare the data from 7 July, 1958, with that from the similar study by Shapley and Knecht (1958) on the 23 February, 1956, event. These authors analyzed data from 14 ionospheric stations in the northern hemisphere.

A flare at 0334 U.T. on 23 February is presumed to have initiated the earlier event, which, however, occurred when the north polar region was in darkness. The data of Shapley and Knecht have been replotted on Fig. 10 in a similar manner to that of Fig. 8.

The delay between the initiating flare and the sudden commencement was 47 hours, and the duration of black-out was about 40 hours for the 1956 event. The low latitude limits for the ionospheric polar cap black-out on 7 July and 23 February events were 59° corrected magnetic latitude (St. John's) and 58° (Kjeller) respectively, corresponding to magnetic rigidities of 9.6×10^8 and 1.2×10^9 electron volts. However, during the daytime when polar cap absorption is more efficient, the effect on 23 February extended to 54° (Fort Monmouth) indicating that particles with rigidities of 1.8×10^9 electron volts, were present. Protons or helium ions of this rigidity would penetrate to very low altitudes, and either the flux was very large, or heavier ions were responsible for this absorption. Cosmic ray data from equatorial latitudes showed, of course, the presence of particles of much greater energy.

The more rapid extension of polar absorption to lower latitudes, and the very marked increase in cosmic ray intensity, show that the 23 February event was the more energetic of the two, even though the duration of black-out was less. Otherwise, there are marked similarities between these two events which show that they were both of the same class of phenomenon.

CONCLUSION

From this study of the July 7, 1958, event, it is clear that polar cap absorption is caused by particle precipitation into the earth's atmosphere which

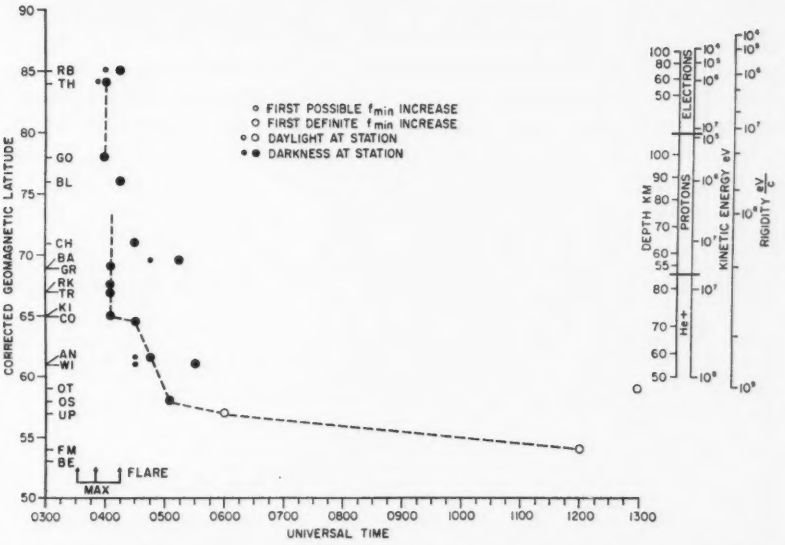

FIG. 10. Time of first increase of f_{min}, arranged in order of corrected geomagnetic latitude, 23 February, 1956 (after Shapley and Knecht).

produced increased ionization and absorption in the lower ionosphere at heights of the order of 50 to 80 km. The earth's magnetic field modified the selected flux of particles, so that a measurable flux did not penetrate to magnetic latitudes below 59°, corresponding to a particle rigidity of 9.6×10^8 ev/c. The necessity for use of a better approximation than the dipole field to determine the precipitation trajectories of particles has been shown.

The later onset of the disturbance in the southern hemisphere apparently was due to the absence of sunlight in the south polar regions, rather than to peculiarities of the particle orbits. The data suggest that electrons first precipitated into the ionosphere causing absorption at latitudes higher than 83° corrected magnetic latitude, and that protons and helium ions then precipitated to lower latitudes.

The polar cap absorption event was followed by a sudden magnetic commencement by auroral absorption, and by a Forbush decrease. The effects were very similar to those of the 23 February, 1956, event but were of longer duration, particularly in the northern hemisphere, though the data suggest that the particles were not quite as energetic as on the earlier occasion.

ACKNOWLEDGMENTS

Acknowledgment is made for the use of I.G.Y. ionospheric data obtained at stations operated by the U.S. Signal Corps, the Norwegian Defence Research Establishment, the Central Radio Propagation Laboratory, the Research Institute of National Defence of Sweden, the Department of Scientific and Industrial Research of the U.K., the University of Alaska, and the Christ-

church Geophysical Observatory of New Zealand. Magnetic data were obtained from the Dominion Observatory, Ottawa. The cosmic ray data were made available by D. C. Rose and the radar aurora data by A. G. MacNamara of the National Research Council, Ottawa. G. C. Reid read the manuscript and made some very helpful suggestions regarding the interpretation of the data.

REFERENCES

ALPHER, R. A. 1950. J. Geophys. Research, **55**, 437.
BAILEY, D. K. 1959. Proc. I.R.E. **47**, 255.
FRIEDMAN, H. 1959. Proc. I.R.E. **47**, 272.
HARANG, L. and TROIM, J. 1959. Planet. Space Sci. **1**, 102.
HEITLER, W. 1954. Quantum theory of radiation. 2nd ed. (The Clarendon Press, Oxford).
HULTQVIST, B. 1958. Arkiv Geofysik, **3**, 63.
——— 1959*a*. Tellus, **11**, 332.
——— 1959*b*. Nature, **183**, 1478.
HULTQVIST, B., AARONS, J., and ORTNER, J. 1959. Tellus, **11**, 319.
KANE, J. A. 1959. J. Geophys. Research, **64**, 133.
LEINBACH, H. and REID, G. C. 1959. Phys. Rev. Letters, **2**, 61.
MEYER, P. 1959. Phys. Rev. **115**, 1734.
NICOLET, M. 1959. J. Geophys. Research, **64**, 2092.
OBAYASHI, T. 1959. Rept. Ionosphere Space Research Japan, **13**, 201.
QUENBY, J. J. and WEBBER, W. R. 1959. Phil. Mag. VIII, **4**, 90.
REID, G. C. and COLLINS, C. 1959. J. Atmospheric and Terrest. Phys. **14**, 63.
SHAPLEY, A. H. 1959. Proc. I.R.E. **47**, 323.
SHAPLEY, A. H. and KNECHT, R. W. 1958. U.S. Dept. of Commerce, NBS Report 5596.
STÖRMER, C. 1955. The polar aurora (Oxford University Press, London).
WHALING, W. 1958. Handbuck der physik, Vol. 34 (Springer-Verlag, Berlin), p. 193.

VELOCITY AUTOCORRELATIONS OF CHARGED PARTICLES IN A MAGNETOIONIC MEDIUM WITH APPLICATIONS TO TURBULENT DIFFUSION[1]

R. C. Bourret

ABSTRACT

A system of charged particles in a slightly ionized medium is considered subject to (1) collisions with members of the neutral species, (2) a constant external magnetic field, and (3) a fluctuating force field, either external or representing the collision forces. On the assumption that their motions are satisfactorily described by the Langevin equation, the cross-correlation functions in time between velocity components of these charged particles are calculated. These functions may be used, as described elsewhere by the author, to describe the self-diffusion of the charged particles. The cases treated are: purely random external forcing, forcing by exponentially correlated (Markovian) forces, and forcing by a random series of pulses corresponding to collision forces.

1. INTRODUCTION

The term "turbulent diffusion" is used here in a slightly extended sense: what is meant is diffusion in which the motion of the diffusate particles is coherent over finite space and time intervals. This contrasts with the completely random motion implicit in the classical (Fickian) diffusion equation. In the particular case in which the diffusion is due to turbulent flow of the medium containing the diffusate particles, such as the diffusion of dissolved salts in the sea, the diffusion is turbulent in the usual sense. All diffusion excepting the limiting classical case is turbulent. In the present article, the time correlation functions of the velocity components will be calculated for a few simple cases. The spatial correlations will be neglected here because (1) it is not known just how they influence the quantitative description of the diffusive process, (2) it is not clear how they may be calculated for the physical systems considered here, and (3) the systems treated here are such that the effect of the spatial correlations is assumed negligible. The characterization of the turbulence will be taken to be the velocity autocorrelations of first order, i.e., quadratic in the velocities, although it is recognized that a complete characterization must include correlations of all orders. These higher order correlations would probably have only a small effect on the diffusive process and, in any case, even the first order correlations have not yet been taken properly into account.

By a well-known kinematical theorem the mean square spread of the diffusate originating at a point depends upon the velocity autocorrelation function (VAF) according to

$$\overline{x_i^2} = 2\int_0^t (t-t')R_{ii}(t')dt' \tag{1}$$

[1]Manuscript received March 14, 1960.
Contribution from the Hughes Research Laboratories, Hughes Aircraft Company, Malibu, California.

where R_{ii} is defined by

$$R_{ii}(t') = \langle v_i(t)v_i(t+t')\rangle \tag{2}$$

the brackets indicating a time average. Thus, given the VAF the growth of the second moment of the diffusate can be described. If less information is needed, the diffusivity along the ith axis can be calculated from the relation

$$D_i = \lim_{t\to\infty} \frac{1}{2}\frac{d}{dt}\overline{x_i^2} = \int_0^\infty R_{ii}(t')dt'. \tag{3}$$

This last is based on the asymptotic agreement of the detailed description (1) with the classical theory for times long compared with all relevant microprocesses (relaxation time, time between collisions, coherence time for external forces, cyclotron orbiting time, etc.). In a previous report (Bourret 1960) a diffusion equation was advanced in which the VAF appears. This equation gives a more complete description of the diffusive process taking into account the VAF characterization of the turbulence. It is not dealt with in detail here, but in Section III its use with the VAF is shown illustratively.

II. THE LANGEVIN EQUATION

What we wish to calculate are the autocorrelation functions of the velocity components of representative diffusate particles. These autocorrelations are to be time correlations rather than space correlations. The latter are of importance in the theory of turbulence and are calculated, after certain simplifying assumptions have been made, from the Navier–Stokes equations of fluid motion or from semiempirical theories. In our present problem no special simplifying assumptions need be made once we have decided upon the form of the equations of motion. Since, however, we wish to describe gaseous systems in which the particles collide we must abandon a strictly deterministic equation and adopt, instead, the Langevin equation which describes not the exact behavior of a single particle but the behavior of a typical particle of the ensemble. The choice of this equation, however, imposes drastic limitations on the kind of information we can obtain. The equation may be written as

$$\frac{d\mathbf{v}}{dt} = \frac{1}{m}\mathbf{F}(t)+\frac{e}{m}\mathbf{v}\times\mathbf{B}-g\mathbf{v}. \tag{4}$$

This says that the acceleration of the average particle is due to an applied force $\mathbf{F}$, which may be due to collisions with other particles, to the deflecting force of the magnetic field $\mathbf{B}$, and to the retarding or "braking" effect of collisions with other particles or with the medium in which it moves. The coefficient of the retarding force, g, may be approximately equated with the collision frequency. Its exact value, however, must be calculated from a consideration of the details of the collision process. (For a detailed discussion of this see Molmud (1959).) The force term, if it could be specified explicitly, would make possible the calculation of the trajectory of the representative particle. In order to study the diffusion of particles it would be necessary to

average over the equations of motion for particles differing in their initial conditions of motion. In that case we would need to know the particle density in phase space in order to obtain the averages. What we shall do, however, is to employ the Boltzmann equation for the distribution in phase space as a basis for the derivation of the Langevin equation. The distribution has thus been taken into account in the formation of the equation with which we begin. We shall consider, too, that the Langevin equation has been derived from the "tight-binding" or relaxation approximation to the collision term in the Boltzmann equation. The derivation from the Brownian motion approximation stipulates conditions which cannot be satisfied in the cases of interest to the present inquiry (see, for example, Wang and Uhlenbeck 1956). In the absence of an explicit force term we must deal with the Langevin equation in a statistical fashion. This is accomplished by characterizing the force by its power spectrum or, equivalently, by its autocorrelation function. It is then possible to determine the power spectrum of the particle motions, and the "initial conditions" of the particle motion do not appear. The only constant of integration which requires specification in this treatment is the mean kinetic energy of the particles. This is equivalent to specifying the temperature of the diffusate gas, and we assume here that the gas is in approximate thermal equilibrium at all times. We see, then, that the Langevin equation itself is never solved when the force is statistically characterized; only the velocity autocorrelations can be deduced from it. It is possible, therefore, to construct from the Langevin equation a differential equation for the velocity autocorrelations themselves, although it generally proves easier to construct an integral expression for these autocorrelations directly rather than to deal with the differential equations which they satisfy.

III. VELOCITY AUTOCORRELATION FUNCTIONS

First we write the three dimensional Langevin equation for charged particles in the presence of a magnetic field. In index notation this reads

$$\frac{dv_\alpha}{dt} = \frac{1}{m} F_\alpha(t) + \Omega_\alpha^\beta v_\beta - g v_\alpha \tag{5}$$

$$\Omega_\alpha^\beta = \omega_0 \begin{bmatrix} 0 & 1 & 0 \\ -1 & 0 & 0 \\ 0 & 0 & 0 \end{bmatrix}, \qquad \omega_0 = \frac{e}{m} B_3 \tag{6}$$

The summation convention is used here and in the following. The term due to the magnetic field has been written in terms of the matrix Ω.

For simplicity the magnetic field is supposed directed along the z-axis. Since all the quantities used are tensorial in character, the effect of a different choice of magnetic-field direction can be corrected for simply by transforming the tensor quantities through an appropriate rotation. The truncated Fourier transform of the force components is defined by

$$\bar{F}_{\alpha,T}(\omega) = \frac{1}{2\pi} \int_{-T/2}^{+T/2} F_\alpha(t) e^{-i\omega t} dt. \tag{7}$$

An analogous definition for the velocity components will be used. If we assume for the moment that the force and velocity components vanish outside of the interval $-T/2$ to $+T/2$ it follows from equation (5) that

$$\bar{v}_{\alpha,T}(\omega) = \frac{1}{m} M_{\alpha}^{\mu}(\omega)\bar{F}_{\mu,T}(\omega) \tag{8}$$

where $M_{\alpha}{}^{\mu}$, the mobility matrix, is given by

$$M_{\alpha}^{\mu}(\omega) = \frac{1}{(i\omega+g)[\omega_0^2+(i\omega+g)^2]}\begin{bmatrix} (i\omega+g)^2, & \omega_0(i\omega+g), & 0 \\ -\omega_0(i\omega+g), & (i\omega+g)^2, & 0 \\ 0, & 0, & \omega_0^2+(i\omega+g)^2 \end{bmatrix}. \tag{9}$$

The velocity autocorrelation functions in which we are interested are defined by

$$R_{\alpha\beta}(\tau) = \lim_{T\to\infty} \frac{1}{T}\int_{-T/2}^{+T/2} v_{\alpha}^{*}(t)v_{\beta}(t+\tau)dt. \tag{10}$$

The set of functions defined by

$$\bar{R}_{\alpha\beta}(\omega) = \lim_{T\to\infty} [\bar{v}_{\alpha,T}^{*}(\omega)\bar{v}_{\beta,T}(\omega)]/T, \tag{11}$$

and called the cross-spectral density or, simply, power spectrum, is related to the velocity autocorrelations according to the Wiener-Khinchine theorem by

$$R_{\alpha\beta}(\tau) = \int_{-\infty}^{+\infty} e^{-i\omega t}\bar{R}_{\alpha\beta}(\omega)d\omega. \tag{12}$$

Analogous to equation (11), the power spectrum of the force functions is defined by

$$\bar{H}_{\mu\lambda}(\omega) \equiv \lim_{T\to\infty} [\bar{F}_{\mu,T}^{*}(\omega)\bar{F}_{\lambda,T}(\omega)]/T. \tag{13}$$

From equation (8) together with the definitions (11) and (13), it follows that

$$\bar{R}_{\alpha\beta}(\omega) = \frac{1}{m^2}\bar{G}_{\alpha\beta}^{\mu\lambda}(\omega)\bar{H}_{\mu\lambda}(\omega) \tag{14}$$

where the symbol $\bar{G}_{\alpha\beta}^{\mu\lambda}$ has been introduced and is defined by

$$\bar{G}_{\alpha\beta}^{\mu\lambda}(\omega) = M^{*\mu}{}_{\alpha}(\omega)M_{\beta}^{\lambda}(\omega). \tag{15}$$

We will have occasion to use the contracted expression

$$\bar{G}_{\alpha\beta}(\omega) = \delta_{\mu\lambda}\bar{G}_{\alpha\beta}^{\mu\lambda}(\omega) \tag{16}$$

which takes the form

$$\bar{G}_{\alpha\beta}(\omega) = \begin{bmatrix} (\omega^2+\omega_0^2+g^2)X^{-1}(\omega) & 2i\omega\omega_0X^{-1}(\omega) & 0 \\ -2i\omega\omega_0X^{-1}(\omega) & (\omega^2+\omega_0^2+g^2)X^{-1}(\omega) & 0 \\ 0 & 0 & (\omega^2+g^2)^{-1} \end{bmatrix} \tag{17}$$

where the auxiliary definitions

$$X(\omega) = (\omega^2-\omega_1^2)(\omega^2-\omega_2^2) \qquad \begin{matrix}\omega_1^2 = (\omega_0+ig)^2 \\ \omega_2^2 = (\omega_0-ig)^2\end{matrix} \tag{18}$$

have been used. The velocity power spectra are given by equation (14). The corresponding autocorrelation functions can be expressed in terms of the quantities

$$G_{\alpha\beta}^{\mu\lambda}(\tau) = \int_{-\infty}^{+\infty} \tilde{G}_{\alpha\beta}^{\mu\lambda}(\omega)e^{-i\omega t}d\omega \tag{19}$$

as follows:

$$R_{\alpha\beta}(\tau) = \frac{1}{2\pi m^2}\int_{-\infty}^{+\infty} G_{\alpha\beta}^{\mu\lambda}(\tau-\tau')H_{\mu\lambda}(\tau')d\tau'. \tag{20}$$

Equations (14) and (20) are usually the best means of obtaining the power spectra of velocity autocorrelation functions of the moving particles.

IV. ISOTROPIC WHITE NOISE FORCING

The kind of force usually treated in connection with the Langevin equation is thermal noise, and this may be described as isotropic white noise, i.e., the three directional components are completely uncorrelated with one another and each component has an autocorrelation function representable by a delta function. In terms of spectral densities this means that there is no cross-spectral density between the components and that the spectral density of a single component is white. This spectral density function we represent by

$$\tilde{H}_{\mu\lambda}(\omega) = P\delta_{\mu\lambda}. \tag{21}$$

The constant P has no very immediate physical significance. Its meaning becomes clear from the normalization of the velocity autocorrelation functions resulting when equation (21) is employed in equation (14). Because of the definition (10) and the assumption of thermal equilibrium of the particle gas the velocity autocorrelations must be normalized according to

$$R_{\alpha\alpha}(0) = \langle v_\alpha^2\rangle = kT/m. \tag{22}$$

The expression kT here refers to the Boltzmann constant times the absolute temperature. This last should be distinguished from the same symbol used previously in a different sense. The former usage will not be repeated in what follows and no confusion should arise. This results in the identification of P as a simple function of the gas temperature through the relation

$$P = gmkT/\pi. \tag{23}$$

The autocorrelations of the velocity components themselves prove to be*

$$R_{\alpha\beta}(\tau) = (kT/m)e^{-g|\tau|}\begin{bmatrix} \cos\ \omega_0\tau & \sin\omega_0|\tau| & 0 \\ -\sin\omega_0|\tau| & \cos\ \omega_0\tau & 0 \\ 0 & 0 & 1\end{bmatrix}. \tag{24}$$

*It may be noted that this VAF corresponds to the "phenomenological" case given in Bourret (1959).

The relation between the autocorrelation functions and the diffusion of the particles has been described elsewhere (Bourret 1960). It is there proposed that the diffusion equation should be, in the absence of sources or singularities,

$$\chi\left(\frac{\partial}{\partial t}\right)\frac{\partial N}{\partial t} = \frac{\partial^2}{\partial x_i \partial x_k}\Psi_{ik}\left(\frac{\partial}{\partial t}\right)N. \tag{25}$$

The two functions ψ_{ik} and χ are the polynomial numerator and denominator of the Laplace transform of the functions (24).

$$\Phi_{ik}(s) = \int_0^\infty e^{-st}R_{ik}(t)dt = \psi_{ik}(s)/\chi(s). \tag{26}$$

If we wish to apply equation (25) to the description of the diffusion of charged particles perpendicular to a magnetic field we first integrate over the co-ordinate z (parallel to the magnetic field) and introduce the definition

$$\int_{-\infty}^{+\infty} N(x, y, z)dz = n(x, y). \tag{27}$$

The functions χ and ψ_{ik} are, in two dimensions,

$$\chi(s) = \omega_0^2 + (s+g)^2 \tag{28}$$

$$\psi_{ik}(s) = kT/m \begin{bmatrix} s+g, & \omega_0 \\ -\omega_0, & s+g \end{bmatrix} \tag{29}$$

and the resulting diffusion equation is

$$\frac{\partial^3 n}{\partial t^3} + 2g\frac{\partial^2 n}{\partial t^2} + (g^2+\omega_0^2)\frac{\partial n}{\partial t} = \frac{kT}{m}g\nabla^2 n + \frac{kT}{m}\frac{\partial}{\partial t}\nabla^2 n. \tag{30}$$

The high order terms in this equation describe transient effects which are of little interest. In any case they are usually small in magnitude compared with the terms of second order or less. Neglecting terms of order higher than the second equation (30) may be written in the form

$$\frac{\partial n}{\partial t} = D\nabla^2 n - \frac{6D}{v^2}\frac{\partial^2 n}{\partial t^2} \tag{31}$$

with

$$D = \frac{kT}{m}\frac{g}{g^2+\omega_0^2} \qquad v^2 = \frac{3kT}{m} \tag{32}$$

This equation is of the form of the Goldstein equation for turbulent diffusion and has been discussed by the present author elsewhere. The diffusivity constant agrees with the standard results (see, for example, Allis 1956).

V. CASE OF ISOTROPIC MARKOVIAN FORCING

If the forces are slightly more coherent than in the previous case, and are, in particular, Markovian, the particle velocity autocorrelations can be

found from equations (12) and (14). We shall assume that the applied forces are Markovian and isotropic and possess correlation functions

$$H_{\lambda\mu}(\tau) = \tfrac{1}{3}\langle F^2\rangle\delta_{\lambda\mu}e^{-\nu|\tau|} \tag{33}$$

and spectral functions

$$\bar{H}_{\lambda\mu}(\omega) = \frac{1}{3\pi}\langle F^2\rangle\delta_{\lambda\mu}\frac{\nu}{\nu^2+\omega^2}. \tag{34}$$

The resulting particle velocity autocorrelations prove to be

$$R_{11}(\tau) = R_{22}(\tau) = \frac{\frac{2}{3}\langle F^2\rangle m^{-2}\nu}{f^2+4g^2\omega_0^2}\left[\frac{h}{2\nu}e^{-\nu|\tau|} + e^{-g|\tau|}\left(\omega_0\sin\omega_0|\tau| + \frac{f}{2g}\cos\omega_0\tau\right)\right] \tag{35}$$

$$R_{33}(\tau) = \frac{\frac{1}{3}\langle F^2\rangle m^{-2}\nu^2 g}{\nu^2-g^2}\left[\nu e^{-g|\tau|} - ge^{-\nu|\tau|}\right] \tag{36}$$

where the notation

$$\begin{aligned} f &= \omega_0^2+\nu^2-g^2 \\ h &= \omega_0^2+g^2-\nu^2 \end{aligned} \tag{37}$$

has been used for brevity. In the limiting case in which $g \to \nu$ (36) assumes the form

$$R_{33}(\tau) = \tfrac{1}{6}\langle F^2\rangle m^{-2}g^3|\tau|e^{-g|\tau|}. \tag{38}$$

These autocorrelation functions are closely approximated by those given by equation (24) in all cases likely to be of physical interest—such as in the ionosphere. If highly coherent radiation were responsible for the forcing, i.e., if g were not very small compared to ν, this approximation would no longer be valid. This is a possibility for laboratory situations. The cross-correlation terms have not been calculated here because they cannot contribute to the diffusion according to the proposed equation (25). This is because the antisymmetrical elements of the $G_{\alpha\beta}$ matrix (equation (17)) cancel in the summation in the diffusion equation. The spectral functions corresponding to expressions (35) and (36) are readily shown to be

$$\bar{R}_{11}(\omega) = \bar{R}_{22}(\omega) = \frac{\frac{1}{3\pi}\langle F^2\rangle m^{-2}\nu}{\nu^2+\omega^2}\cdot\frac{\omega^2+(\omega_0^2+g^2)}{\omega^4-2\omega^2(\omega_0^2-g^2)+(\omega_0^2+g^2)^2}, \tag{39}$$

$$\bar{R}_{33}(\omega) = \frac{1}{3\pi}\langle F^2\rangle m^{-2}\frac{\nu}{\nu^2+\omega^2}\cdot\frac{1}{g^2+\omega^2}. \tag{40}$$

VI. THE CASE OF FORCING BY COLLISION IMPULSES

If the charged diffusate particles are mixed with a much larger number of neutral particles, such as may occur in a slightly ionized gas, the driving

force will consist principally of a random sequence of impulses due to collisions with members of the neutral species. The force correlation matrix is defined by

$$F_{ij}(t) = \widetilde{\langle F_i(t')F_j(t'+t)\rangle} \tag{41}$$

where the brackets indicate an ensemble average and the wavy line means an average over all incident directions in the collision. This last is equivalent to averaging the matrix F_{ij} over the rotation group in three dimensions. The result of this averaging is simply to eliminate the off-diagonal elements, i.e.,

$$F_{ij}(t) = \tfrac{1}{3}\delta_{ij}\langle F_1(t')F_1(t'+t)+F_2(t')F_2(t'+t)+F_3(t')F_3(t'+t)\rangle. \tag{42}$$

Since the collisions are assumed isotropic each of the bracketed terms will have the same average value and we may write

$$H_{ij}(t) = \delta_{ij}\langle F(t')F(t'+t)\rangle \tag{43}$$

where $F(t)$ is a typical force component. This force component consists of a random series of positive and negative pulses of functional form $f(t)$. It will be assumed that the positive and negative pulses occur with average frequencies ν_+ and ν_- respectively. The autocorrelation function appearing in (43) can be evaluated by means of a generalization of Campbell's theorem (see Appendix) for a random series of positive and negative pulses which states

$$\langle F(t)F(t+\tau)\rangle = (\nu_+ + \nu_-)\int_{-\infty}^{+\infty} f(t)f(t+\tau)dt + (\nu_+ - \nu_-)^2\left[\int_{-\infty}^{+\infty} f(t)dt\right]^2. \tag{44}$$

For the individual pulse we assume the simple form

$$f(t) = \frac{\tau_0 \Delta p/\pi}{t^2+\tau_0^2} \tag{45}$$

in which τ_0 is the effective duration of the collision and Δp the total impulse. Substituting this pulse shape into equation (44) gives for the force autocorrelation matrix (43) the expression

$$H_{ij}(t) = \delta_{ij}\frac{\nu}{3\pi}(\Delta p)^2\frac{2\tau_0}{t^2+(2\tau_0)^2}, \qquad \nu = \nu_+ + \nu_-. \tag{46}$$

It will be noticed that the second term of equation (44) vanishes because the pulse series is assumed to have equal numbers of positive and negative pulses. From (46) we readily find the spectral matrix of the forces to be

$$\bar{H}_{ij}(\omega) = \delta_{ij}\frac{\nu}{6\pi}(\Delta p)^2 e^{-2\tau_0|\omega|}. \tag{47}$$

From this the spectral matrix for the velocities is found from equation (14)

$$\bar{R}_{ij}(\omega) = \bar{G}_{ij}(\omega)\frac{\nu}{6\pi}(\Delta p)^2 e^{-2\tau_0|\omega|}. \tag{48}$$

The classical diffusivities are given by equation (3) and are given by

$$D_i = \bar{R}_{ii}(0) = \bar{G}_{ii}(0)\frac{\nu}{6\pi}(\Delta p)^2. \tag{49}$$

From equation (17) this becomes

$$\left.\begin{aligned} D_1 = D_2 &= \frac{\nu}{6\pi}\frac{(\Delta p)^2}{\omega_0^2+g^2} \\ D_3 &= \frac{\nu}{6\pi}\frac{(\Delta p)^2}{g^2} \end{aligned}\right\} \tag{50}$$

By equation (20) the VAF are determined by the integral

$$R_{ij}(t) = \frac{1}{2\pi}\int_{-\infty}^{+\infty} G_{ij}^{\mu\lambda}(t-t')F_{\mu\lambda}(t')dt'. \tag{51}$$

For the case with no magnetic field this yields

$$R_{ij}(t) = \delta_{ij}\frac{kT}{m}(\tau_0\nu)[I(t)+I(-t)] \tag{52}$$

where the following notation has been used

$$I(t) = -\mathrm{Im}[e^{-z}Ei(z)] \tag{53}$$

$$z = \nu(t+2i\tau_0) \tag{54}$$

$$Ei(z) = -\int_{-z}^{\infty} e^{-x}\,dx/x \tag{55}$$

and where the normalizing constant has been determined by the relation

$$R_{ii}(0) = \langle v_i^2\rangle = kT/m. \tag{56}$$

VII. CONCLUSION

It was mentioned in the Introduction that velocity correlations in space would not be taken into account here. This omission makes it impossible to apply the results obtained to plasmas undergoing collective oscillations since it is of the nature of these oscillations to imply spatially coherent motion of the charged particles. The discussion given here, moreover, does not include a description of oscillating particles subject to random forcing, collision damping, and magnetic field deflections. Just how such a situation might be legitimately described by a Langevin equation is not yet entirely clear. The effect of the oscillation on the VAF may prove to be very similar to that of the magnetic field, i.e., it may simply add a periodic factor to the result. This, as well as the problem of spatial VAF, will be taken up by the author elsewhere.

REFERENCES

ALLIS, W. P. 1956. Motions of ions and electrons, Research Laboratory of Electronics, Massachusetts Institute of Technology, Technical Report No. 299.
BOURRET, R. C. 1960. Can. J. Phys. **38**, 665.

MOLMUD, P. 1959. Phys. Rev. **114**, 29.
RICE, S. O. 1954. *In* Noise and stochastic processes, *edited by* N. Wax (Dover Publications, Inc., New York).
WANG CHANG, C. W. and UHLENBECK, G. E. 1956. The kinetic theory of a gas in alternating outside force fields, University of Michigan Technical Report, ONR, Nonr-1224-(15).

APPENDIX

We wish to construct the autocorrelation function of a series composed of randomly occurring identical positive and negative pulses. For this purpose we must construct a slight generalization of Campbell's theorem, which, in its ordinary form, is applicable only to a series of a single kind of pulse. The pulses will have the functional form $f(t)$, and a subscript will indicate the algebraic sign of the pulse, thus

$$f(t) = f_+(t) = -f_-(t). \tag{57}$$

The entire series of positive and negative pulses will be designated by $F(t)$, and it will be written as the sum of a series of positive pulses plus a series of negative pulses as follows:

$$F(t) = F_+(t)+F_-(t) = \sum_\alpha f_+(t-t_\alpha)+\sum_\beta f_-(t-t_\beta). \tag{58}$$

The t_α and the t_β are the random times of occurrence of the positive and negative pulses, respectively. The ensemble average to be used in forming the autocorrelation function will be indicated by brackets. In this notation the autocorrelation function for the series may be written out as a sum of four terms

$$\langle F(t)F(T+\tau)\rangle = \langle F_+(t)F_+(t+\tau)\rangle+\langle F_-(t)F_-(t+\tau)\rangle+\langle F_+(t)F_-(t+\tau)\rangle + \langle F_-(t)F_+(t+\tau)\rangle. \tag{59}$$

We assume that the average numbers of positive and negative pulses per unit time are ν_+ and ν_-, respectively. The form of Campbell's theorem given, for example, by Rice (1954) allows us to write down the autocorrelation functions for the first two terms of the preceding equation as follows:

$$\langle F_+(t)\ F_+(t+\tau)\rangle = \nu_+\int_{-\infty}^{\infty} f(t)\,f(t+\tau)dt+\nu_+^2\left[\int_{-\infty}^{\infty} f(t)dt\right]^2 \tag{60}$$

$$\langle F_-(t)\ F_-(t+\tau)\rangle = \nu_-\int_{-\infty}^{\infty} f(t)\,f(t+\tau)dt+\nu_-^2\left[\int_{-\infty}^{\infty} f(t)dt\right]^2. \tag{61}$$

The third term we write out as

$$\langle F_+(t)\ F_-(t+\tau)\rangle = \left\langle \sum_\alpha f_+(t-t_\alpha)\ \sum_\beta f_-(t-t_\beta+\tau)\right\rangle. \tag{62}$$

Carrying out the averaging over all possible values of the t_α and t_β* and indicating the average total number of pulses per interval T by N_+ and N_-

$$\lim_{T\to\infty}\frac{1}{T}\int_0^{\ } dt_\alpha\,\frac{1}{T}\int_0^T dt_\beta\ \sum_\alpha^{N_+} f_+(t-t_\alpha)\ \sum_\beta^{N_-} f_-(t-t_\beta+\tau) \tag{63}$$

*This assumes, of course, that the *ensemble* average may be replaced by a *time* average.

$$= \lim_{T\to\infty} -\frac{N_+}{T}\int_0^T f(\xi)d\xi \frac{N_-}{T}\int_0^T f(\eta)d\eta \tag{64}$$

and finally

$$= -\nu_+\nu_-\left[\int_{-\infty}^{+\infty} f(t)dt\right]^2 \tag{65}$$

since

$$\lim_{T\to\infty}\frac{N_+}{T} = \nu_+, \qquad \lim_{T\to\infty}\frac{N_-}{T} = \nu_-. \tag{66}$$

The last term of the complete expression for the autocorrelation of the series gives the same result as the above. Combining these formulas with the results given by Campbell's theorem for the first two terms of equation (59) gives finally the desired generalization

$$\langle F(t)F(t+\tau)\rangle = (\nu_+ + \nu_-)\int_{-\infty}^{+\infty} f(t)\,f(t+\tau)dt + (\nu_+ - \nu_-)^2\left[\int_{-\infty}^{+\infty} f(t)dt\right]^2. \tag{67}$$

NOTES

THE SUDDEN INCREASE IN COSMIC RAY INTENSITY OF MAY 4, 1960*

D. C. Rose

A sudden increase in cosmic ray intensity occurred on May 4 at approximately 10:30 U.T. Previous events of this type are rare and have been interpreted as a burst of particles coming from the sun or the immediate neighborhood with energies sometimes up to a few decades of billion electron volts. The last event of this particular type and the largest yet recorded occurred on February 23, 1956, though an unusual event on July 17, 1959, had some similar features. The sudden increases of the type that occurred on May 4 are believed always to be associated with an intense solar flare but by no means occur with every intense flare.

Four stations in Canada are operated by the Division of Pure Physics of the National Research Council. Each station is equipped with a cubical telescope (24 inches to a side) and a standard neutron monitor. The stations are listed as follows.

Name	Geographic		Altitude (meters)	Geomagnetic	
	Lat.	Long.		Lat.	Long.
Resolute	74.7° N.	94.9° W.	17	82.9°	289.3°
Churchill	58.8° N.	94.2° W.	39	68.7°	322.7°
Sulphur Mountain	51.2° N.	115.6° W.	2283	52.9°	300.4°
Ottawa	45.4° N.	75.6° W.	101	56.8°	351.4°

The records from the four stations have been measured and the intensity variation is shown in Fig. 1. The top four curves represent the changes in the intensity of the nucleon component as measured by a standard neutron monitor at each of the above four stations. The 100% base represents the mean between from 0900 to 1030 G.M.T. in each case. With our method of recording, the pips can be read off the recorder in any time interval, though there is an increasing reading error for shorter intervals. The shortest interval used was 1 minute. The reading error may be represented as the number of counts in ± 0.05 minutes though in fact this error is probably not a normal statistical error and depends on the reading technique used. This error should be combined with the standard error for the Poisson distribution when the intervals are short but for intervals of 10 minutes or more it can be neglected. The counting rates at the 100% level are shown in Table I.

For the main curves of Fig. 1 the counting interval was varied from 20 to 2 minutes depending on the rate of change. The inserted curves for Churchill,

*Issued as N.R.C. No. 5790.

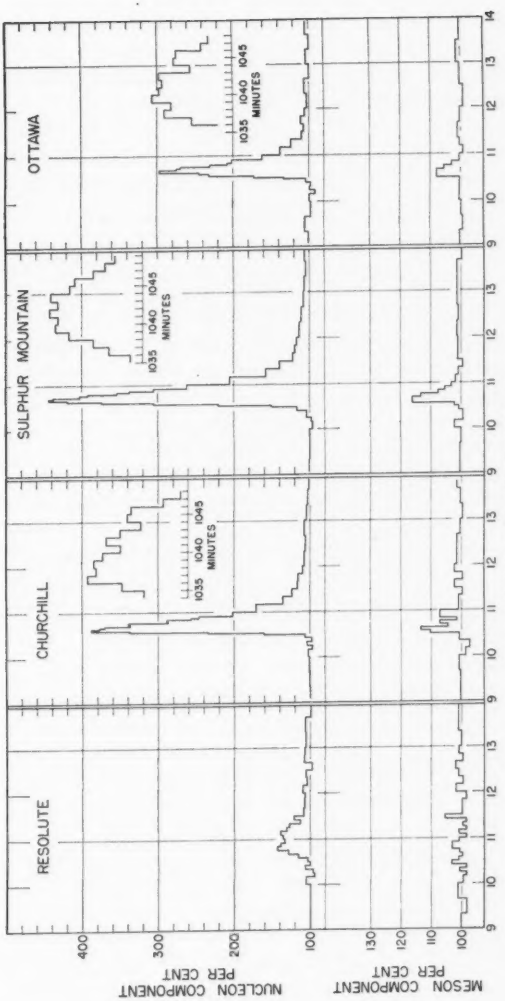

FIG. 1. The intensity increases at Resolute, Churchill, Sulphur Mountain, and Ottawa. Upper curves: the nucleon component. (The insert curves are 1-minute readings with an expanded time scale.) Lower curves: the meson component. The data are not corrected for pressure. The 100% level is the average intensity from 0900 to 1030 hours in each case.

Sulphur Mountain, and Ottawa show an independent set of measurements using minute intervals with an expanded time scale. These are included to show the shape of the peak intensity. This is well rounded in each case, there being no evidence of an appreciable higher counting rate even for a few seconds. No barometer corrections have been made for any of these data but the barometric pressures were not changing rapidly enough to affect the results appreciably. The lower curves represent the meson intensity change at the four stations measured with standard cubical telescopes. The times of

TABLE I

Counting rate at the 100% level in counts per hour divided by the scaling factor

Station	Nucleon component		Meson component	
	Pips/hour	Scaling factor	Pips/hour	Scaling factor
Resolute	220.7	64	51.2	1024
Churchill	265.9	64	61.8	1024
Sulphur Mountain	203.0	512	80.9	1024
Ottawa	262.3	64	57.1	1024

onset and times of the peak are listed in Table II. The times of onset are estimated by the point where a straight line through the rapid increasing part of the curve crosses the 100% axis and for the nucleon component are probably accurate to better than 1 minute. The times of maximum are estimated using a certain amount of smoothing of the minute values but cannot be in error by more than about 2 minutes. In the case of the meson component the accuracy is lower because of the much lower amplitude of the event.

TABLE II

Time of onset and time and height of the maximum intensity (G.M.T.)

Station	Time of onset	Time of maximum	% at maximum
Nucleon component			
Resolute	1032	1050–1105	142
Churchill	1030	1037	390
Sulphur Mountain	1029	1042	420
Ottawa	1029	1040	298
Meson component			
Resolute	—	—	100
Churchill	1028	1036	113
Sulphur Mountain	1031	1038	116
Ottawa	1028	1035	108

The striking feature of the results are:

(1) the low value of the increase at Resolute in relation to the other stations. The increase is either lacking or insignificant in the case of the meson component.

(2) the time delay in reaching maximum at Resolute. This is quite significant, the maximum being at least 10 minutes later than at other stations.

(3) the high intensity at Churchill relative to Ottawa and Resolute, all of which are at low altitude.

(4) the rise at Churchill seems to be steeper and the maximum slightly earlier than at Sulphur Mountain and Ottawa.

(5) the high intensity at Sulphur Mountain, which may be at least partly due to its altitude. Sulphur Mountain and Ottawa have about the same geomagnetic latitude.

(6) the relative heights of the nucleon and meson components are roughly consistent at the different stations.

Before drawing definite conclusions about this increase, the data from other stations should be studied but certain preliminary qualitative conclusions can be presented.

In consideration of calculations of Lüst (1957), none of these stations were in impact zones at the time of this increase, though Sulphur Mountain may have been not very far from one. The declination of the sun was $+16°$.

The flare reported to be associated with this increase was of very short duration, and, according to the preliminary listing, started well before the cosmic ray increase, namely, at 1020 (Preliminary Report of Solar Activity from the High Altitude Observatory, Boulder, Colorado, TR 453 May 6, 1960) and was over at 1025. The times of onset in Table II indicate that there was a delay of between 4 and 9 minutes in the arrival of particles. This delay is of the same order as that found in the February 23 event, 1956, for non-impact zone stations (Lüst and Simpson 1957).

The small intensity at Resolute suggests that the isotropy suggested by Meyer, Parker, and Simpson (1956) was not achieved during the major part of the event. A superposition of the part of the increase after about 1110 shows a close resemblance between the curves for Resolute, Churchill, and Ottawa, indicating that isotropy was probably reached about then or 40 minutes after onset.

The data from which the curves in Fig. 1 are drawn have been distributed to World Data Centers and the I.G.Y. cosmic ray stations with which data exchange has been arranged for some time. Spare copies are available.

The author would like to express appreciation of the prompt forwarding of data by Dr. F. Terentiuk from Sulphur Mountain, Mr. K. Gustafson from Churchill, and Mr. P. Bridges from Resolute.

LÜST, R. 1957. Phys. Rev. **105**, 1827.
LÜST, R. and SIMPSON, J. A. 1957. Phys. Rev. **108**, 1563.
MEYER, P., PARKER, E. N., and SIMPSON, J. A. 1956. Phys. Rev. **104**, 768.

RECEIVED JUNE 21, 1960.
DIVISION OF PURE PHYSICS,
NATIONAL RESEARCH COUNCIL,
OTTAWA, CANADA.

LETTERS TO THE EDITOR

Under this heading brief reports of important discoveries in physics may be published. These reports should not exceed 600 words and, for any issue, should be submitted not later than six weeks previous to the first day of the month of issue. No proof will be sent to the authors.

Frequency Measurement of Standard Frequency Transmissions[1, 2]

Measurements are made at Ottawa, Canada, using N.R.C. caesium-beam frequency resonator[3] as reference standard (with an assumed frequency of 9 192 631 770 c.p.s.). Frequency deviations from nominal are quoted in parts per 10^{10}. A negative sign indicates that the frequency is below nominal.

Date, June 1960	MSF, 60 kc/s	GBR, 16 kc/s		WWVB 60 kc/s
		5-hour average*	24-hour average	
1	−163	−153	−150	−19
2	−165	−152	−152	−83
3	−166	−158	−159	−82
4	−162	−155	−158	N.M.
5	−161	−156	−157	N.M.
6	−167	−159	−159	−80
7	−158	−150	−148	−87
8	−155	−143	−144	−80
9	−158	−153	−156	−44
10	−157	−150	−148	−12
11	−155	−156	−156	N.M.
12	−152	−153	−154	N.M.
13	−150	−153	−153	− 7
14	−157	−146	−144	+ 2
15	−155	−149	−151	+ 3
16	−152	−144	−145	−74
17	−158	−154	−155	−71
18	−160	−155	−158	N.M.
19	−158	−152	−150	N.M.
20	−155	−150	−147	−71
21	N.M.	−151	−152	−71
22	−149	−147	−150	−71
23	−144	−149	−150	−70
24	−154	−151	−151	N.M.
25	−161	−150	−147	N.M.
26	−161	−154	−152	N.M.
27	−150	−137	−135	N.M.
28	−151	−143	−145	−65
29	−144	−138	−135	−66
30	−144	−144	−145	−66
Midmonthly mean	−156	−150	−150	
Midmonthly mean of WWV	−144			

NOTE: N.M. no measurement.
*Time of observations: 01.30 to 03.30 U.T.; 10.00 to 13.00 U.T.

RECEIVED JULY 18, 1960.
S. N. KALRA
DIVISION OF APPLIED PHYSICS,
NATIONAL RESEARCH COUNCIL,
OTTAWA, CANADA.

[1]Issued as N.R.C. No. 5783.
[2]Cf. Kalra, S. N. 1959. Can. J. Phys. 37, 1328.
[3]Values published previous to this issue were subject to an additional uncertainty due to the method of assessment of the magnetic field correction used in the resonator.

NOTES TO CONTRIBUTORS

Canadian Journal of Physics

MANUSCRIPTS

General.—Manuscripts, in English or French, should be typewritten, double spaced, on paper 8½×11 in. **The original and one copy are to be submitted.** Tables and captions for the figures should be placed at the end of the manuscript. Every sheet of the manuscript should be numbered. Style, arrangement, spelling, and abbreviations should conform to the usage of recent numbers of this journal. Greek letters or unusual signs should be written plainly or explained by marginal notes. Characters to be set in boldface type should be indicated by a wavy line below each character. Superscripts and subscripts must be legible and carefully placed. Manuscripts and illustrations should be carefully checked before they are submitted. Authors will be charged for unnecessary deviations from the usual format and for changes made in the proof that are considered excessive or unnecessary.

Abstract.—An abstract of not more than about 200 words, indicating the scope of the work and the principal findings, is required, except in Notes.

References.—References should be listed **alphabetically by authors' names,** unnumbered, and typed after the text. The form of the citations should be that used in current issues of this journal; in references to papers in periodicals, titles should not be given and only initial page numbers are required. The names of periodicals should be abbreviated in the form given in the most recent *List of Periodicals Abstracted by Chemical Abstracts.* All citations should be checked with the original articles and each one referred to in the text by the authors' names and the year.

Tables.—Tables should be numbered in roman numerals and each table referred to in the text. Titles should always be given but should be brief; column headings should be brief and descriptive matter in the tables confined to a minimum. Vertical rules should not be used. Numerous small tables should be avoided.

ILLUSTRATIONS

General.—All figures (including each figure of the plates) should be numbered consecutively from 1 up, in arabic numerals, and each figure referred to in the text. The author's name, title of the paper, and figure number should be written in the lower left corner of the sheets on which the illustrations appear. Captions should not be written on the illustrations.

Line drawings.—Drawings should be carefully made with India ink on white drawing paper, blue tracing linen, or co-ordinate paper ruled in blue only; any co-ordinate lines that are to appear in the reproduction should be ruled in black ink. Paper ruled in green, yellow, or red should not be used. All lines must be of sufficient thickness to reproduce well. Decimal points, periods, and stippled dots must be solid black circles large enough to be reduced if necessary. Letters and numerals should be neatly made, preferably with a stencil (**do NOT use typewriting**) and be of such size that the smallest lettering will be not less than 1 mm high when the figure is reduced to a suitable size. Many drawings are made too large; originals should not be more than 2 or 3 times the size of the desired reproduction. Whenever possible two or more drawings should be grouped to reduce the number of cuts required. In such groups of drawings, or in large drawings, full use of the space available should be made; the ratio of height to width should conform to that of a journal page (4¾×7½ in.), but allowance must be made for the captions. **The original drawings and one set of clear copies (e.g. small photographs) are to be submitted.**

Photographs.—Prints should be made on glossy paper, with strong contrasts. They should be trimmed so that essential features only are shown and mounted carefully, with rubber cement, on white cardboard, with no space between those arranged in groups. In mounting, full use of the space available should be made. **Photographs are to be submitted in duplicate; if they are to be reproduced in groups one set should be mounted, the duplicate set unmounted.**

REPRINTS

A total of 100 reprints of each paper, without covers, are supplied free. Additional reprints, with or without covers, may be purchased at the time of publication.

Charges for reprints are based on the number of printed pages, which may be calculated approximately by multiplying by 0.6 the number of manuscript pages (double-spaced typewritten sheets, 8½×11 in.) and including the space occupied by illustrations. Prices and instructions for ordering reprints are sent out with the galley proof.

Contents

L. W. Gold—The cracking activity in ice during creep - - - - - - - 1137

R. B. Moore and W. White—Tables of rotational energy levels of deformed even-even nuclei - - - - - - - - - - - - - - - - - - 1149

Robert C. Smith and Robert T. Sharp—Central three-body forces in heavy nuclei - 1154

Malcolm McMillan and W. Opechowski—On the temperature dependence of the shape of paramagnetic resonance lines - - - - - - - - - 1168

Archibald W. Smith and Gerald W. Williams—Domain structure in yttrium iron garnet - - - - - - - - - - - - - - - - - - - 1187

John H. Chapman—The polar radio black-out of the ionosphere of 7 July, 1958 - 1195

R. C. Bourret—Velocity autocorrelations of charged particles in a magneto-ionic medium with applications to turbulent diffusion - - - - - - 1213

Notes:

D. C. Rose—The sudden increase in cosmic ray intensity of May 4, 1960 - 1224

Letters to the Editor:

S. N. Kalra—Frequency measurement of standard frequency transmissions 1228

Printed in Canada *by* University of Toronto Press